Title
Observational constraints on the photochemistry of non-acyl peroxy nitrates and organic nitrates on regional and global scales

Author
Browne, Eleanor Carol

Publication Date
2012

Peer reviewed|Thesis/dissertation

Observational constraints on the photochemistry of non-acyl peroxy nitrates and organic nitrates on regional and global scales

By

Eleanor Carol Browne

A dissertation submitted in partial satisfaction of the

requirements for the degree of

Doctor of Philosophy

in

Chemistry

in the

Graduate Division

of the

University of California, Berkeley

Committee in charge:

Professor Ronald C. Cohen, Chair
Professor Stephen R. Leone
Professor Allen H. Goldstein

Fall 2012

Observational constraints on the photochemistry of non-acyl peroxy nitrates and organic nitrates on regional and global scales

by

Eleanor Carol Browne

Abstract

Observational constraints on the photochemistry of non-acyl peroxy nitrates and organic nitrates on regional and global scales

by

Eleanor Carol Browne

Doctor of Philosophy in Chemistry

University of California, Berkeley

Professor Ronald C. Cohen, Chair

Reduced chemicals that are for the most part insoluble in water are emitted to the atmosphere from a wide range of natural and industrial processes. The self-cleansing nature of the atmosphere subsequently oxidizes these chemicals to products such as HNO_3, CO_2 and H_2O. The oxidants in this chemistry are primarily OH, O_3 and NO_3 with an additional contribution from H_2O_2 in the liquid phase. The concentrations of these gas phase oxidants are regulated by the availability of NO_x ($NO_x = NO + NO_2$) radicals. Consequently, understanding the sources of NO_x and its removal from the atmosphere is crucial to understanding the composition of the atmosphere and thus air quality and climate. In this thesis I investigate processes controlling NO_x concentrations in remote continental environments and in the upper troposphere. Using upper tropospheric data collected during the NASA Arctic Research of the Composition of the Troposphere from Aircraft and Satellites (ARCTAS) experiment, I find that methyl peroxy nitrate ($CH_3O_2NO_2$) is an important sink of NO_x and that it may account for the long standing discrepancy between measured and modeled ratios of NO to NO_2. Incorporation of $CH_3O_2NO_2$ chemistry into a global chemical transport model shows that the formation of $CH_3O_2NO_2$ has important impacts on atmospheric chemistry at temperatures below 240 K. Next, I focus on the lower troposphere over the remote continents and investigate the role of emissions from the biosphere as they affect the NO_x removal rate. During the oxidation of biogenic organics, non-peroxy organic nitrates (molecules of the form $RONO_2$ which will be referred to as ΣANs) are formed. Using a simplified representation of low NO_x, high biogenic volatile organic compound chemistry, I find that the reactions leading to formation of ΣANs control the NO_x lifetime over most of the continents. Comparison of these results to both ARCTAS observations and calculations using a regional 3-D chemical transport model (the Weather Research and Forecasting model with chemistry - WRF-Chem) confirm the importance of ΣANs in determining NO_x lifetime. In addition to their confirmation of ΣANs as a NO_x sink, the ARCTAS data imply that the lifetime of ΣANs is shorter than that of HNO_3. The chemical lifetimes and the products of oxidative chemistry of ΣANs are not well known. I identify two mechanisms that are capable of explaining the short lifetime of ΣANs, one of which returns NO_x to the atmosphere and the other which removes it permanently. These two mechanisms are expected to result in different spatial patterns of NO_x concentrations. The ARCTAS data is unique in its extensive coverage over the boreal forest where monoterpene emissions are

especially high. I show that the observations imply that the reactions that produce monoterpene nitrates represent a NO_x sink that is roughly equal to the rate of the $OH+NO_2$ reaction to form HNO_3. Using WRF-Chem I show how this chemistry affects OH, O_3, and peroxy nitrate concentrations and describe how current uncertainties in our understanding of monoterpene nitrate chemistry affect predictions of the concentrations of those species and of NO_x.

Contents

List of Tables

List of Figures

Acknowledgements

All the work that has gone into this thesis would not have been possible without the support of numerous people these past six years. I would first like to thank my advisor, Ron Cohen for his support and intellectual guidance. By allowing me the freedom to pursue research topics that interested me while always challenging me to think about the big picture science, Ron has shaped my scientific career. Ron is always available and listens to what I have to say, treating me more as a colleague than as a student. His attention to developing the communication skills of the group members has greatly improved my writing and presentation skills.

I would also like to thank Paul Wooldridge, without whom none of the field measurements described here, or any of the other field campaigns I participated in, would have been possible. Paul taught me almost everything I know about the instruments with incredible patience for which I will always be grateful. Paul's help with the instruments, as well as the discussions regarding the data and other science have greatly influenced my scientific work.

This work would also have not been possible with the support of current and past Cohen group members. In particular, I would like to thank Brian LaFranchi for his patience and help in my first few years of graduate school and with the BEARPEX campaigns. I would also like to thank Ashley Russell and Luke Valin for all the help over the years in lab, classes, teaching, and in life.

The last six years would not have been possible without the support of Rex Lake, who has been there for the highs and lows and always knows what I need to hear. This last year in particular would not have been possible without him telling me to calm down and knowing when we should order take-out rather than cook. I would also like to thank my parents and brother for their continued and unwavering support.

I also gratefully acknowledge financial support from NASA grant NNX08AR13G and a NASA Earth Systems Science Fellowship. I would also like to thank all the participants of the BEARPEX, ARCTAS, and CalNex field campaigns. The field campaigns were amazing learning opportunities, where I learned not just about my own research, but also about what everyone else was doing and how all our work fits together. The conversations I had during field campaigns have made me a better scientist. The comments and advice I have received from my co-authors on the various manuscripts has also been invaluable. Their comments and suggestions have improved the quality of my work and have provided interesting scientific insights.

Chapter 2 has been adapted from the following peer-reviewed publication:
Global and regional effects of the photochemistry of $CH_3O_2NO_2$: evidence from ARCTAS, Atmospheric Chemistry and Physics, 11, 4209-4219, 2011.
It has been modified for presentation here and was coauthored by:
A. E. Perring[1,*,**], P. J. Wooldridge[1], E. Apel[2], S. R. Hall[2], L. G. Huey[3], J. Mao[4], K. M. Spencer[5], J. M. St. Clair[6], A. J. Weinheimer[2], A. Wisthaler[7], and R. C. Cohen[1,8]

[1]Department of Chemistry, University of California Berkeley, Berkeley, CA, USA
[2]Atmospheric Chemistry Division, National Center for Atmospheric Research, Boulder, CO, USA
[3]School of Earth and Atmospheric Sciences, Georgia Institute of Technology, Atlanta, GA, USA

[4]School of Engineering and Applied Science, Harvard University, Cambridge, MA, USA
[5]Division of Chemistry and Chemical Engineering, California Institute of Technology, Pasadena, CA, USA
[6]Division of Geology and Planetary Sciences, California Institute of Technology, Pasadena, CA, USA
[7]Institut für Ionenphysik & Angewandte Physik, University of Innsbruck, Innsbruck, Austria
[8]Department of Earth and Planetary Sciences, University of California Berkeley, Berkeley, CA, USA
[*]now at: Chemical Sciences Division, Earth Systems Research Laboratory, National Oceanic and Atmospheric Administration, Boulder, CO, USA
[**]now at: Cooperative Institute for Research in Environmental Sciences, University of Colorado, Boulder, CO, USA

Chapter 1

Introduction

Nitrogen oxides, collectively known as NO_x ($NO_x = NO + NO_2$) are emitted into the atmosphere from soils, lightning, and combustion processes. As shown in Fig. 1.1, in the presence of volatile organic compounds (VOCs) and sunlight, NO and NO_2 rapidly interconvert producing ozone (an air pollutant and climate forcer) and regenerating OH (the primary control over the atmospheric lifetime of trace gases). NO_x is removed from this cycle (Fig. 1.2) when either NO or NO_2 react with other radicals forming one of three main classes of molecular products: nitric acid, peroxy nitrates, or non-peroxy organic nitrates. Peroxy nitrates are molecules of the form RO_2NO_2 and can be further subdivided into acyl and non-acyl peroxy nitrates. Acyl peroxy nitrates ($RC(O)O_2NO_2$) contain a peroxycarboxylic group whereas non-acyl peroxy nitrates contain the peroxy functionality without the carbonyl (i.e., they are of the form HO_2NO_2 or RO_2NO_2). In this thesis total peroxy nitrates, the sum of all acyl and non-acyl peroxy nitrates, will be referred to as ΣPNs. Non-peroxy organic nitrates are molecules of the form $RONO_2$ where R represents an alkyl group (alkyl nitrates) or a carbon backbone with additional functional groups such as hydroxyl groups (multifunctional nitrates). In this thesis, this class of molecules is referred to as total alkyl and multifunctional nitrates or ΣANs.

The identity of the molecular nitrogen product formed (HNO_3, ΣPNs, or ΣANs) depends on the VOC mixture, NO_x concentration, temperature, pressure and solar illumination. Subsequent chemical reactions characteristic of each of these families of higher oxides of nitrogen lead to either the return of NO_x to the active pool of free radicals or deposition to the Earth's surface. The branching between pathways that permanently remove NO_x versus those that temporarily sequester NO_x, as well as the time scales on which sequestered NO_x is returned to the free radical pool, remain one of the major uncertainties in our understanding of atmospheric chemistry. These uncertainties in regional and global budgets of O_3, OH, and NO_x in turn affect our understanding of processes controlling air quality and climate. In this thesis, I explore the role of two of these classes of NO_x loss reactions in the non-urban atmosphere where most of the chemistry on the planet occurs. I examine the formation of non-acyl peroxy nitrates and their role in the low temperature chemistry of the upper troposphere, and the role of chemicals emitted by the biosphere as a source of ΣANs – molecules that serve to control the concentration and lifetime of NO_x loss in remote continental environments.

In the textbook view of atmospheric chemistry, all VOC chemistry can be simplified as a representation of reactivity equivalent reactions of CO and CH_4. In this model atmosphere, the formation of HNO_3 through the reaction of NO_2 with OH is the only loss process of NO_x. Due to its long lifetime with respect to oxidation and photolysis (on the order of weeks) and short lifetime with respect to deposition (~ half a day in the boundary layer), the formation of HNO_3 is considered a permanent sink of NO_x from the atmosphere.

It is widely recognized that the atmospheric nitrogen cycle is more complex than this textbook view. In particular the formation of ΣPNs from the reaction of NO_2 and RO_2 (generally an acyl peroxy radical, $RC(=O)O_2$), can constitute a significant NO_x loss in NO_x source regions. ΣPNs have a steep temperature dependence to thermal decomposition, which results in a wide

range of lifetimes in the earth's atmosphere. They are formed in source regions where NO_x and organics are present in high concentrations even though the ΣPNs' lifetime in these regions is short (44 min at 298 K). The lifetime is 13.3 h at 280 K and weeks to months at lower temperatures, thus if ΣPNs are lofted into the free troposphere, they can be transported on intercontinental scales and then will release their NO_x when the air parcel containing them descends to warmer temperatures. This model has important implications for the redistribution of NO_x on the planet, but the basic textbook model, in which permanent NO_x removal is essentially exclusively through the OH+NO_2 reaction, is unaltered.

Evidence that other chemical reactions affecting the NO_x lifetime, including the chemistry of non-acyl peroxy nitrates HO_2NO_2 and $CH_3O_2NO_2$ (Wennberg et al., 1999; Murphy et al., 2004; Kim et al., 2007; Spencer et al., 2009) and the chemistry of ΣANs (Horowitz et al., 2007; Perring et al., 2009a, 2010; Farmer et al., 2011; Fiore et al., 2011; Paulot et al., 2012) is growing, especially in urban plumes. Here, I focus on the role of these mechanisms in the remote atmosphere.

In Chapter 2, I use ARCTAS measurements to show that methyl peroxy nitrate ($CH_3O_2NO_2$) is present in concentrations of ~5–15 pptv in the springtime arctic upper troposphere and investigate the regional and global effects of $CH_3O_2NO_2$ by including its chemistry in the GEOS-Chem 3-D global chemical transport model that is driven by Goddard Earth Observing System (GEOS) meteorology. I find that at temperatures below 240 K, inclusion of $CH_3O_2NO_2$ chemistry results in decreases of up to ~20% in NO_x, ~20% in N_2O_5, ~5% in HNO_3, ~2% in ozone, and increases in methyl hydrogen peroxide of up to ~14%. Larger changes are observed in biomass burning plumes lofted to high altitude. Additionally, by sequestering NO_x at low temperatures, $CH_3O_2NO_2$ decreases the cycling of HO_2 to OH, resulting in a larger upper tropospheric HO_2 to OH ratio. These results may impact some estimates of lightning NO_x sources as well as help explain the long-standing discrepancy between modeled and measured NO to NO_2 ratios.

In contrast to HNO_4 and $CH_3O_2NO_2$, ΣANs are important NO_x sinks at high temperatures where complex VOCs are abundant. ΣANs are formed from the minor channel of the reaction of RO_2 with NO and can be considered the most poorly understood NO_x sink. This is partly due to the chemical complexity of this class of molecules, whose formation depends on the specific identity of the RO_2, as well as the analytical difficulties associated with their measurement in the atmosphere. Although the formation rate (e.g., Arey et al., 2001) and lifetime (Clemitshaw et al., 1997; Talukdar et al., 1997a, 1997b; Atkinson and Arey, 2003) are relatively well constrained for simple alkyl nitrates, the products of alkyl nitrate oxidation (e.g., Aschmann et al., 2011, 2012) as well as the formation and fate of more complex nitrates are poorly constrained (e.g., Horowitz et al., 2007; Paulot et al., 2009; Perring et al., 2009; Lockwood et al., 2010; Fiore et al., 2011; Paulot et al., 2012). This is particularly true for isoprene and other biogenic nitrates that are believed to account for a large fraction of ΣANs. Consequently, the extent to which these molecules act as a sink versus reservoir of NO_x represents a large uncertainty in tropospheric chemistry.

In Chapter 3, I present a framework for understanding how the formation of ΣANs impacts the tropospheric NO_x budget. I focus on conditions of low NO_x and high biogenic volatile organic compound (BVOC) concentrations; conditions characteristic of most continental boundary layers. Using a steady-state model, I show that below 500 pptv of NO_x, the NO_x lifetime is extremely sensitive to ΣAN formation rates and find that even for ΣAN formation

rates that are an order of magnitude smaller than is typical for continental conditions, significant reductions in NO_x lifetime are caused by nitrate forming reactions. I compare the results of the steady-state box model to a 3-D chemical transport model (CTM). This confirms that the concepts illustrated by the simpler model are a useful approximation to predictions provided by the full CTM.

In Chapter 4, I use measurements from the NASA Arctic Research of the Composition of the Troposphere from Aircraft and Satellites (ARCTAS) experiment to test the theory presented in Chapter 3 and as a guide to thinking about the role of ΣANs in the continental NO_x budget. I show that ΣANs account for ~20% of total oxidized nitrogen and that their instantaneous production rate is larger than that of HNO_3. This confirms the primary role of reactions producing ΣANs as a control over the lifetime of NO_x. However, HNO_3 is generally present in larger concentrations than ΣANs indicating that the atmospheric lifetime of ΣANs is shorter than the HNO_3 lifetime. I investigate a range of proposed loss mechanisms that would explain the inferred lifetime of ΣANs, finding two processes that are consistent with the observations: 1) rapid ozonolysis of isoprene nitrates where at least ~35% of the ozonolysis products release NO_x from the carbon backbone and/or 2) hydrolysis of organic nitrates in aerosol waters with HNO_3 as a product. Implications of these ideas for our understanding of NO_x and NO_y budget in remote and rural locations are described.

The ARCTAS measurements presented in Chapter 4 suggest that the formation of monoterpene nitrates is a large NO_x sink. Due at least in part to the numerous uncertainties associated with isoprene chemistry and the dominance of isoprene emissions on the global scale, the formation of monoterpene nitrates has largely been ignored. Monoterpenes, however, are known to be emitted in higher quantities than isoprene from some ecosystems (including the boreal forest) and are widely recognized as important precursors to secondary organic aerosol (SOA). Using the WRF-Chem regional chemical transport model, I investigate the impact of monoterpene nitrates on the NO_x budget of the boreal forest in Chapter 5 and find that monoterpene nitrates may equal the importance of HNO_3 as a NO_x sink in this environment. I also investigate how the NO_x budget responds to changes in the formation and fate of monoterpene nitrates and find changes in OH, O_3, and ΣPNs that are large enough that the chemistry of monoterpenes cannot be ignored without accepting significant errors in the gas phase chemistry.

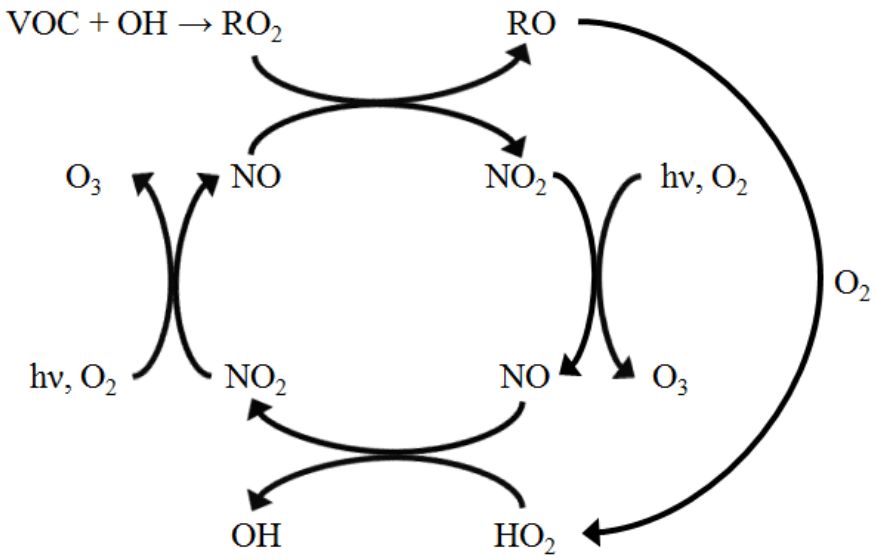

Figure 1.1 Simplified representation of tropospheric NO_x-HO_x (HO_x = OH + HO_2 + RO_2) chemistry.

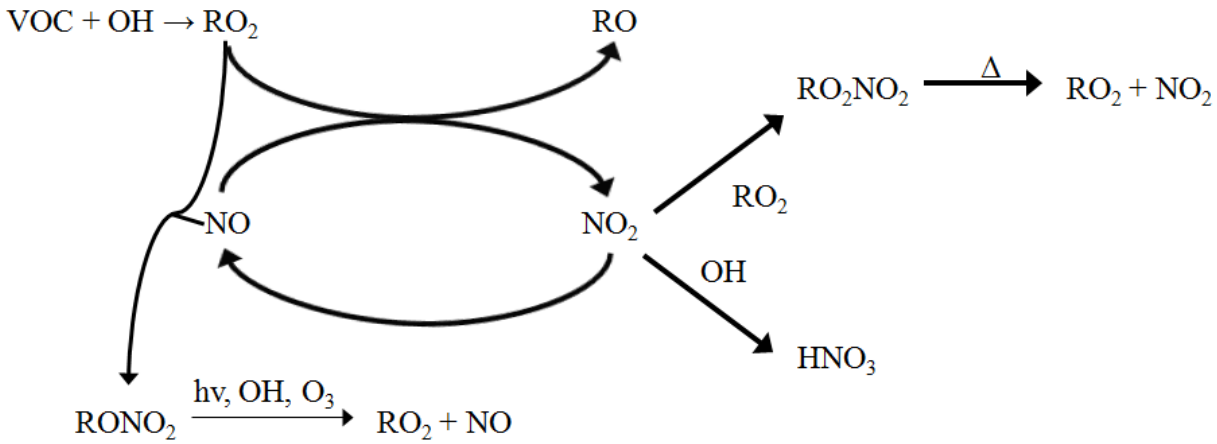

Figure 1.2 NO_x loss processes. HNO_3 serves as a permanent NO_x loss. Peroxy nitrates (RO_2NO_2) are generally considered to be in thermal equilibrium with their precursors. Some fraction of non-peroxy nitrates ($RONO_2$) serve as permanent sinks of NO_x while the remainder are oxidized or photolyzed to release NO_x.

Chapter 2

Global and regional effects of the photochemistry of $CH_3O_2NO_2$: Evidence from ARCTAS

2.1 Introduction

Non-acyl peroxynitrates (e.g. HO_2NO_2, $CH_3O_2NO_2$) are weakly bound molecules that play a role in the chemistry of the troposphere where it is cold (Slusher et al., 2002; Murphy et al., 2004; Kim et al., 2007) or where peroxy radicals and NO_x (NO_x =NO+NO_2) have especially high concentrations (Spencer et al., 2009). Initial observations and calculations focused on understanding the role these molecules play in the stratospheric HO_x (HO_x =OH+HO_2) balance (e.g., Wennberg et al., 1999). More recently, in-situ observations of non-acyl peroxynitrates in the troposphere (Slusher et al., 2002; Murphy et al., 2004; Kim et al., 2007; Spencer et al., 2009) have resulted in increased interest in the role of these compounds in NO_x and HO_x budgets in the lower troposphere. During the NCAR Tropospheric Ozone Production about the Spring Equinox (TOPSE) experiment (Atlas et al., 2003), measurements in the Arctic upper troposphere, where temperatures were on average ~230 K, showed that non-acyl peroxy nitrates, primarily HO_2NO_2, were, on average, 30% of NO_y (NO_y =NO + NO_2 + HO_2NO_2 + $CH_3O_2NO_2$ + HNO_3 + HONO + acyl peroxy nitrates + organic nitrates + NO_3 + 2×N_2O_5) (Murphy et al., 2004). These observations imply that HO_2NO_2 represents a significant sink of HO_x and acts as a large reservoir of NO_x in the Arctic during winter and spring. Measurements from the NASA Intercontinental Chemical Transport Experiment- North America (INTEX-NA) demonstrated that HO_2NO_2 is present in the mid-latitude upper troposphere at mixing ratios of approximately 76 pptv between 8 km and 9 km, accounting for about 5% of NO_y and 10% of the local HO_x sink (Kim et al., 2007).

HO_2NO_2 is formed by the association reaction of HO_2 and NO_2 and methyl peroxy nitrate ($CH_3O_2NO_2$) is formed by the analogous association reaction of CH_3O_2 with NO_2. Although CH_3O_2 is the second most abundant peroxy radical in the atmosphere (after HO_2), much less attention has been devoted to $CH_3O_2NO_2$ chemistry. To my knowledge the indirect measurement of the sum of HO_2NO_2 and $CH_3O_2NO_2$ during the TOPSE campaign by Murphy et al. (2004) is the only previous in-situ evidence for $CH_3O_2NO_2$. $CH_3O_2NO_2$ chemistry has been previously considered in some box and one dimensional models. Thompson et al. (1997) used a 1-D tropospheric chemical model and upper tropospheric measurements from the Pacific Exploratory Mission in the Western Pacific Ocean (PEM-West B) and predicted a mean concentration of 27 pptv for $CH_3O_2NO_2$ at 10 km in the mid-latitudes (35^o–45^o N) during February and March. During TOPSE, a steady-state model indicated that at temperatures around 250K $CH_3O_2NO_2$ should be present at average concentrations of 70 pptv (at 40^o–60^o N) and 27 pptv (at 60^o– 85^o N) (Cantrell et al., 2003b). Here, I present experimental evidence from observations during the Arctic Research of the Composition of the Troposphere from Aircraft and Satellites (ARCTAS) experiment for the presence of $CH_3O_2NO_2$. I use the GEOS-Chem (Bey et al., 2001) 3-D chemical transport model to investigate the effects of $CH_3O_2NO_2$ chemistry on the distribution of NO_x, O_3, NO_y, and HO_y (HO_y =OH + HO_2 +HONO+HO_2NO_2 +CH_3OOH+ 2×H_2O_2) species. I

find that at temperatures below 240 K, the addition of $CH_3O_2NO_2$ chemistry to GEOS-Chem decreases regional concentrations of NO_x by 20% and of O_3 by 2 %. Additionally, concentrations of N_2O_5 decrease by ~20% and methyl hydrogen peroxide concentrations increase by ~14 %.

2.2 Measurements

The ARCTAS measurement campaign has been described in detail by Jacob et al. (2010). Here I focus on the spring portion of ARCTAS (ARCTAS-A) that took place 1–19 April 2008. ARCTAS-A consisted of two transit flights between Palmdale, CA and Fairbanks, Alaska (65^o N, 148^o W) and seven arctic flights. The arctic flights included three local flights as well as flights to and from Thule, Greenland (77^o N, 69^o W) and Iqaluit, Nunavut (64^o N, 69^o W). In this analysis I only consider data collected north of 55^o N. The payload of the DC-8 consisted of an extensive suite of gas phase and aerosol measurements (Jacob et al., 2010). I use the measurements listed in Table 2.1. All data are available in a public archive (http://www-air.larc.nasa.gov/cgi-bin/arcstat-c). Although OH and HO_2 were measured both by the NCAR chemical ionization mass spectrometer (Cantrell et al., 2003a) and the Pennsylvania State laser induced fluorescence (LIF) techniques (Faloona et al., 2004), I use the LIF OH and HO_2 measurements in the model due to the more extensive coverage at high altitudes.
The core measurements for this analysis are from the UC Berkeley nitrogen oxides instrument. Briefly, total peroxy nitrates (ΣPNs), total alkyl and multifunctional nitrates (ΣANs), and NO_2 were measured using the Thermal Dissociation-Laser Induced Fluorescence (TD-LIF) instrument described in detail by Wooldridge et al. (2010). NO_2 is measured using laser induced fluorescence (Thornton et al., 2000) with supersonic expansion (Cleary et al., 2002). A 7 kHz, Q-switched, frequency doubled Nd:YAG laser pumps a tunable dye laser utilizing a mixture of pyrromethene 597 in isopropanol. This produces narrowband radiation (0.06 cm^{-1}) at 585 nm. The laser light is focused through two multipass white cells and the red-shifted fluorescence (wavelengths long of 700 nm) is detected using a red sensitive photomultiplier tube (Hamamatsu H7421-50). Prompt scatter is eliminated using time gated detection and scattered light with wavelengths less than 700 nm is rejected by bandpass filters. Fluorescence counts are collected at 4 Hz and averaged to one second for reporting to the data archive. The dye laser is tuned on and off an isolated rovibronic feature of the jet-cooled NO_2 at 585 nm. The frequency is held at the peak of the feature for 9 s and then moved to the offline position in the continuum absorption of NO_2 for 3 s. The difference between these two signals is directly proportional to the NO_2 mixing ratio. The ratio between the peak and background NO_2 fluorescence is 10 to 1 at 760 Torr backing pressure behind the expansion nozzle. The detection cells are kept at a pressure of approximately 0.2 torr. Calibration is performed at least every two hours during a level flight leg using a 4.5 ppm NO_2 reference standard diluted to ~2–8 ppbv in zero air. Stability of the NO_2 reference is verified by comparing a library of 6–8 different NO_2 standards approximately twice a year. These standards have been observed to remain stable for up to 5 years and to be accurate at atmospherically relevant mixing ratios to within 1% (Bertram et al., 2005a). As described in Thornton et al. (2000), correction for fluorescence quenching by water is made using the diode laser hygrometer measurements (Sachse et al., 1987; Diskin et al., 2002).

The configuration of the instrument for ARCTAS consisted of two detection cells. Sample flow was directed through a short (18 cm) inlet heated to approximately 25 ^{o}C and then split into two sampling lines. Two-thirds of the flow is directed down 154.5 cm of Teflon PFA

(perfluoroalkoxy) tubing at cabin temperature before splitting in two. Half of this flow is directed to detection cell 1 for ambient NO_2 measurement. The other half is heated in a quartz tube at 200 ^oC to thermally dissociate peroxy nitrates and then passes through PFA tubing to detection cell 2. The remaining third of the sample flow is passed directly into a heated quartz tube (375 ^oC) followed by PFA tubing for ΣANs detection in detection cell 2. NO_2 was measured continuously in cell 1 while cell 2 alternately sampled the NO_2 + ΣPNs signal (50% of the time) and the NO_2 + ΣPNs + ΣANs signal (50% of the time).

During ARCTAS, NO_2 was also measured by photolytic conversion to NO with detection via chemiluminescence from the reaction of NO and ozone (Weinheimer et al., 1994). For the one minute merged data (version 11) the measurements agree within the stated uncertainties. A linear least squares non-weighted fit (as in Cantrell (2008)) of the chemiluminescence data versus the LIF data resulted in a slope of 0.95±0.01 with an intercept of −8.1±0.8 pptv and an R^2 value of 0.95.

2.3 Observational evidence of $CH_3O_2NO_2$

Methyl peroxy nitrate is weakly bound (~95 kJ mol^{-1}) and calculations (performed after ARCTAS was completed) suggest that it dissociates with high efficiency in the inlet lines of the TD-LIF instrument after which it is detected in the NO_2 channel. The interference from $CH_3O_2NO_2$ is expected to affect both the LIF and chemiluminescence NO_2 measurements. It is likely that past measurements of NO_2 in the upper troposphere and arctic are subject to this interference from $CH_3O_2NO_2$. This may explain discrepancies between observed and modeled upper tropospheric NO_2 in past experiments (e.g., Crawford et al., 1996). Additionally, it is consistent with the improvement between upper tropospheric measured and modeled NO_2 observed by Bradshaw et al. (1999) between the 1991 PEM-West-A experiment and 1996 PEM-Tropics-A experiment when the inlet was redesigned to decrease the residence time to 40 ms (from 2 s). Here I focus on $CH_3O_2NO_2$ and its behavior in the LIF instrument as it was configured during ARCTAS. In what follows I refer to this measurement as XNO_2 to indicate that it is a measurement of the sum of NO_2 and a fraction of these thermally labile nitrogen compounds.

Given a 300 K cabin temperature (approximate mean cabin temperature during ARCTAS) and a pressure of 300 torr, the thermal decomposition lifetime of $CH_3O_2NO_2$ is 700 ms, while that of HO_2NO_2 is 17.9 s. Although the residence time of an ambient sample in the detection system is quite short (~350–850ms), I calculate that between 48 and 77% of $CH_3O_2NO_2$ and 3 to 6% of HO_2NO_2 thermally dissociate prior to reaching the NO_2 detection cell. HO_2NO_2 dissociation is minimal and results in a median calculated NO_2 interference of less than 1 ppt (6% of the XNO_2 signal) and a maximum absolute interference during a 1 minute period of 10.3 ppt (19% of the NO_2 signal). This molecule is detected with near unit efficiency in the ΣPNs channel as described previously (Murphy et al., 2004; Wooldridge et al., 2010).

The ambient $CH_3O_2NO_2$ concentration is calculated using an instantaneous photostationary state model subject to the constraint that the sum of the model NO_2 and the fractions of HO_2NO_2 and $CH_3O_2NO_2$ that dissociate in the LIF inlet are equal to the LIF measurement of XNO_2. I used measured concentrations of HO_2NO_2 to calculate the contribution of HO_2NO_2 to the XNO_2 measurement. Since the validity of the photostationary state assumption requires that the source and sink reactions of a molecule vary slowly in comparison to the

lifetime of that molecule, I perform this calculation only when the lifetime of $CH_3O_2NO_2$ is less than 12 h, or there is greater than 20 h of sunlight per day as in Murphy et al. (2004). Additionally, I filter the data to exclude locations where tropospheric composition has been recently perturbed. These include times when the DC-8 sampled fresh NO_x emissions (defined as $NO_x/NO_y > 0.2$ and when NO was more than ±3 standard deviations of the median value within ±0.5 km altitude), ozone depletion events ($O_3 < 20$ ppb), stratospheric influences (defined as $O_3/CO > 0.75$), and solar zenith angle greater than 85 degrees. These restrictions exclude measurements from the coldest temperatures/highest altitudes sampled during ARCTAS: conditions under which high concentrations of $CH_3O_2NO_2$ are expected.

The reactions included in the photostationary state calculation are shown in Table 2.2. All measured values are from the archived one minute merged data, version 11. In addition to the XNO_2 measurement, concentrations of species listed in Table 2.1 were used to constrain the model. The use of the measured OH and HO_2 concentrations enables us to exclude HO_x source reactions from the photostationary state model. As the IUPAC recommended UV cross sections for $CH_3O_2NO_2$ (Atkinson et al., 2006) are identical to HO_2NO_2 (Atkinson et al., 2004), I set the UV photolysis of $CH_3O_2NO_2$ equal to the measured UV photolysis rate of HO_2NO_2. I do not consider infrared overtone photolysis of $CH_3O_2NO_2$ due to the shorter thermal decomposition lifetime of $CH_3O_2NO_2$ and the lower expected cross section of C-H overtones (Nizkorodov et al., 2005; Vaida, 2009). The model is run to steady state concentrations (±0.001 %) for peroxyacetyl radical, methyl peroxy radical, and $CH_3O_2NO_2$. I do not attempt to fill in missing data points from any of the measured species and calculate concentrations for the 480 one minute averaged data points that meet the selection criteria.

Uncertainties in the model calculations of NO_2 and $CH_3O_2NO_2$ will be a combination of systematic and random uncertainties in the measured concentrations and systematic uncertainties in the photolysis rates, the rate constants, and the estimated residence time in the instrument prior to detection. Uncertainties in the rate constants for $CH_3O_2NO_2$ formation and dissociation and in the instrument residence time will have the largest systematic effect on the results. In the calculation I use the JPL-2006 (Sander et al., 2006) rate recommendations for $CH_3O_2NO_2$ reactions. This recommendation is based on the recent work of Golden (2005), who has re-evaluated the data for formation and dissociation of $CH_3O_2NO_2$. This re-evaluation includes the new measurements of the association reaction of CH_3O_2 and NO_2 by Bacak et al. (2006). The measurement of Bacak et al. (2006) at 223 K represents the first measurements of the rate constant below 253 K, thus significantly reducing the uncertainty in this reaction at low temperatures. Adjusting the uncertainties to the JPL-2006 one sigma values for the rate constants of formation and decomposition of $CH_3O_2NO_2$ results in changes to the calculated NO_2 values of ~±23% (~1.2 ppt) and of ∓40% (~2.3 ppt) for $CH_3O_2NO_2$ in the temperature range of 230–235 K. This range of NO_2 concentrations is within the uncertainty of a simpler calculation of steady state NO_2 using only the measured NO_2 photolysis rate and the NO, ozone, and HO_2 concentrations.

The residence time in the UC Berkeley LIF was determined in the laboratory after ARCTAS was completed by varying inlet and outlet pressures to simulate aircraft conditions while measuring the flows. Due to the difficulties in simulating aircraft conditions in the lab, I assign an uncertainty of ±25% to the residence time. An increase of 25% in the residence time leads to decreases of approximately 10% in both NO_2 and $CH_3O_2NO_2$ concentrations at 230–235 K. A decrease in residence time of 25% results in ~10% increases of NO_2 and $CH_3O_2NO_2$ in the

same temperature range. A decrease in residence time results in an increase in both NO_2 and $CH_3O_2NO_2$ because the decreased residence time results in smaller fractions of $CH_3O_2NO_2$ and HO_2NO_2 that dissociate in the inlet. Since the sum of dissociated $CH_3O_2NO_2$, dissociated HO_2NO_2, and calculated NO_2 is forced to equal the measured XNO_2, the decrease in the fractions of $CH_3O_2NO_2$ and HO_2NO_2 that dissociate results in a larger concentration of NO_2 and thus a higher calculated steady state $CH_3O_2NO_2$.

The concentrations of $CH_3O_2NO_2$ calculated by the photostationary state model and constrained by the XNO_2 observations reach values of up to ~5–15 pptv in the coldest conditions sampled during ARCTAS (Fig. 2.1). It is probable that larger concentrations of $CH_3O_2NO_2$ were present during ARCTAS in conditions under which the photostationary state assumption fails. Under these conditions, the median $CH_3O_2NO_2$ mixing ratio is ~1.6 times larger than that of NO_2. As shown in Fig. 2.2, at temperatures below 240 K, $CH_3O_2NO_2$ ranges from ~27–43% of XNO_2 while thermal dissociation of HO_2NO_2 contributes ~11–14 %. The resulting NO_2 shows improved agreement with NO_2 predicted from measured NO, HO_2, and NO_2 photolysis values at temperatures ~245K and below (not shown). Since $CH_3O_2NO_2$ is approximately equal to NO_2 at temperatures below 240 K, it serves as an important NO_x reservoir that will release NO_x when the air mass warms, potentially doubling the NO_2 concentration. This source of CH_3O_2 and NO_2 radicals will increase ozone production and affect NO_x and HO_x chemistry. In order to investigate this more completely, I added $CH_3O_2NO_2$ chemistry to the global 3-D chemical transport model GEOS-Chem.

2.4 Global 3-D CTM results

The GEOS-Chem model (version 08-02-02) was run at 2×2.5 degree resolution. The standard chemistry in the model is described in detail in Mao et al. (2010). Two separate runs were conducted: one with $CH_3O_2NO_2$ reactions added to the standard chemistry (hereinafter referred to as the methyl peroxy nitrate or MPN case) and one with only the standard chemistry (hereinafter referred to as the base case). The $CH_3O_2NO_2$ reactions consisted of Reactions (R7), (R8) and (R13) from Table 2.2. As in the photostationary state model, photolysis of $CH_3O_2NO_2$ was calculated assuming that the UV cross sections were equal to those of HO_2NO_2 and that IR photolysis of $CH_3O_2NO_2$ resulting from vibrational overtone excitation was negligible.

Both models were run from January–December 2007 to remove memory of the initialization. I analyze output for January–December 2008. Twenty-four hour averaged concentrations are saved for both the first and second half of each month. In this analysis I focus on the resulting changes in tropospheric concentrations to NO_x, ozone, N_2O_5, HO_2NO_2, HNO_3, and methyl hydrogen peroxide. These species are chosen as examples to illustrate that due to the highly coupled, non-linear relationship between NO_x and HO_x, altering NO_x concentrations by including $CH_3O_2NO_2$ chemistry changes: the cycling of NO_x (and thus ozone concentrations), both short (N_2O_5, HO_2NO_2) and long-term (HNO_3) NO_x reservoirs and sinks, and HO_x reservoirs (CH_3OOH). I do not attempt a thorough budget analysis of the changes in all of these species; my goal is to illustrate how changes resulting from inclusion of $CH_3O_2NO_2$ chemistry affect tropospheric composition. Significant changes in tropospheric composition, particularly at cold temperatures, result when $CH_3O_2NO_2$ chemistry is included. I present seasonal mean results for the North American Arctic (defined here as 175°W–35°W and 65° N–85° N) and summertime (June, July, August) results from the tropics (defined here as 180°W–180° E and 20° S–20° N). I

restrict this analysis to the troposphere by only using results in the model's vertical layers below the layer containing the tropopause.

2.4.1 North American Arctic

As shown in Fig. 2.3, the mean value for modeled $CH_3O_2NO_2$ in the coldest conditions (~220 K) during the summertime (June, July, August) in the North American Arctic is ~40 pptv. During winter (December, January, February), concentrations are lower due to decreased production. The spring (March, April, May) concentrations are slightly higher than the concentrations inferred from the ARCTAS observations of XNO_2 (Chapter 2.3). It is expected that part of this discrepancy is due to exclusion of non-photostationary state conditions from the ARCTAS observations. $CH_3O_2NO_2$ acts as a NO_x reservoir and including it in the GEOS-Chem model results in ~14–23% less NO_x (~12 pptv in the summer) (Fig. 2.4a) as compared to the base case. As a result, in the summer, when photochemistry is most active, ozone is reduced by 1.2% (1.3 ppbv) (Fig. 2.4b). In the winter, ozone is reduced by 0.6% (0.5 ppbv). Although NO_y concentrations remain unchanged, substantial differences in the partitioning of NO_y is observed. At the coldest temperatures N_2O_5 concentrations are reduced by ~10–20% (~0.2 pptv) (Fig. 2.4c) due to sequestration of NO_2 by $CH_3O_2NO_2$. At temperatures above ~230–240 K, $CH_3O_2NO_2$ causes increases in N_2O_5 of up to 20% in the fall (September, October, November) and 30% in winter. Increases in HO_2NO_2 concentrations are also seen in the fall and winter (Fig. 2.4d). These increases result from an increase in chemical production of N_2O_5 and HO_2NO_2 in the MPN case relative to the base case. The increase in chemical production is due to increased NO_2 concentrations (at 240 K NO_2 is 20% larger in the winter and 16% larger in fall). This increase in NO_2 is presumably due to thermal dissociation of $CH_3O_2NO_2$. It should be noted that although these are large relative changes, they represent absolute changes of generally less than 1 pptv.

By sequestering NO_x, $CH_3O_2NO_2$ reduces NO concentrations resulting in a decreased conversion of HO_2 to OH. Consequently, OH concentrations are lower (not shown). These reductions in NO_x and OH by $CH_3O_2NO_2$ chemistry result in up to 4% less HNO_3 (~6 pptv) in the winter and 5.5% less HNO_3 (~15 pptv) in the summer (Fig. 2.4e). The HO_y species methyl hydrogen peroxide shows increases up to 14% (~3 pptv) at ~220K in the summertime (Fig. 2.4f). Smaller increases occur at other times of the year. The changes in methyl hydrogen peroxide concentrations are due to increases in chemical production (resulting from higher HO_2 concentrations), increases in lifetime due to the lower OH concentrations, and changes in the concentrations transported into the region. At 220 K, chemical production is increased ~4% in the MPN case relative to the base case in the spring and in the summer it is increased by ~10 %. The lifetime of methyl hydrogen peroxide in the MPN case relative to the base case increases by ~6% in the spring and ~9% in the summer.

2.4.2 Tropics

Although overall results from the tropics are similar to the results in the North American Arctic there are two distinct differences. First, temperatures in the upper troposphere of the tropics are lower than in the mid latitudes and polar regions due to the higher tropopause. Consequently, $CH_3O_2NO_2$ concentrations peak at temperatures of ~215K and decrease at lower temperatures (Fig. 2.5) as do the differences between the base and MPN cases (Figs. 2.6 and

2.7). The decrease occurs because of a reduction in CH_3O_2 formation due to the slower rate of OH+CH_4 at colder temperatures. The second important difference from the North American Arctic is the presence of large modeled spikes in $CH_3O_2NO_2$ concentrations (and the resulting large spikes in differences between the base and MPN cases) on the otherwise smooth curve that has the temperature dependence of $CH_3O_2NO_2$ chemistry. These spikes are due to elevated concentrations of $CH_3O_2NO_2$ downwind of biomass burning events as confirmed by large concentrations of peroxyacetyl nitrate and CO in these plumes (not shown). These spikes appear at regular intervals due to the decreased vertical resolution of the model in the upper troposphere. Each group of points are the results from a different vertical level of the model. In these particular biomass burning events, $CH_3O_2NO_2$ chemistry results in maximum changes of ~20-40% (25–70 pptv) less NO_x (Fig. 2.6a), ~2–4% (1.5–2.6 ppbv) less ozone (Fig. 2.6b), ~20–35% (0.7–1.2 pptv) less N_2O_5 (Fig. 2.6c), ~7–20% (1.5–6 pptv) less HO_2NO_2 (Fig. 2.6d), ~7–14% (15–40 pptv) less HNO_3 (Fig. 2.6e), and ~30–75% (20–60 pptv) more methyl hydrogen peroxide (Fig. 2.6f) as compared to the base case. As in the arctic, changes in methyl hydrogen peroxide are due to a combination of increased chemical production and increased lifetime in the MPN case compared to the base case. In the biomass burning plumes chemical production is up to ~90% faster in the MPN case and the lifetime is~29% longer. Additionally, the MPN case has approximately 14– 28% less OH (Fig. 2.7a) and 10–25% more HO_2 (Fig. 2.7b) in these plumes than in the base case.

2.5 Implications

Through sequestration of NO_x, $CH_3O_2NO_2$ will directly affect the NO_x budget of the upper troposphere. Since lightning emits NO_x directly into the upper troposphere, these emissions will result in proportionally more $CH_3O_2NO_2$ production than surface NO_x sources. Recently, several studies have attempted to constrain the lightning NO_x source by varying emissions in models and using top-down constraints from aircraft (e.g., Hudman et al., 2007) or satellite (e.g., Martin et al., 2007) measurements. It is possible that inclusion of $CH_3O_2NO_2$ chemistry will necessitate an increase in these lightning NO_x estimates; however this effect will be sensitive to the altitude of lightning NO_x emissions. Over the tropics the $CH_3O_2NO_2$ to NO_x ratio peaks at ~30% between 11 and 12 km altitude and then decreases to ~15% by ~9.9 km and ~14 km. Consequently, calculations of lightning NO_x emitted between 11 and 12 km will be most strongly affected by $CH_3O_2NO_2$ chemistry.

The decrease in upper tropospheric NO_x from inclusion of $CH_3O_2NO_2$ results in increases in HO_2 and decreases in OH in the upper troposphere, thus increasing the HO_2 to OH ratio. During the Intercontinental Chemical Transport Experiment-A (INTEX-A) Ren et al. (2008) found that the observed HO_2/OH ratio was larger than box-model predictions in the upper troposphere. Although the box model used in Ren et al. (2008) contains $CH_3O_2NO_2$ chemistry, it was constrained to measured NO_2 concentrations. It is likely that these concentrations are measurements of XNO_2. I expect that the difference in the box model results constrained to XNO_2 versus the results constrained to NO_2 would be qualitatively similar to the changes observed between the base case and MPN case GEOS-Chem runs. The magnitude of the change in HO_2 between the MPN and base case runs is significantly smaller than the measurement-model differences observed during INTEX-A by Ren et al. (2008). I conclude that $CH_3O_2NO_2$ interference in the NO_2 measurement during INTEX-NA may be responsible for part of the

difference between measured and modeled HO_x and NO_x during INTEX-NA, but there are still unexplained measurement-model discrepancies.

It is also interesting to note that because both the reaction with OH and IR photolysis are negligible loss process for $CH_3O_2NO_2$, $CH_3O_2NO_2$ has a longer lifetime than HO_2NO_2 at temperatures below ~225 K (symbols in Fig. 2.8) under daytime conditions. Therefore, in the coldest conditions of the upper troposphere during the day, $CH_3O_2NO_2$ is a more effective reservoir of NO_x and HO_x than HO_2NO_2. However, at night the lifetimes of $CH_3O_2NO_2$ and HO_2NO_2 will be controlled only by thermal decomposition (lines in Fig. 2.8) and $CH_3O_2NO_2$ will have a much shorter lifetime. For instance, assuming nine hours of darkness at 225 K, 40% of $CH_3O_2NO_2$ will decompose, releasing CH_3O_2 and NO_2, whereas HO_2NO_2 will remain intact. Thus, these two species will have different diurnal effects on the radical concentrations.

By using reduced pressures, shorter residence times (e.g. Bradshaw et al., 1999), or some combination thereof, it is possible for future inlet designs for upper tropospheric NO2 measurements to minimize the interference of $CH_3O_2NO_2$. In the TD-LIF system this would enable detection of $CH_3O_2NO_2$ solely in the peroxy nitrates channel. Although TD-LIF provides the sum measurement of all peroxy nitrate species, an indirect measurement of $CH_3O_2NO_2$ would be possible using the difference between the TD-LIF signal and speciated peroxy acetyl nitrates and pernitric acid measurements.

2.6 Conclusions

Measurements from ARCTAS indicate that the thermally unstable $CH_3O_2NO_2$ dissociates in the inlet of NO_2 instruments resulting in upper tropospheric measurements of NO_2 that are better described as thermally labile nitrogen (XNO_2). Using the measurements of XNO_2 during ARCTAS I show that in the coldest conditions sampled, $CH_3O_2NO_2$ is present at concentrations approximately equal to or greater than NO_2. Inclusion of $CH_3O_2NO_2$ chemistry in the GEOS-Chem model results in changes in concentrations of NO_x and HO_x and their reservoirs (such as N_2O_5, HNO_3, and methyl hydrogen peroxide). The magnitude of the changes vary by season and region, however the results indicate that the addition of $CH_3O_2NO_2$ chemistry to GEOS-Chem results in significant changes whenever the temperature is below 240 K. These changes affect the calculated production and loss rates of NO_x and HO_x, the upper tropospheric HO_2 to OH ratio and the spatial distribution of NO_x and HO_x reservoirs. As shown by the results from the North American Arctic, addition of $CH_3O_2NO_2$ chemistry to models results in changes to the seasonal cycles of NO_y and HO_y species, particularly in the increase in N_2O_5 and HO_2NO_2 between 230 K and 260 K. The results from the tropics also indicate that $CH_3O_2NO_2$ plays an important role in the evolution of biomass burning plumes that are lofted to high altitudes. By sequestering both CH_3O_2 and NO_2, $CH_3O_2NO_2$ changes the chemical evolution and ozone production potential of these plumes.

Species	Method	Reference
NO, O_3	Chemiluminescence	Weinheimer et al. (1994)
XNO_2	LIF[a]	Thornton et al. (2000); Cleary et al. (2002)
Pernitric acid, peracetic acid, methyl hydrogen peroxide	CIMS[b]	Crounse et al. (2006, 2009); St. Clair et al. (2010)
Acetone	PTR-MS[c]	Wisthaler et al. (2002)
Acetaldehyde	GC-MS[d]	Apel et al. (2003)
Peroxyacetyl nitrate	CIMS[b]	Slusher et al. (2004); Kim et al. (2007)
CH_4	TDLAS[e]	Sachse et al. (1987); Diskin et al. (2002)
OH,HO_2	LIF[a]	Faloona et al. (2004)
	CIMS[b]	Cantrell et al. (2003a)
UV photolytic frequencies	Spectral radiometry	Shetter and Müller (1999)

[a]Laser Induced Fluorescence [b]Chemical ionization mass spectrometry [c]Proton transfer reaction mass spectrometry [d]Gas chromatography - mass spectrometry [e]Tunable diode laser absorption spectroscopy

Table 2.1 Measurements used in this analysis to constrain the photostationary state model. XNO_2 refers to the sum of NO_2 and the NO_2 from the partial thermal dissociation of $CH_3O_2NO_2$ and HO_2NO_2 in the inlet of the LIF instrument.

	Reaction	Rate Constant
1	$CH_4 + OH + O_2 \rightarrow CH_3O_2 + H_2O$	$2.45 \times 10^{-12} \times \exp(-1775/T)$ [a]
2	$CH_3C(O)O_2 + NO \rightarrow CH_3O_2 + CO_2 + NO_2$	$8.1 \times 10^{-12} \times \exp(270/T)$ [a]
3	$CH_3C(O)CH_3 + h\nu + 2\ O_2 \rightarrow CH_3C(O)O_2 + CH_3O_2$	Measured
4	$CH_3C(O)O_2 + CH_3C(O)O_2 + 2\ O_2 \rightarrow 2\ CH_3O_2 + 2\ CO_2 + O_2$	$2.9 \times 10^{-12} \times \exp(500/T)$ [a]
5	$CH_3OOH + OH \xrightarrow{70\%} CH_3O_2 + H_2O$	$3.8 \times 10^{-12} \times \exp(200/T)$ [a]
6	$CH_3C(O)H + h\nu + O_2 \rightarrow CH_3O_2 + HCO$	Measured
7	$CH_3O_2NO_2 + h\nu \rightarrow CH_3O_2 + NO_2$	Assumed to be equal to measured HO_2NO_2 value
8	$CH_3O_2NO_2 + h\nu \rightarrow CH_3O + NO_3$	Assumed to be equal to measured HO_2NO_2 value
9	$CH_3O_2 + NO \rightarrow CH_3O + NO_2$	$2.8 \times 10^{-12} \times \exp(300/T)$ [a]
10	$CH_3O_2 + HO_2 \rightarrow$ Products	$3.8 \times 10^{-13} \times \exp(780/T)$ [b]
11	$CH_3O_2 + CH_3C(O)O_2 \rightarrow$ Products	$2.0 \times 10^{-12} \times \exp(500/T)$ [a]
12	$CH_3O_2 + CH_3O_2 \rightarrow$ Products	$9.5 \times 10^{-14} \times \exp(390/T)$ [a]
13	$CH_3O_2 + NO_2 + M \leftrightarrow CH_3O_2NO_2 + M$	Low Pressure Limit = $1.0 \times 10^{-30} \times (T/300)^{-4.8}$ High Pressure Limit = $7.2 \times 10^{-12} \times (T/300)^{-2.1}$ Keq = $9.5 \times 10^{-29} \times \exp(11234/T)$ [a]
14	$CH_3C(O)O_2NO_2 + h\nu \rightarrow CH_3C(O)O_2 + NO_2$	Measured
15	$CH_3C(O)O_2NO_2 \leftrightarrow CH_3C(O)O_2 + NO_2$	Low Pressure Limit = $9.7 \times 10^{-29} \times (T/300)^{-5.6}$ High Pressure Limit = $9.3 \times 10^{-12} \times (T/300)^{-1.5}$ Keq = $9.0 \times 10^{-29} \times \exp(14000/T)$ [a]
16	$CH_3C(O)OOH + OH \rightarrow CH_3C(O)O_2 + H_2O$	3.7×10^{-12} [c]
17	$CH_3C(O)H + OH + O_2 \rightarrow CH_3C(O)O_2 + H_2O$	$4.7 \times 10^{-12} \times \exp(345/T)$ [b]
18	$CH_3C(O)O_2 + HO_2 \rightarrow$ Products	$5.2 \times 10^{-13} \times \exp(980/T)$ [b]

[a] JPL 2006 (Sander et al., 2006) [b]Atkinson et al., 2006 (web version last updated 2009 http://www.iupac-kinetic.ch.cam.ac.uk/show_datasheets.php?category=Gas-phase+organics%3A+HOx+%2B+VOC+%28C1-C3%29)
[c]Master Chemical Mechanism v3.1 (Saunders et al., 2003)

Table 2.2 Reactions and rates used in the photostationary state model.

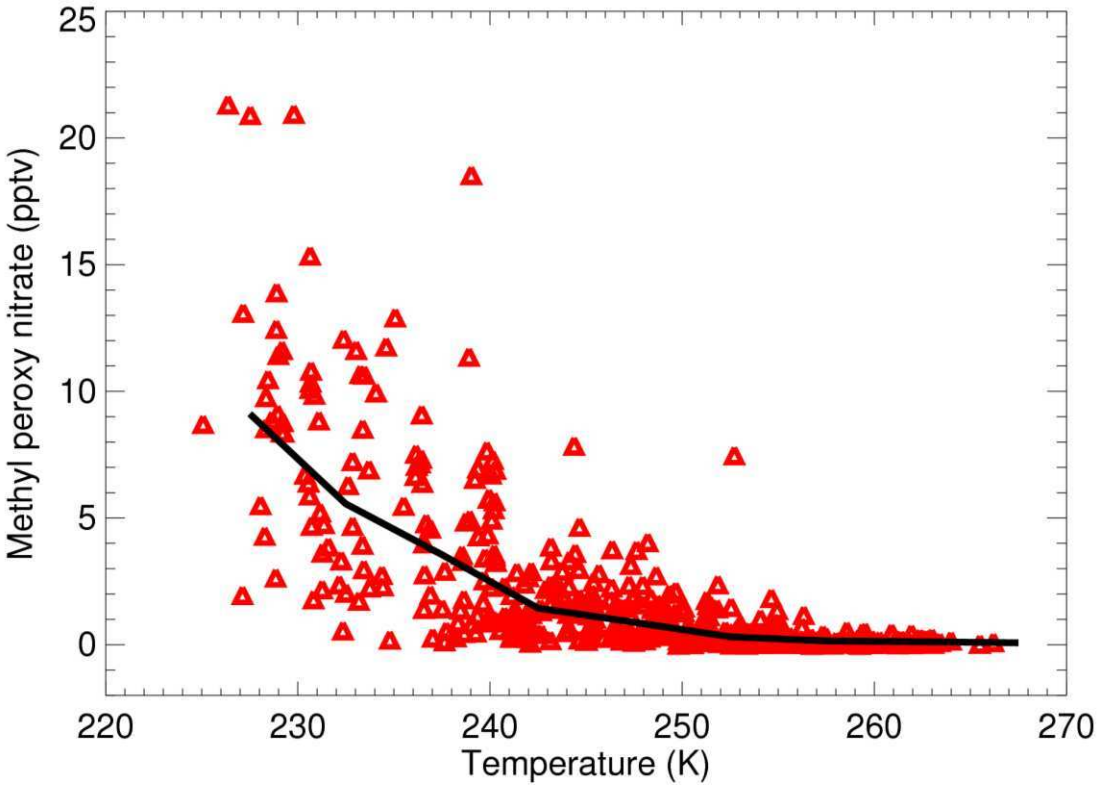

Figure 2.1 Methyl peroxy nitrate concentration inferred from observations. The black line represents temperature binned median values.

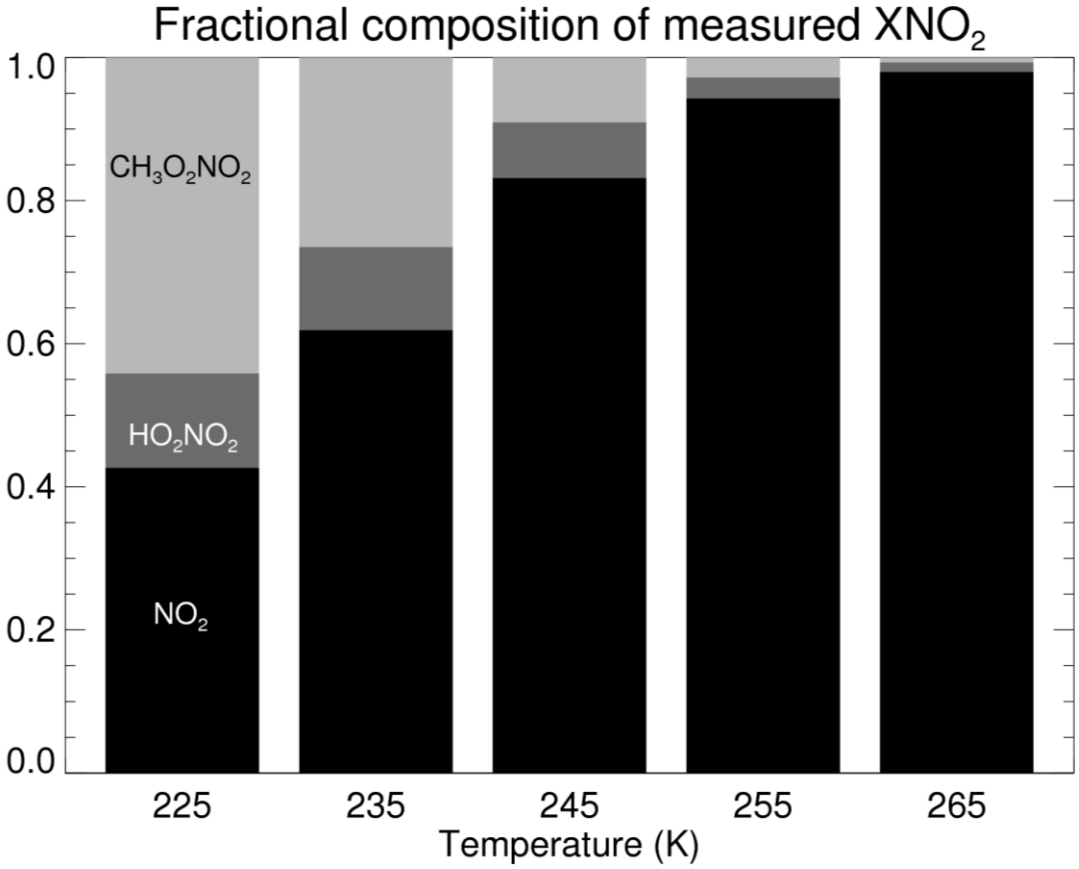

Figure 2.2 Fractional composition of the XNO_2 measured by the UC Berkeley LIF nitrogen oxides instrument calculated using the photostationary state model constrained to total measured XNO_2. We estimate that 48–77% of $CH_3O_2NO_2$ and 3–6% of HO_2NO_2 dissociate in the inlet prior to detection.

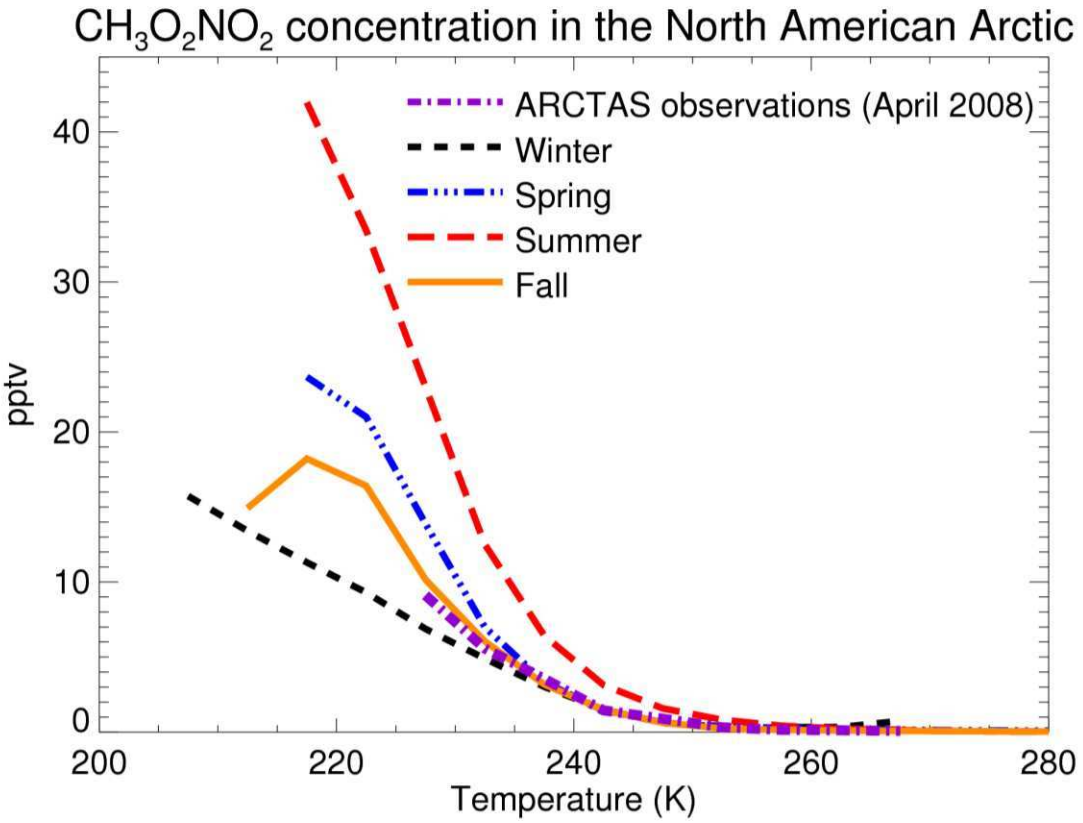

Figure 2.3 Temperature binned mean values of the GEOS-Chem modeled $CH_3O_2NO_2$ 24 h average concentrations over the North American Arctic for each season.

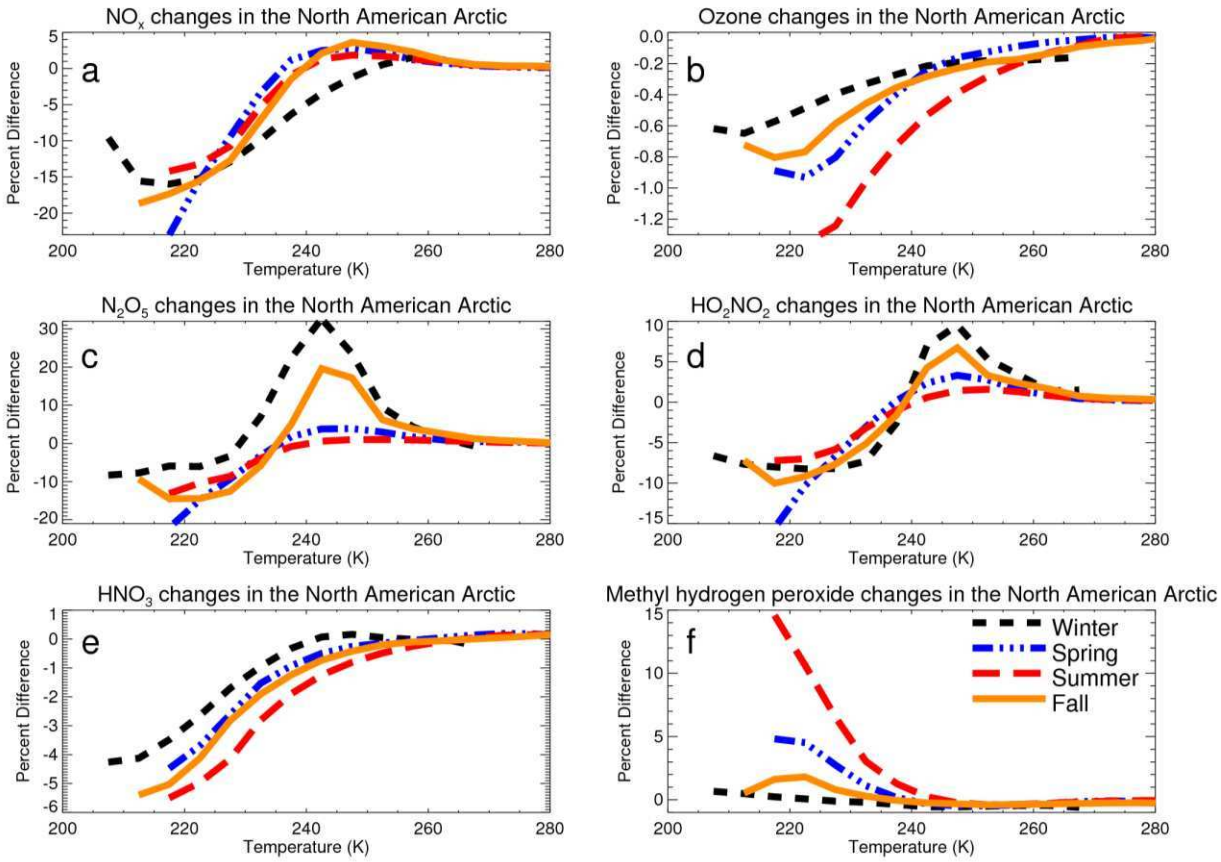

Figure 2.4 Differences between the GEOS-Chem base case and MPN case (((MPN-BASE)/BASE)×100) over the North American Arctic versus temperature for **(a)** NO_x, **(b)** ozone, **(c)** N_2O_5, **(d)** HO_2NO_2, **(e)** HNO_3, and **(f)** methyl hydrogen peroxide. These results are temperature binned means of 24 h averaged concentrations.

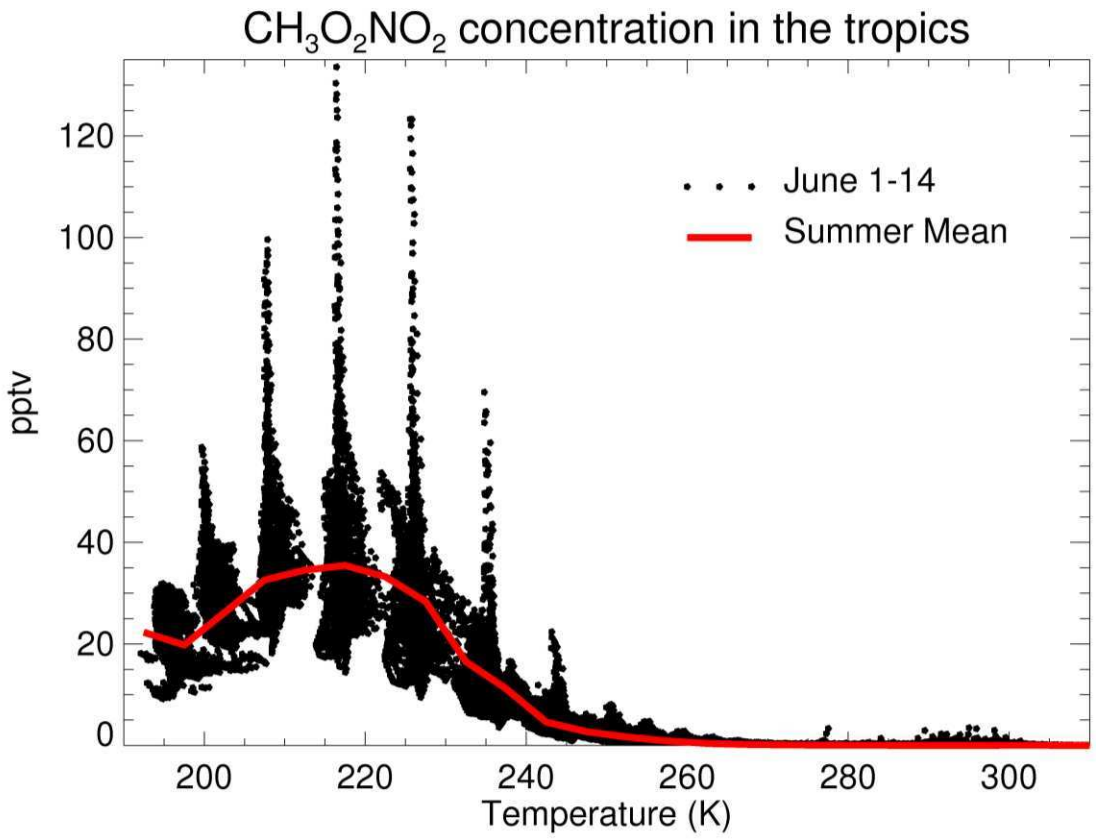

Figure 2.5 Tropospheric concentrations of $CH_3O_2NO_2$ versus temperature over the tropics. The individual points are the 24 h average value of 1–14 June 2008. The red line is the summer mean concentration. The regular temperature intervals at low temperatures are a result of decreasing vertical resolution in the model at increasing altitudes.

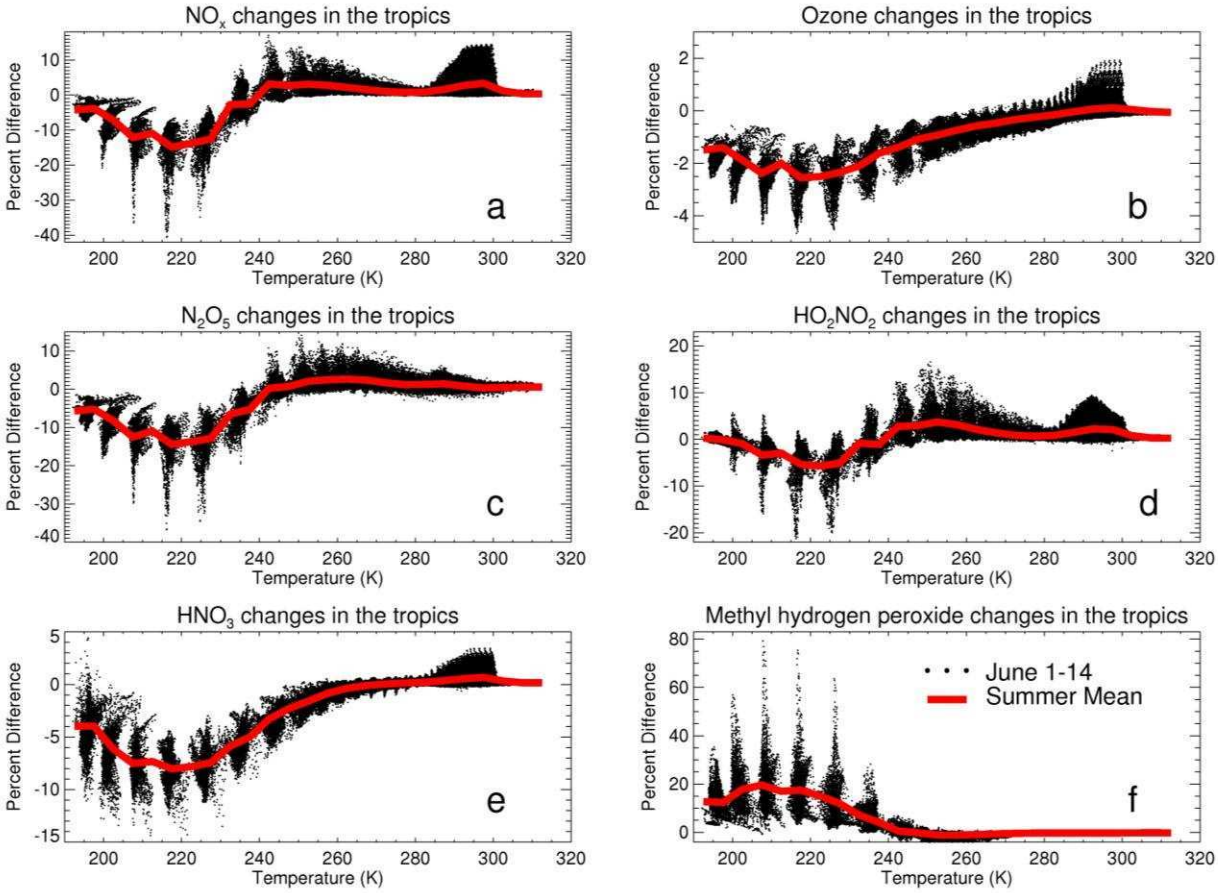

Figure 2.6 Differences between the GEOS-Chem base case and MPN case (((MPN BASE)/BASE)×100) over the tropics versus temperature for **(a)** NO_x, **(b)** ozone, **(c)** N_2O_5, **(d)** HO_2NO_2, **(e)** HNO_3, and **(f)** methyl hydrogen peroxide. The individual points are the 24 h average value of 1–14 June 2008. The red line is the summer mean concentration. The regular temperature intervals at low temperatures are a result of decreasing vertical resolution in the model at increasing altitudes.

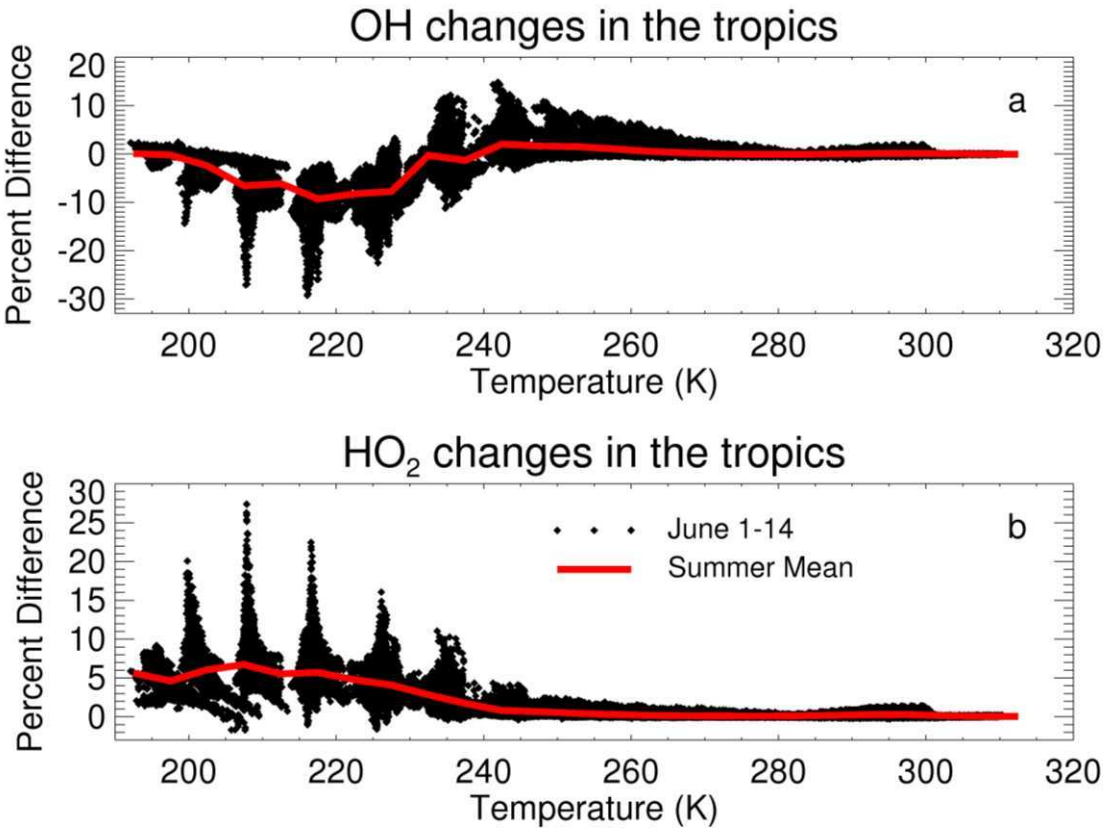

Figure 2.7 Differences between the GEOS-Chem base case and MPN case (((MPN-BASE)/BASE)×100) over the tropics versus temperature for **(a)** OH and **(b)** HO_2. The individual points are the 24 h average value of 1–14 June 2008. The red line is the summer mean concentration. The regular temperature intervals at low temperatures are a result of decreasing vertical resolution in the model at increasing altitudes.

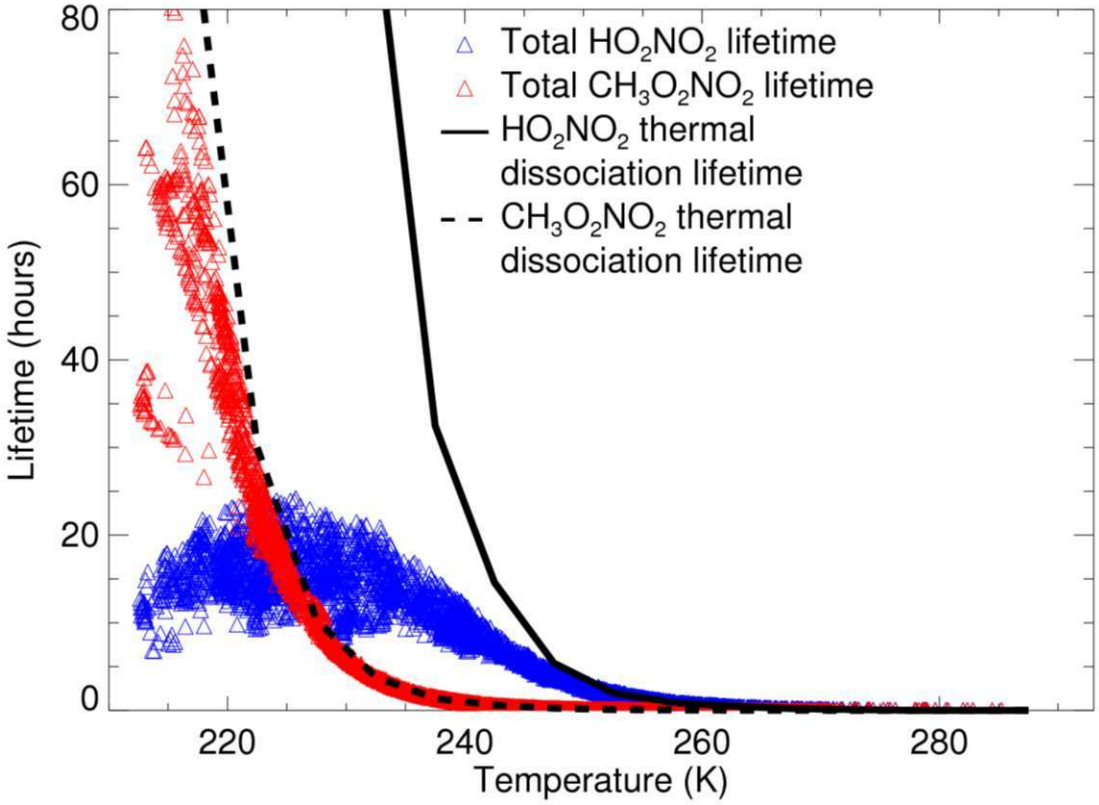

Figure 2.8 Temperature dependence of $CH_3O_2NO_2$ and HO_2NO_2 lifetimes for conditions sampled during ARCTAS. Symbols represent total lifetimes and solid lines are 5 K binned thermal lifetimes. IR photolysis for HO_2NO_2 is estimated as $1\times10{-}5\ s^{-1}$ (~27.8 h).

Chapter 3

Effects of biogenic nitrate chemistry on the NO_x lifetime in remote continental regions

3.1 Introduction

Nitrogen oxides enter the atmosphere as a result of bacterial processes in soils, high temperature chemistry in lightning, and combustion of fossil fuels and biomass. Current estimates are that human creation of reactive nitrogen (both oxidized and reduced nitrogen) has increased by over an order of magnitude from ~15 Tg N yr^{-1} to ~187 Tg N yr^{-1} from 1860 to 2005 (Galloway et al., 2008). This increase is one of the primary causes of air pollution, contributing directly to the production of urban ozone and secondary organic aerosol. The increase in NO_x also results in an increase in the global background of OH and thus affects air pollution by increasing the global background ozone concentration and making it more difficult for individual cities to reduce ozone. This increase in ozone also affects climate directly, and both the NO_x and the ozone affect climate indirectly by their influence on the global lifetime of CH_4 (e.g., Fuglestvedt et al., 1999; Wild et al., 2001; Derwent et al., 2008; Fry et al., 2012). Several studies have shown that the net global impact of NO_x emissions on climate forcing is highly dependent on the location and seasonal cycle of the emissions (e.g., Fuglestvedt et al., 1999; Derwent et al., 2008; Fry et al., 2012). Consequently, there has been a significant research effort to understand emissions of NO_x from different sources such as fossil fuel combustion (e.g., van der A et al., 2008; Dallmann and Harley, 2010; Jaeglé et al., 2005), lightning (e.g., van der A et al., 2008; Hudman et al., 2007; Schumann and Huntrieser, 2007), biomass burning (e.g., van der A et al., 2008; Alvarado et al., 2010; Jaeglé et al., 2005; Mebust et al., 2011; Wiedinmyer et al., 2006), and soils (e.g., van der A et al., 2008; Bertram et al., 2005; Ghude et al., 2010; Hudman et al., 2010; Jaeglé et al., 2005). In contrast, the lifetime of NO_x, knowledge of which is necessary to determine concentrations from emissions, is not as well studied.

In the vicinity of emissions, the lifetime of NO_x is a steeply nonlinear function of the concentration of NO_x (Valin et al., 2011 and references therein). In the remote continental atmosphere, emissions are more uniformly distributed and NO_x concentrations vary more slowly. Textbooks suggest that the chemical lifetime of NO_x in these regions is largely set by its reaction with OH to produce HNO_3. However, several analyses have quantified the effect of isoprene nitrate formation on the NO_x budget, showing that isoprene nitrate formation is a major sink of NO_x and implying a strong effect on NO_x lifetime (e.g., Trainer et al., 1991; Horowitz et al., 2007; Ito et al., 2007; Wu et al., 2007; Paulot et al., 2012).

In this chapter I present a framework for understanding the impact of organic nitrates ($RONO_2$) on the NO_x budget in low NO_x, high BVOC environments. This framework serves as a guide for thinking about how one would expect 3-D chemical transport models to respond to changes in assumptions about $RONO_2$ chemistry and for thinking about measurements of NO_x and $RONO_2$ in environments comprised of different BVOC mixtures. I find that the instantaneous NO_x lifetime, and consequently ozone production efficiency, is extremely sensitive to $RONO_2$ production even when production rates are an order of magnitude smaller than typical

for continental conditions. Calculations using the WRF-Chem model (Weather Research and Forecasting model with chemistry (Grell et al., 2005) with detailed $RONO_2$ chemistry added to the chemical mechanism are shown to be consistent with the conceptual model.

3.2 Background

Daytime chemistry in the lower troposphere encompasses two chemical regimes: a low NO_x ($NO_x = NO + NO_2$) regime in which HO_x ($HO_x = OH+HO_2+RO_2$) self-reactions (e.g., $HO_2 + RO_2$) dominate HO_x loss processes, and a high NO_x regime in which radicals are lost through nitric acid production. Although low NO_x chemistry has generally been synonymous with methane and carbon monoxide chemistry, recent field observations have shown that in the presence of high biogenic volatile organic compound (BVOC) concentrations, low NO_x chemistry is significantly more complex than this textbook view. Most of these recent low NO_x, high BVOC studies have focused on understanding the production and loss processes of HO_x radicals (e.g., Lelieveld et al., 2008; Stavrakou et al., 2010; Stone et al., 2011; Taraborrelli et al., 2012; Whalley et al., 2011; Mao et al., 2012). Here, I focus on understanding the nitrogen radical budget under these conditions.

Chemical loss of NO_x is generally considered to be dominated by nitric acid formation:

$$OH + NO_2 \rightarrow HNO_3 \qquad (R1)$$

Close to source regions, where NO_x concentrations are high, NO_x will also be lost through the formation of peroxy nitrates:

$$RO_2 + NO_2 + M \leftrightarrow ROONO_2 + M \qquad (R2)$$

It is well known that peroxy nitrates act as a NO_x reservoir; they may be transported to rural and remote locations where they will dissociate, resulting in a net source of NO_x downwind from the emissions.

Chemical NO_x loss also occurs via the formation of alkyl and multifunctional organic nitrates of the form $RONO_2$ from the minor branch of the NO and peroxy radical reaction:

$$NO + RO_2 \rightarrow RONO_2 \qquad \alpha \qquad (R3a)$$

$$NO + RO_2 \rightarrow NO_2 + RO \qquad (1-\alpha) \qquad (R3b)$$

Measurements of total $RONO_2$ by thermal dissociation laser induced fluorescence (Day et al., 2002) have shown that $RONO_2$ account for a substantial fraction of oxidized nitrogen (NO_y = $NO + NO_2 + NO_3$ + total peroxy nitrates + total alkyl and multifunctional nitrates + HNO_3 + $2*N_2O_5$ + HONO + …) in urban (Rosen et al., 2004; Cleary et al., 2005; Perring et al., 2010; Farmer et al., 2011) and rural (Murphy et al., 2006; Farmer and Cohen, 2008; Day et al., 2009; Perring et al., 2009a; Beaver et al., 2012) locations as well as downwind of the continents (Perring et al., 2010).

Isoprene nitrates are thought to be a large fraction of the organic nitrate source. Global modeling studies investigating the impact of isoprene-derived nitrates on NO_x and O_3 have found large sensitivities in the net global and regional budgets of O_3 and OH to assumptions about formation, lifetime, and oxidation products of isoprene-derived nitrates (e.g., Horowitz et al., 1998, 2007; von Kuhlmann et al., 2004; Fiore et al., 2005; Ito et al., 2007, 2009; Wu et al., 2007; Paulot et al., 2012). Paulot et al. (2012) used a global CTM to calculate the impact of isoprene-derived nitrates on the NO_x budget in the tropics and found that up to 70% of the local net NO_x sink is from the formation of isoprene-derived nitrates.

Recently, simultaneous field measurements of speciated multifunctional nitrates using chemical ionization mass-spectrometry (St. Clair et al., 2010) and measurements of total $RONO_2$ by thermal dissociation laser induced fluorescence provided the first opportunity for a comparison of the total $RONO_2$ measurement in a complex chemical environment. The sum of the individual compounds was ~65% of the total $RONO_2$ when only isoprene (first and second generation) and 2-methyl-3-buten-2-ol nitrates were included, and was almost closed when all nitrogen containing masses were included. The measurements confirmed that biogenic $RONO_2$ represent the vast majority of the total in a rural environment (Beaver et al., 2012). Recent measurements from the NASA Arctic Research of the Composition of the Troposphere from Aircraft and Satellites (ARCTAS) campaign (Jacob et al., 2010) show that in the low NO_x, high BVOC environment of the Canadian boreal forest, $RONO_2$ account for 20% of NO_y and often account for at least half of the instantaneous NO_x sink (Chapter 4).

3.3 Steady-state calculations

Low NO_x, high BVOC environments, such as boreal and tropical forests, are generally characterized by large expanses of relatively homogeneous emissions. Consequently, even while transport can be long-range, the lifetime of NO_x can be short relative to changes in sources and sinks. Thus, NO_x is expected to be in steady-state where sources are balanced by chemical loss. HO_x radicals have a shorter lifetime and are also expected to be in a steady-state. Using this assumption, I calculate the rate of NO_x loss to $RONO_2$ and to HNO_3 during the day and night. Analysis is restricted to NO_x concentrations less than 500 pptv. Discussion on the effects of $RONO_2$ chemistry at higher NO_x concentrations can be found in Farmer et al. (2011) and are reviewed by Perring et al. (2012).

3.3.1 Daytime

Here, I use a simplified representation of daytime chemistry (Table 3.1) where $P(HO_x)$ represents primary HO_x production from all sources including $O(^1D)+H_2O$, photolysis of species such as H_2O_2 and HCHO, and any others. I assume that 80% of HO_x production results in OH and the remainder in HO_2 (from HCHO photolysis). In addition to CO and CH_4 chemistry, a lumped VOC that reacts with OH to form a lumped peroxy radical (RO_2 in Table 3.1) is included. When this lumped RO_2 species reacts with NO, it either propagates the radicals (R3a) or forms an organic nitrate (R3b). The fraction of the time that an organic nitrate is formed (R3b/(R3a+R3b)) is referred to as the branching ratio (α). For specific molecules, α increases with increasing carbon number, lower temperature, and higher pressure (Arey et al., 2001).

For the other RO_2 reactions, I assume that the RO_2 species behaves like a primary or secondary peroxy radical. Following the MCM protocol, the RO_2+RO_2 reaction then results in 1.2 alkoxy radicals (Jenkin et al., 1997). In the model, the alkoxy radical either instantaneously isomerizes or decomposes (i.e., I ignore the reaction with O_2) to produce a peroxy radical that is lumped with CH_3O_2 (i.e., no formation of organic nitrates upon reaction with NO). The $RO_2+CH_3O_2$ reaction follows the same assumptions resulting in 0.6 CH_3O_2 and 0.6 HO_2. The RO_2 species undergoes an isomerization reaction with products of OH and HO_2. This reduced complexity is designed to mimic the low NO_x chemistry of isoprene (e.g., Peeters et al., 2009; Peeters and Müller, 2010; Crounse et al., 2011, 2012).

For illustrative purposes, I use the mean conditions sampled during ARCTAS at low altitude and removed from recent biomass burning influence (Table 3.2) as inputs to the model. I run the model at specified NO concentrations until the radicals (RO_2, CH_3O_2, HO_2, OH, and NO_2) are in steady-state and then calculate the formation of $RONO_2$ and nitric acid.

Values of α equal to 0%, 0.1%, 1%, 5%, and 10% are used to illustrate a range of conditions that vary from remote conditions removed from the continents (α=0% and α=0.1%) to areas influenced primarily by BVOCs (e.g., monoterpenes, isoprene) with high $RONO_2$ formation (α=5-10%).

It should be noted that the α value in the steady-state model is different from what has been referred to in the literature as the "effective branching ratio" (Rosen et al., 2004; Cleary et al., 2005; Perring et al., 2010; Farmer et al., 2011). The effective branching ratio refers to the average branching ratio of the entire VOC mixture (including CO, CH_4, etc) and is therefore smaller than the branching ratio of the RO_2 species. Observations suggest that the effective branching ratio for VOC mixtures for urban regions ranges from 4-7% (Cleary et al., 2005; Farmer et al., 2011; Perring et al., 2010; Rosen et al., 2004). The effective branching ratio for the situations calculated here ranges from 0.06-8.74% and is dependent on NO_x due to changes in the ratio of CH_3O_2 to RO_2 with NO_x (Table 3.3). Full details regarding the calculation of α_{eff} and discussion of how it varies with NO_x can be found in Appendix A.

3.3.2 Nighttime

Nighttime chemical loss of NO_x occurs via NO_3 reactions with alkenes that have organic nitrate products, heterogeneous hydrolysis of N_2O_5, and reactions of NO_3 with aldehydes. The latter two loss processes both result in the formation of HNO_3. I consider a nighttime VOC mix that consists of three VOCs: isoprene, α-pinene, and acetaldehyde.

The reaction of NO_3 with alkenes results in an NO_3-alkene adduct that either retains or releases the nitrate functionality upon reaction with other radicals. The parameter β is used to represent the fraction that retains the nitrate functionality. Recent measurements of organic $RONO_2$ yields for the reaction of biogenic VOC with NO_3 suggest that β for isoprene is ~65-70% (Rollins et al., 2009; Perring et al., 2009b), ~40-45% for β-pinene (Fry et al., 2009), and ~30% for limonene (Fry et al., 2011). I assign a β value of 30% for α-pinene, and 70% for isoprene.

Since there is no suitable ARCTAS data to constrain the nighttime concentrations of alkenes and aldehydes, output from the WRF-Chem model is used to guide the choice of input concentrations (Table 3.4). I choose a lower estimate of 400 pptv of alkenes (which I split evenly between isoprene and α-pinene) and a mid-range concentration of 2 ppbv of acetaldehyde. The model is run using lifetimes of N_2O_5 (ranging from 10 min to 3 hr) with respect to heterogeneous hydrolysis. With this simplified representation of the chemistry of these VOCs and the inorganic reactions of NO_x and O_3 shown in Table 3.5, I calculate the loss of NO_x to HNO_3 and to $RONO_2$ by prescribing the NO_2 concentration and assuming NO_3 and N_2O_5 are in instantaneous steady-state.

3.4 NO_x lifetime

3.4.1 Daytime

I compute the lifetime of NO_x with respect to chemical loss to $RONO_2$ and nitric acid using Eq. (3.1):

$$\tau_{NO_x} = \frac{[NO_x]}{Loss(NO_x)} = \frac{[NO_x]}{\sum_i \alpha_i k_{RO_{2i}+NO}[RO_{2i}]\,[NO] + k_{OH+NO_2}[OH][NO_2]} \quad (3.1)$$

For NO_x concentrations less than 500 pptv when α=0%, HNO_3 formation is the sole mechanism for NO_x loss, and the NO_x lifetime is longest at low NO_x and decreases as NO_x increases (Fig. 3.1). This decrease is roughly proportional to $1/[OH]$ (not shown), which at low NO_x concentrations, increases as NO_x concentrations increase due to an increase of OH recycling from HO_2+NO.

As α increases, the NO_x lifetime decreases, most significantly at the lowest NO_x concentrations. At 100 pptv NO_x, for α values in the range expected in remote forested regions, $RONO_2$ production results in a NO_x lifetime of less than 8 hours (α=5%) and less than 5 hours (α=10%), compared to a NO_x lifetime of greater than one day (~27 hours) for α=0%. The lifetime of NO_x peaks near NO_x concentrations of ~20 pptv (α=1%) to ~210 pptv (α=10%) for α values of at least 1% (Fig. 3.1). This reflects the dependence of $RONO_2$ production on RO_2 concentrations. At low NO_x concentrations, RO_2 concentrations change rapidly as a function of NO_x, resulting in the NO_x lifetime curve behaving approximately as $1/[RO_2]$. As NO_x increases, the change in RO_2 with NO_x slows, and the OH term becomes more important. The resulting maximum in NO_x lifetime depends on the weighting of the RO_2 term (the α value) and shifts to higher NO_x concentrations as α increases (Fig. 3.1).

The relative effects of HNO_3 versus $RONO_2$ formation on NO_x lifetime are shown in Fig. 3.2, where the fraction of NO_x loss to $RONO_2$ (solid lines) and to HNO_3 (dashed lines) is shown versus NO_x. The fraction of NO_x loss to $RONO_2$ is significant at NO_x below 100 pptv-even if α is as low as 1%. That fraction decreases as NO_x increases.

For the α=5% and α=10% cases that are expected to be typical of BVOC emissions from forests, $RONO_2$ production represents more than half of the NO_x loss at NO_x concentrations below ~400 pptv and ~950 pptv, respectively. Consequently, in remote regions with high BVOC emissions where one expects NO_x concentrations of ~20-300 pptv, $RONO_2$ formation accounts for over 50% of the instantaneous NO_x loss. It is notable that even for the α=1%, which is similar to the measured value for ethane of 1.2% ± 0.2% (Atkinson et al., 1982), ~31% of NO_x loss is due to $RONO_2$ at 100 pptv NO_x and ~15% of NO_x loss at 500 pptv NO_x. I note that the total VOC reactivity of 2 s^{-1} that I use in these calculations is much too high for ethane to affect the $RONO_2$ yield (~370 ppbv of ethane are required to have a reactivity of 2 s^{-1}). Since the importance of $RONO_2$ decreases with decreasing VOC reactivity, it is expected that $RONO_2$ formation would be low in pure ethane, CO, CH_4 chemistry. However, only ~740 pptv of isoprene (α ~10%) is needed to achieve a reactivity of 2 s^{-1} and 74 pptv of isoprene with a reactivity of 0.2 s^{-1} would have the effect of α ~1%. Even a small addition of isoprene or other highly reactive BVOC will result in a reactivity and α in the range of these calculations.

The exact numbers presented in Fig. 3.1 and Fig. 3.2 are sensitive to the parameters chosen for HO_x production, VOC reactivity, and peroxy radical reaction rates. I have tested the effects of much slower or faster peroxy radical self reaction rates and the effects of varying the HO_x production and NMVOC reactivity. I find that the basic structure of the results is insensitive to wide variations in the assumed parameters.

3.4.2 Nighttime

The nighttime formation of $RONO_2$ from NO_3 chemistry also has important implications for the chemical loss of NO_x, especially since the branching ratio for $RONO_2$ formation is much higher for NO_3 chemistry and N_2O_5 is present at very low concentrations due to low concentrations of NO_2. I calculate the NO_x lifetime at night with respect to the formation of $RONO_2$ and HNO_3 using Eq. (3.2) and Eq. (3.3) respectively.

$$\tau_{NO_x \to RONO_2} = \frac{[NO_2]+[NO_3]+2*[N_2O_5]}{\beta_{\alpha-pinene} k_{NO_3+\alpha-pinene}[\alpha-pinene][NO_3]+\beta_{isoprene} k_{NO_3+isoprene}[Isoprene][NO_3]} \quad (3.2)$$

$$\tau_{NO_x \to HNO_3} = \frac{[NO_2]+[NO_3]+2*[N_2O_5]}{2k_{N_2O_5 hydrolysis}[N_2O_5]+k_{NO_3+aldehyde}[Aldehyde][NO_3]} \quad (3.3)$$

For NO_x concentrations less than 500 pptv, the NO_x lifetime with respect to $RONO_2$ formation is just under 40 hours and varies by ~8% for a range of assumptions about the N_2O_5 lifetime to hydrolysis and acetaldehyde concentrations (Fig. 3.3a). The lifetime shows relatively little sensitivity to reasonable changes in alkene concentration since any increase in alkenes decreases the steady-state NO_3 concentration. The NO_x lifetime with respect to nighttime production of HNO_3 is much longer (at least several days -Fig. 3.3b) and varies by over an order of magnitude. Consequently, at NO_x concentrations less than 500 pptv, the NO_x lifetime at night (not shown) is dominated by the loss to $RONO_2$. The net lifetime with respect to both sinks at 100 pptv NO_x is ~34-36 hours (for all cases). At 500 pptv NO_x, the lifetime varies from ~27 hours for an N_2O_5 hydrolysis lifetime of 10 min, to just under 36 hours for an N_2O_5 hydrolysis lifetime of 180 min (and 2 ppbv acetaldehyde concentration).

This lifetime is highly sensitive to the assumed value of β; as β increases and the loss of NO_x through NO_3 reactions becomes more efficient, the NO_x lifetime will be limited by the NO_2+O_3 rate. Under this condition, the NO_x lifetime is

$$\tau = \frac{[NO_x]}{Fk_{NO_2+O_3}[NO_2][O_3]} \quad (3.4)$$

where F is a number between 1 (loss through NO_3 dominates) and 2 (loss through N_2O_5 dominates). Under low NO_x conditions F will be close to 1 and the lifetime has a limiting value at high BVOC or high β of ~12 hours.

The fractional NO_x loss to HNO_3 and $RONO_2$ is shown in Fig. 3.4. Loss to HNO_3 becomes important only for the shortest N_2O_5 hydrolysis lifetime; a lifetime that is likely much too fast for a remote environment. Furthermore, increasing the HNO_3 production through the aldehyde+NO_3 reaction by increasing the acetaldehyde concentration by a factor of 3 (to 6 ppbv) results in minor differences. Even if acetaldehyde is replaced with pinonaldehyde (which reacts an order of magnitude more quickly), the fraction of NO_x loss to $RONO_2$ is high: at 100 pptv

NO_x it is ~92% for pinonaldehyde concentrations of 2 ppbv and 80% for 6 ppbv pinonaldehyde (for a N_2O_5 lifetime of 180 min).

3.4.3 Twenty-four hour average lifetime

The average NO_x lifetime will be a combination of the nighttime and daytime sinks. However, the NO_x lifetime at night is much longer than the daytime value except at α=0% where the two are nearly equal. Thus, the diurnal average lifetime will be similar to the daytime lifetime (Fig. 3.1).

3.5 Ozone production efficiency

Since the production of $RONO_2$ reduces the NO_x lifetime, it will reduce the number of ozone molecules produced per NO_x removed (the ozone production efficiency-OPE) (Fig. 3.5). OPE is calculated using Eq. (3.5):

$$OPE = \frac{P(O_3)}{L(NO_x)} = \frac{k_{HO_2+NO}[HO_2][NO] + k_{CH_3O_2+NO}[CH_3O_2][NO] + (1-\alpha)k_{RO_2+NO}[RO_2][NO]}{k_{OH+NO_2}[NO_2][OH] + \alpha k_{RO_2+NO}[RO_2][NO]} \quad (3.5)$$

At 100 pptv NO_x OPE decreases from ~110 for α=0% to ~19 for the α=10% case. The shape of the OPE versus NO_x curve also changes with α; the slope of the OPE versus NO_x line decreases in steepness as α increases. The shallow slope of OPE versus NO_x for the higher α cases occurs because both ozone production and ozone loss depend on RO_2. For the low α cases, NO_x loss depends primarily on OH concentration, which, as discussed earlier, decreases as NO_x decreases. Since the RO_2 concentration increases as NO_x decreases, this results in a high OPE at low NO_x.

NO_x reservoirs, such as peroxy nitrates, transport NO_x from high NO_x, low OPE environments (urban areas) to areas downwind at lower NO_x and high OPE. Fig. 3.5 suggests that if this downwind area is over the continents, that the OPE may be significantly lower than the traditional textbook view of low NO_x chemistry would assume. This high sensitivity of OPE to the $RONO_2$ formation potential also suggests that small errors in $RONO_2$ representation may lead to larger errors in the calculated ozone burden.

The value of OPE in the atmosphere has often been estimated using the correlation between NO_z ($NO_z = NO_y - NO_x$) and O_3, however, this is a difficult comparison due to the different lifetimes of O_3 and NO_z, as well as the variability in lifetimes of the different NO_z components. These problems are more significant in the boundary layer of remote environments where there are large contributions of peroxy nitrates and HNO_3 to NO_z. However, measurements from a forest in northern Michigan suggest an OPE of ~22 for NO_x concentrations around 300 pptv (Thornberry et al., 2001), an OPE value that lies between the α=5% and α=10% values expected for a forested environment.

3.6 Boreal Forest: Comparison to a 3D chemical transport model

I compare the steady state calculations described above to the WRF-Chem 3D chemical transport model simulations carried out using a domain that includes a large fraction of Canada where low NO_x concentrations coupled with high BVOC emissions from the boreal forest are

expected to have a strong effect on NO_x lifetime. Details regarding the WRF-Chem model simulations can be found in Chapter 4.

The WRF-Chem model allows us to account for effects from NO_x reservoirs with long lifetimes relative to changes in sources and sinks (i.e. ones for which transport plays an important role in determining concentration) such as: formation and decomposition of peroxy nitrates and the release of NO_x from oxidation and photolysis of $RONO_2$. The NO_x lifetime is defined with respect to the net chemical loss of NO_x. If the net chemical loss to any class of species (e.g., peroxy nitrates, $RONO_2$, nitric acid) is less than zero, then that species has zero contribution to the chemical loss of NO_x at that NO_x concentration. Figure 6 shows the NO_x lifetime to net chemical loss as a function of NO_x, binned by the effective α value calculated using Eq. (A2). In the calculation of α_{eff} I assume that the ozone production rate defined in Eq. (A3) is equivalent to Eq. (3.6):

$$P(O_3) = j_{NO_2}[NO_2] - k_{NO+O_3}[NO][O_3] \quad (3.6)$$

I note that in the WRF-Chem results I report use 24-hour averaged data to calculate α_{eff}. This allows us to sort the airmasses by their $RONO_2$ production rates; however, the exact value of α_{eff} differs slightly from what would be calculated using only the daytime data.

Within the domain there are examples of airmasses with α_{eff} ranging from ~0.4-8%. Both the full 3-D calculations (Fig. 3.6) and the box model (Fig. 3.1) show the same general dependence of the lifetime on α. The most notable difference between the two is that the NO_x lifetime from the 3-D calculations decreases more steeply as NO_x increases than it does for the steady-state results. This is due to an increase in the loss due to peroxy nitrate formation (Fig. 3.7c) as NO_x increases, an effect that is not represented in the steady-state model, which assumed peroxy nitrates were at steady-state and thus could be ignored.

The fractional net NO_x loss to $RONO_2$, peroxy nitrates, and HNO_3 is shown in Fig. 3.7. The NO_x concentrations predicted by WRF-Chem cover the range (~30-250 pptv); over this small range, large changes in the fractional composition of the products of NO_x loss reactions are predicted by both the steady-state model (Fig. 3.2) and the WRF-Chem calculations (Fig. 3.7). In both calculations the fraction of net NO_x loss to $RONO_2$ (Fig. 3.7a) approaches unity as NO_x decreases and as the effective α value increases. Interestingly, the WRF-Chem predictions for the fractional net NO_x loss to HNO_3 shows only a slight increase as a function of NO_x (Fig. 3.7b) and the decrease in fractional NO_x loss to $RONO_2$ is compensated by an increase in the net NO_x loss to peroxy nitrates when NO_x is greater than ~50-80 pptv (Fig. 3.7c). I note that a plot of the fractional instantaneous gross loss when only $RONO_2$ and HNO_3 are considered (which is a direct comparison to Fig. 3.2), does show the fractional contribution of HNO_3 decreasing with increasing NO_x (not shown). The fractional net NO_x loss to peroxy nitrates exhibits little variation with respect to α_{eff}, indicating that peroxy nitrates are acting to buffer NO_x. A full investigation of this effect, however, would require a larger NO_x range and attention to the effects of temperature and transport. Many of these aspects have been discussed previously (Sillman and Samson, 1995). I note that due to the thermal instability of peroxy nitrates, the importance of peroxy nitrates as a NO_x reservoir will be highly dependent on temperature and large differences are expected between seasons and between boreal and tropical forests. In no regime does peroxy nitrate chemistry change the conclusion that the lifetime of NO_x is controlled by $RONO_2$ production rates at low NO_x concentrations.

3.7 Discussion

In low NO_x, high BVOC environments, the formation of $RONO_2$ accounts for the majority of the instantaneous NO_x sink, resulting in decreased NO_x lifetime and decreased OPE relative to chemistry dominated by CO and CH_4. However, the ultimate regional and global impact of the $RONO_2$ chemistry is dependent on the extent to which these molecules serve as permanent versus temporary NO_x sinks; a value which, in general, is not well known. For instance, if I assume that $RONO_2$ predominately serve as temporary NO_x sinks that transport NO_x to areas with higher OPE (e.g., areas with lower NO_x or areas at the same NO_x but lower α), I expect an increase in the ozone burden as a result of accounting for $RONO_2$ chemistry. In contrast, if the $RONO_2$ are lost primarily through deposition, they may increase nitrogen availability in the biosphere. Since many areas are nitrogen limited, introduction of nitrogen will also affect the carbon storage capacity of an ecosystem (e.g., Holland et al., 1997; Thornton et al., 2007, 2009; Bonan and Levis, 2010). A recent study observed the direct foliar uptake of $RONO_2$ and subsequent incorporation of the nitrogen into amino acids (Lockwood et al., 2008), indicating that (at least some) $RONO_2$ will affect plant growth.

It is interesting to consider how the effects of $RONO_2$ on climate and air quality may impact our understanding of both preindustrial and future climates. For instance, it is likely that during the preindustrial era when NO_x concentrations were lower, that $RONO_2$ formation was a more important NO_x sink than it is today. Model predictions of preindustrial climate often predict larger ozone concentrations than the semi-quantitative measurements of the late 19^{th}/early 20^{th} century indicate (e.g., Mickley et al., 2001; Archibald et al., 2011). Although there may be problems with the ozone measurements or with the emissions estimates used in the models, this may also indicate that models are missing a NO_x sink in the preindustrial era. As shown in Fig. 3.5, I calculate that the OPE is very sensitive to the assumed branching ratio, indicating that a small error in $RONO_2$ formation may have a large effect on the ozone burden.

In industrialized countries, NO_x emissions are currently decreasing due to air quality control measures (e.g., van der A et al., 2008; Dallmann and Harley, 2010; Russell et al., 2010, 2012). Coupling this decrease in NO_x with the increase in biogenic VOC emissions expected in a warmer climate, suggests that $RONO_2$ chemistry will begin to play a more important role in NO_x termination in urban and suburban areas. As discussed in Section 4.1, the crossover from $RONO_2$ to nitric acid accounting for over 50% of NO_x loss occurs at ~400 pptv for a 5% branching ratio and at ~950 pptv for a 10% branching ratio. Past studies have constrained the effective branching ratio in urban areas at 4-7% (Cleary et al., 2005; Farmer et al., 2011; Perring et al., 2010; Rosen et al., 2004) – a value that suggests that in future climates, it will be necessary to correctly simulate $RONO_2$ chemistry in order to understand regional pollution and air quality.

In order to improve our understanding of the impact of $RONO_2$ on atmospheric chemistry, particularly on the global and regional NO_x and HO_x budgets, laboratory studies on the formation of $RONO_2$ (particularly for biogenic species other than isoprene), oxidation, physical loss, and oxidation products are necessary. These measurements must be supplemented by field measurements spanning NO_x concentrations from near zero to a few ppbv. In one such analysis, I use measurements from the ARCTAS campaign (Chapter 4). However, a thorough understanding will require measurements in environments with different classes of BVOC emissions (e.g. pine forests which are dominated by monoterpenes (α ~ 18%) and oak forests which are dominated by isoprene (α~10%)). These field measurements will provide constraints

on how the importance of $RONO_2$ versus nitric acid changes as a function of NO_x and will test the representation of $RONO_2$ chemistry in reduced chemical mechanisms.

3.8 Conclusions

Recent field measurements have indicated that low NO_x, high BVOC chemistry is significantly more complex than the textbook view of low NO_x chemistry being controlled by methane and carbon monoxide. Most of the work on low NO_x, high BVOC chemistry has focused on the implications for the HO_x budget. In this chapter I present a framework for understanding the NO_x budget under these conditions. I find that production of $RONO_2$ accounts for the majority of the instantaneous NO_x sink in low NO_x, high BVOC environments in both a steady-state model and a 3-D chemical transport model. Furthermore, the NO_x lifetime and OPE are highly sensitive to $RONO_2$ production. These findings suggest that proper representation of $RONO_2$ formation and NO_x recycling are necessary for accurate calculation of past, present, and future ozone concentrations and the corresponding climate effects.

Reaction	Rate
$CH_4 + OH \xrightarrow{O_2} CH_3O_2 + H_2O$	$1.85\times10^{-12}\exp(-1690/T)$[a]
$CH_3O_2 + NO \longrightarrow NO_2 + HO_2 + HCHO$	$2.8\times10^{-12}\exp(300/T)$[b]
$CH_3O_2 + HO_2 \longrightarrow products$	$4.1\times10^{-13}\exp(750/T)$[b]
$CH_3O_2 + CH_3O_2 \longrightarrow 0.66HO_2 + products$	$9.5\times10^{-14}\exp(390/T)$[b]
$NMVOC + OH \xrightarrow{O_2} RO_2$	See Table 3.2
$RO_2 + NO \longrightarrow (1-\alpha)HO_2 + (1-\alpha)NO_2 + \alpha RONO_2$	$2.7\times10^{-12}\exp(360/T)$[c]
$RO_2 + HO_2 \longrightarrow products$	$2.06\times10^{-13}\exp(1300/T)$[d]
$RO_2 + RO_2 \xrightarrow{2O_2} 1.2CH_3O_2 + products$	1.4×10^{-12} [e]
$RO_2 \longrightarrow HO_2 + OH$	$4.12\times10^{8}\exp(-7700/T)$[e]
$RO_2 + CH_3O_2 \xrightarrow{2O_2} 0.6CH_3O_2 + 0.6HO_2 + products$	1.4×10^{-12} [f]
$CO + HO \xrightarrow{M,O_2} HO_2 + CO_2$	$k_0=1.5\times10^{-13}(T/300)^{0.6}$ $k_\infty=2.1\times10^{9}(T/300)^{6.1}$ [b]*
$CO + OH \xrightarrow{M} HOCO \xrightarrow{O_2} HO_2 + CO_2$	$k_0=5.9\times10^{-33}(T/300)^{-1.4}$ $k_\infty=1.1\times10^{-12}(T/300)^{1.3}$ [b]
$P(HO_x) \longrightarrow 0.8OH + 0.2HO_2$	See Table 3.2
$OH + O_3 \longrightarrow HO_2 + O_2$	$1.7\times10^{-12}\exp(-940/T)$[a]
$OH + H_2 \xrightarrow{O_2} HO_2 + H_2O$	$7.7\times10^{-12}\exp(-2100/T)$[a] H_2=531 ppb**
$HCHO + OH \longrightarrow HO_2 + CO_2 + H_2O$	$5.4\times10^{-12}\exp(135/T)$[a]
$H_2O_2 + OH \longrightarrow HO_2 + H_2O$	$2.9\times10^{-12}\exp(-160/T)$[a]
$HO_2 + OH \longrightarrow H_2O + O_2$	$4.8\times10^{-11}\exp(250/T)$[a]
$HO_2 + O_3 \longrightarrow OH + 2O_2$	$1.0\times10^{-14}\exp(-490/T)$[b]
$HO_2 + HO_2 \xrightarrow{M} H_2O_2 + H_2O$	$(2.1\times10^{-33}\times M\times\exp(920/T) +$ $3.0\times10^{-13}\exp(460/T)) \times$ $(1 + [H_2O]\times1.4\times10^{-21}\exp(2200/T))$[b]
$HO_2 + NO \longrightarrow OH + NO_2$	$3.45\times10^{-12}\exp(270/T)$[a]
$NO + O_3 \longrightarrow NO_2 + O_2$	$1.4\times10^{-12}\exp(-1310/T)$[a]
$NO_2 + OH \xrightarrow{M} HNO_3$	$k_0 = 1.49\times10^{-30}(T/300)^{-1.8}$ $k_\infty=2.58\times10^{-11}$ [g]
$NO_2 + h\nu \xrightarrow{O_2} NO + O_3$	See Table 3.2

[a]IUPAC (Atkinson et al., 2004, 2006) [b]JPL 2010 (Sander et al., 2006) *Calculated using the JPL 2010 termolecular rate for chemical activation reactions [c]MCM v3.2 (Jenkin et al., 1997; Saunders et al., 2003) [d]MCM v3.2 RO_2+HO_2 for five carbon RO_2 [e](Crounse et al., 2011) using MCM v3.2 RO_2+HO_2 reaction rate with a 5 carbon RO_2 to represent isoprene peroxy + HO_2 [f](Jenkin et al., 1997) RO_2 reactions secondary RO_2 with β-OH **(Novelli et al., 1999) [g](Henderson et al., 2012)

Table 3.1 Reactions and rate coefficients used in the steady-state modeling of daytime chemistry.

Species	Value
Temperature	285 K
Photolysis rate of NO_2	6.2×10^{-3} s^{-1}
CH_4	1865 ppbv
CO	130 ppbv
O_3	40 ppbv
HO_x production rate	4.1×10^{6} molecules cm^{-3} s^{-1}
HCHO	1.48 ppbv
H_2O_2	2.04 ppbv
H_2O	1.18×10^{4} ppm
NMVOC+OH	2 s^{-1}

Table 3.2 Parameters used in the daytime steady-state model. The value of the parameters (except for NMVOC + OH) are based on the median ARCTAS measurements from less than 2 km pressure altitude and excluding data with recent anthropogenic or biomass burning influence.

α	α_{eff} 10 pptv NOx	α_{eff} 100 pptv NOx	α_{eff} 500 pptv NOx
0.1%	0.06%	0.08%	0.09%
1%	0.64%	0.81%	0.87%
5%	3.22%	4.03%	4.37%
10%	6.43%	8.06%	8.74%

Table 3.3 Effective α value at various NO_x concentrations. These are calculated using Eq. A2.

Species	Value
Temperature	285 K
O_3	40 ppbv
α-pinene	200 pptv
isoprene	200 pptv
acetaldehyde	2 ppbv
$\beta_{isoprene}$	0.7
$\beta_{\alpha\text{-pinene}}$	0.3
N_2O_5 hydrolysis	τ= 180, 120, 60, or 10 min

Table 3.4 Parameters used in the nighttime steady-state model.

Reaction	Rate
$NO_2 + O_3 \longrightarrow NO_3$	$1.2\times10^{-13}\exp(-2450/T)$[a]
$NO_3 + NO_2 \xrightarrow{M} N_2O_5$	$k_0=2.0\times10^{-30}(T/300)^{-4.4}$ $k_\infty=1.4\times10^{-12}(T/300)^{-0.7}$ [a]
$N_2O_5 \xrightarrow{M} NO_3 + NO_2$	$K_{eq} = 2.7\times10^{-27}\exp(11000/T)$ [b]
$\alpha - pinene + NO_3 \longrightarrow \beta_{\alpha-pinene} RONO_2 + products$	$1.2\times10^{-12}\exp(490/T)$ [c]
$Isoprene + NO_3 \longrightarrow \beta_{isoprene} RONO_2 + products$	$3.15\times10^{-12}\exp(-450/T)$[c]
$Acetaldehyde + NO_3 \longrightarrow HNO_3 + products$	$1.4\times10^{-12}\exp(-1860/T)$ [c]
$N_2O_5 \xrightarrow{H_2O,surface} 2HNO_3$	See Table 5

[a]JPL 2010 (Sander et al., 2006)

[b]JPL 2010 calculated from $\frac{k_{NO_3+NO_2}}{K_{eq}}$

[c]IUPAC (Atkinson et al., 2006)

Table 3.5 Reactions and rate coefficients used in the steady-state modeling of nighttime chemistry.

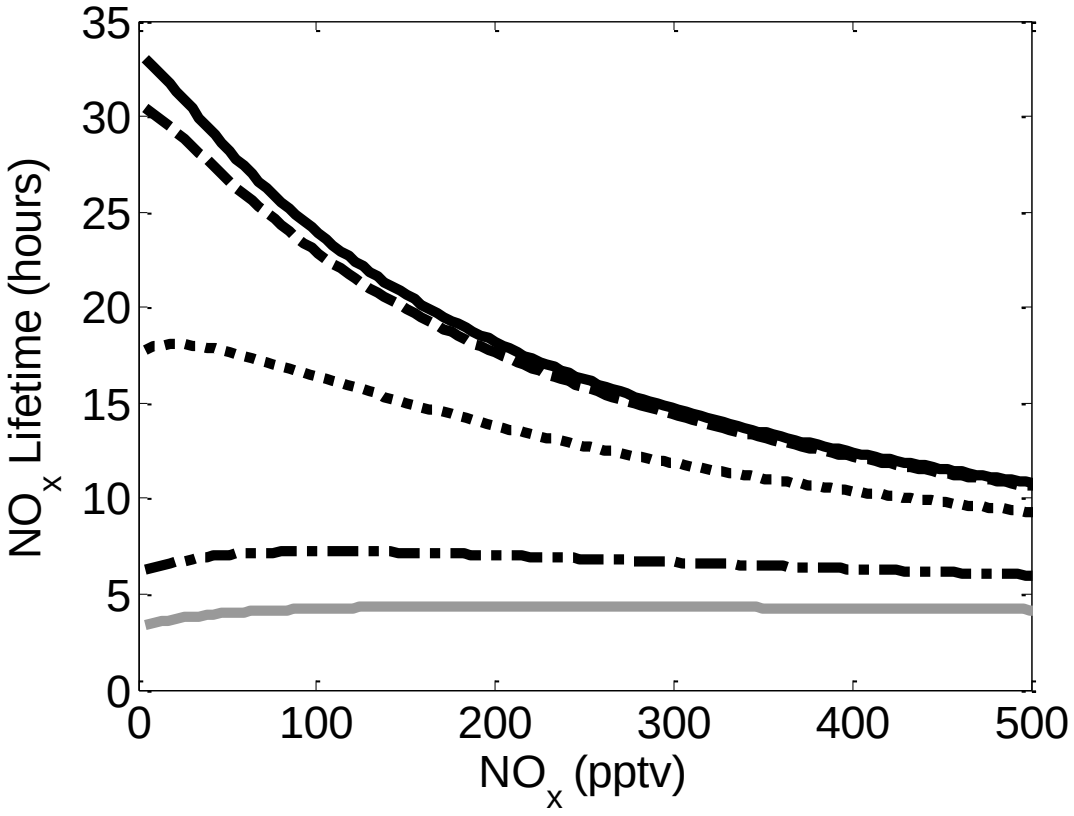

Figure 3.1 Steady-state model results of NO_x lifetime to chemical loss versus NO_x concentration for α=0% (solid black line), α=0.1% (dashed black line), α=1% (dotted black line), α=5% (dash-dot black line), and α=10% (grey solid line).

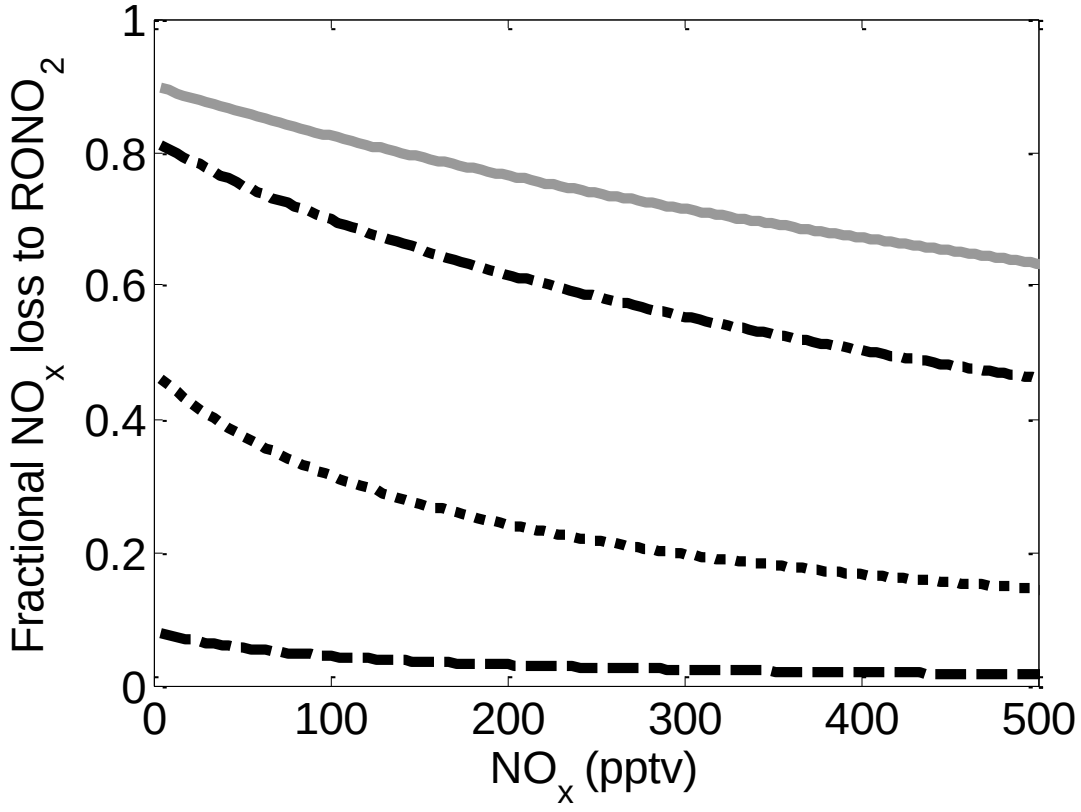

Figure 3.2 Steady-state model results of fractional chemical NO_x loss to $RONO_2$ versus NO_x concentration for α=0.1% (dashed black line), α=1% (dotted black line), α=5% (dash-dot black line), and α=10% (grey solid line). HNO_3 production accounts for the remainder of the NO_x loss.

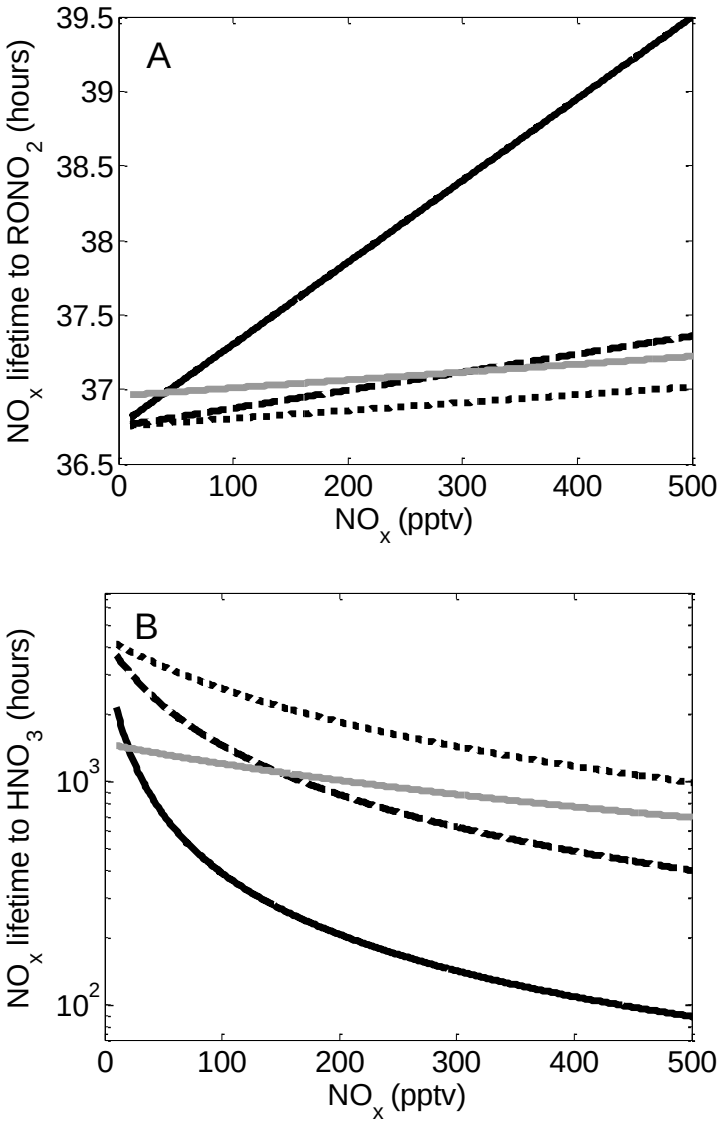

Figure 3.3 Steady state model calculation of NO_x lifetime at night to **A)** organic nitrate formation and **B)** to nitric acid formation through both NO_3 reaction with aldehydes and N_2O_5 hydrolysis. The solid black line is for an N_2O_5 hydrolysis lifetime of 10 min with 2 ppbv of acetaldehyde, the dashed black line for an N_2O_5 hydrolysis lifetime of 60 min with 2 ppbv of acetaldehyde, the dotted black line for an N_2O_5 hydrolysis lifetime of 180 min with 2 ppbv of acetaldehyde, and the solid grey line for an N_2O_5 hydrolysis lifetime of 180 min with 6 ppbv of acetaldehyde.

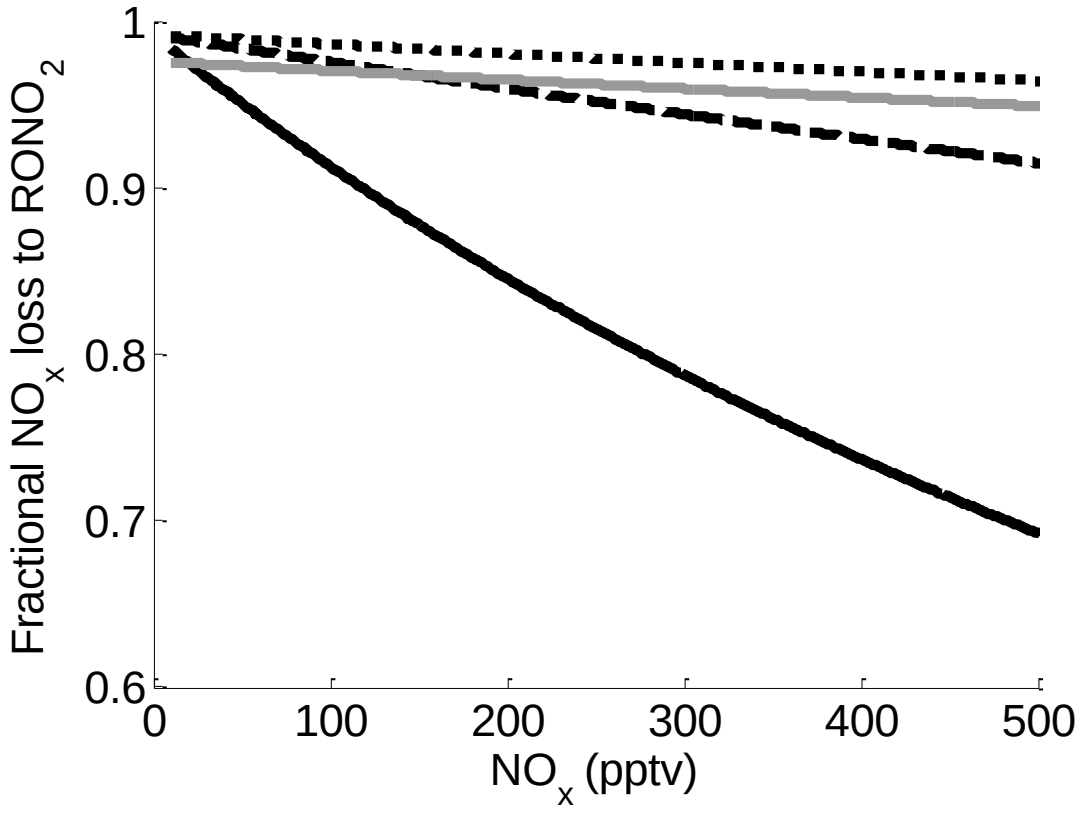

Figure 3.4 Fractional NO_x loss to $RONO_2$ at night in the steady-state model for an N_2O_5 hydrolysis lifetime of 10 min with 2 ppbv of acetaldehyde (solid black line), N_2O_5 hydrolysis lifetime of 60 min with 2 ppbv of acetaldehyde (dashed black line), N_2O_5 hydrolysis lifetime of 180 min with 2 ppbv of acetaldehyde (dotted black line), and an N_2O_5 hydrolysis lifetime of 180 min with 6 ppbv of acetaldehyde (solid grey line). HNO_3 production accounts for the remainder of the NO_x loss.

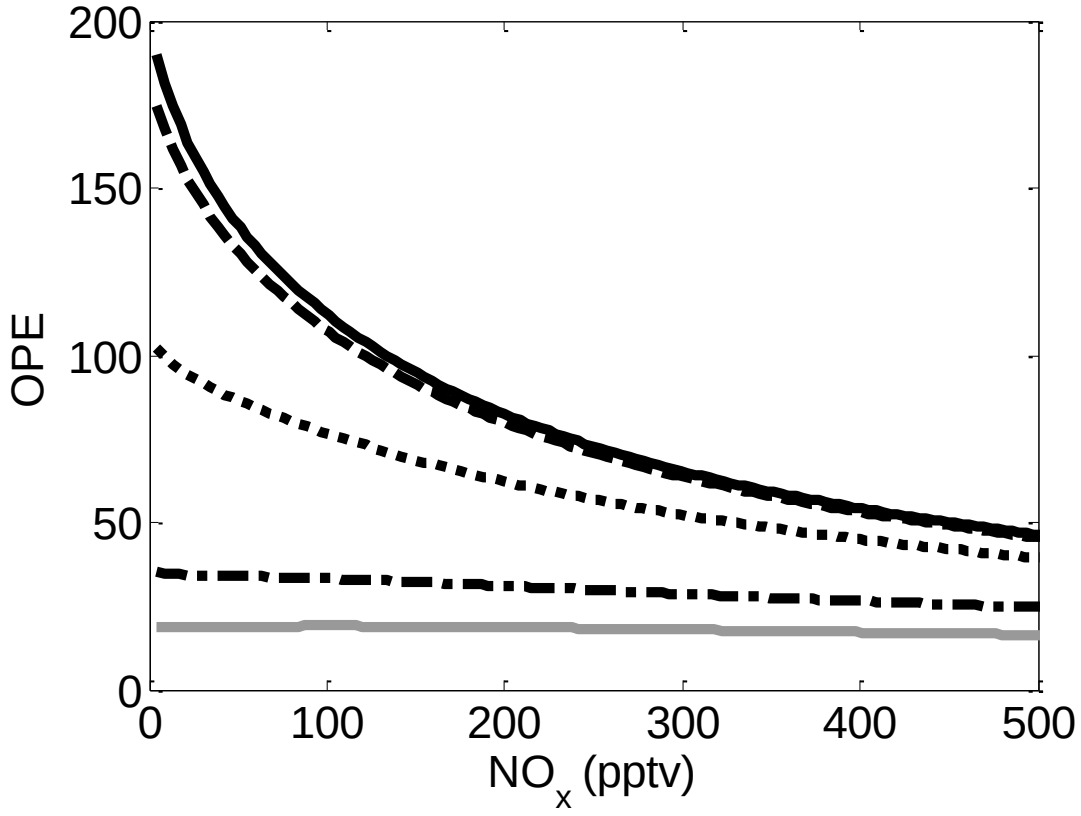

Figure 3.5 Steady-state model results for ozone production efficiency (OPE) versus NO_x concentration for α=0% (solid black line), α=0.1% (dashed black line), α=1% (dotted black line), α=5% (dash-dot black line), and α=10% (grey solid line).

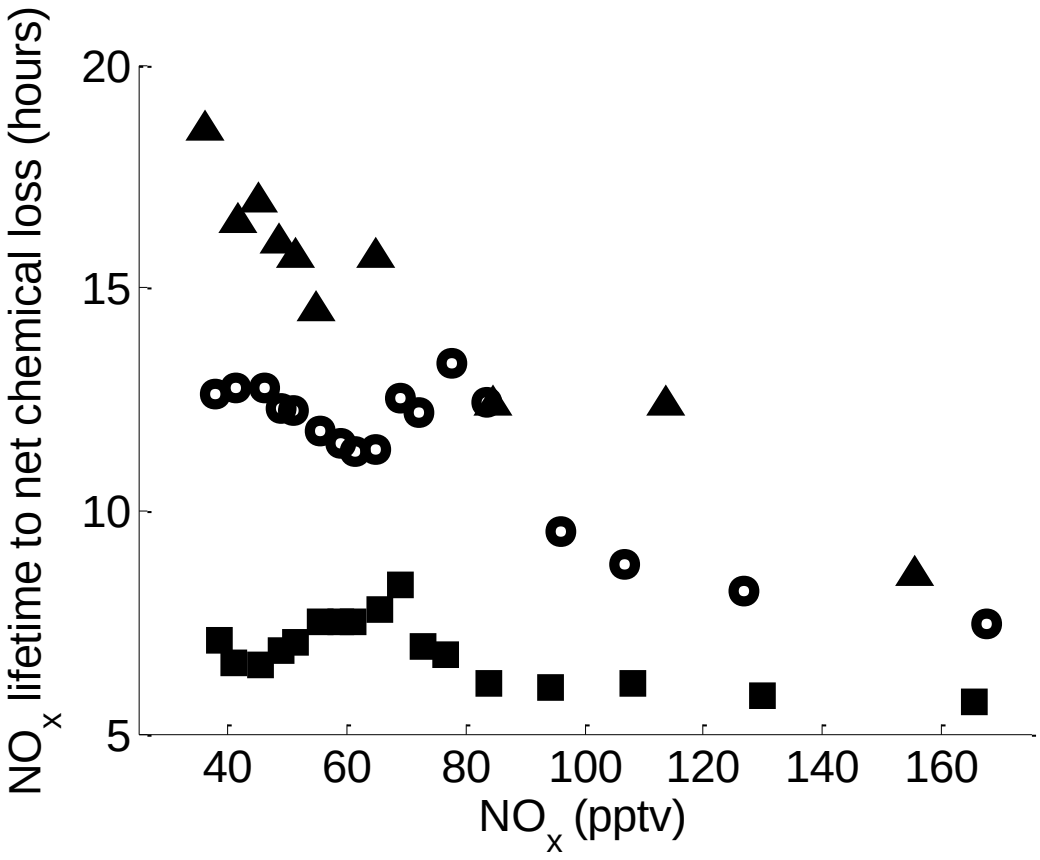

Figure 3.6 WRF-Chem predication of the NO_x lifetime to net chemical loss over Canada (north of 53°N) averaged over two weeks in July. The net chemical loss is defined as the sum of the net chemical loss to different classes of NO_y including $RONO_2$, RO_2NO_2, and HNO_3 (full details can be found in Appendix B). If the net chemical loss is less than zero for any particular class, the net loss is set to zero. The results are sorted by the effective α_{eff} value as calculated using Eq. A2. The triangles represent $0.5\% \leq \alpha_{eff} < 2\%$, the open circles are $3\% \leq \alpha_{eff} < 4\%$, and the squares are $\alpha_{eff} \geq 5\%$.

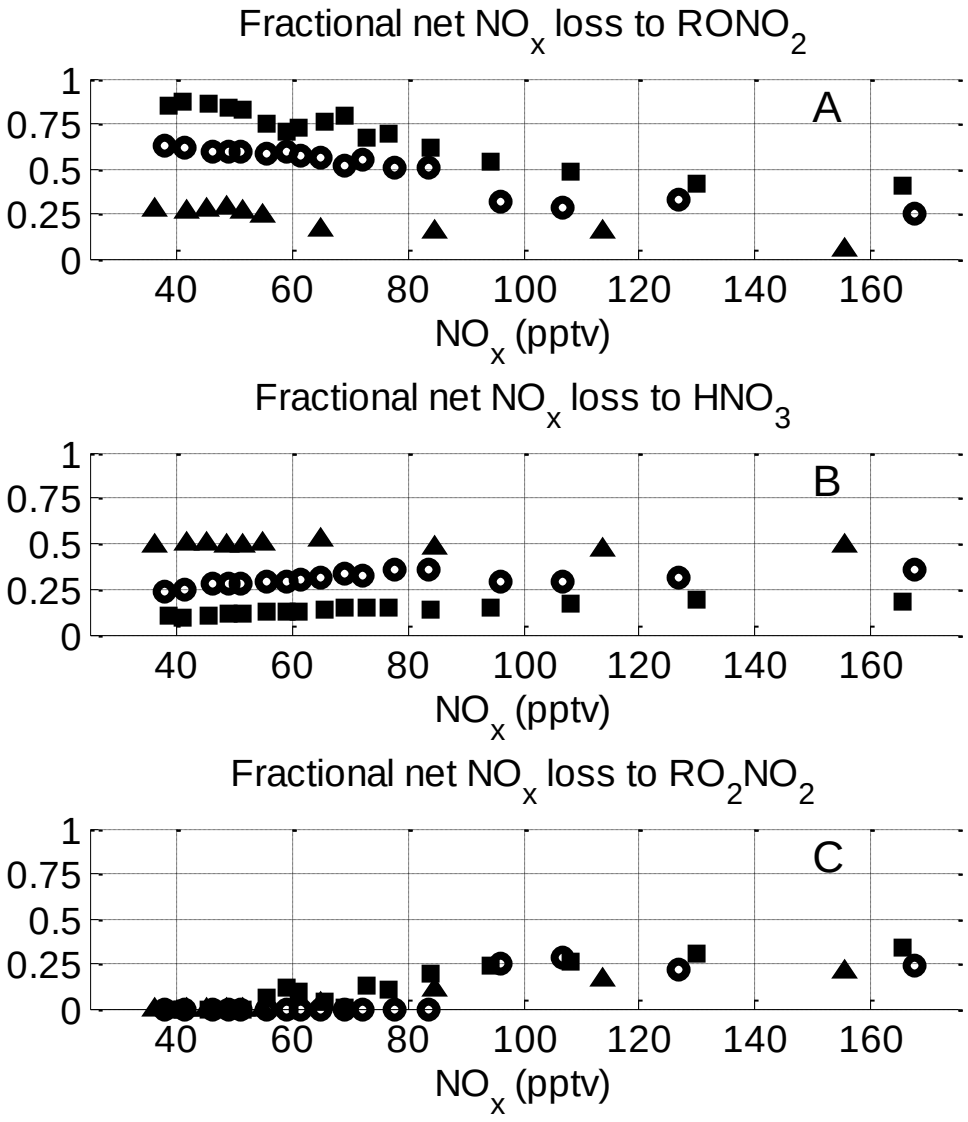

Figure 3.7 WRF-Chem results for **A)** fractional net NO_x loss to organic nitrates, **B)** fractional net NO_x loss to HNO_3, and **C)** fractional net NO_x loss to peroxy nitrates. The net chemical loss is defined as the sum of the net chemical loss to different classes of NO_y including organic nitrates, peroxy nitrates, and nitric acid (full details can be found in Chapter 4). If the net chemical loss is less than zero for any particular class, the net loss is set to zero. The results are sorted by the effective α_{eff} value as calculated using Eq. A2. The triangles represent $0.5\% \leq \alpha_{eff} < 2\%$, the open circles are $3\% \leq \alpha_{eff} < 4\%$, and the squares are $\alpha_{eff} \geq 5\%$.

Chapter 4

Observations of total $RONO_2$ over the Boreal Forest: NO_x sinks and HNO_3 sources

4.1 Introduction

In remote, continental regions, isoprene, terpenes and other biogenic volatile organic compounds (BVOCs) rival CH_4 and CO as controls over the free radical chemistry of the atmospheric boundary layer, affecting global distributions of oxidants (OH, O_3, NO_3) and oxidant precursors (e.g., NO_x, HCHO). In turn, these oxidants affect the burden of tropospheric ozone and of organic compounds (e.g., CH_4, CH_3Br) with effects on radiative balance and therefore on climate and stratospheric ozone. Consequently, the oxidative chemistry of BVOC has been the subject of extensive research. Recent advances in laboratory and field measurements have focused on the products of BVOC oxidation and have inspired renewed examination of how the mechanisms of BVOC oxidation affect atmospheric composition. In particular, the impact of BVOC on the HO_x budget has been highlighted (e.g., Thornton et al., 2002; Lelieveld et al., 2008; Stavrakou et al., 2010; Stone et al., 2011; Whalley et al., 2011; Paulot et al., 2012; Taraborrelli et al., 2012).

Oxidation of BVOC results in peroxy radicals that may react with NO_x (NO_x = NO + NO_2), with other peroxy radicals, or - in some cases - may isomerize (potentially regenerating OH). The reaction of peroxy radicals with NO_2 results in the formation of peroxy nitrates (RO_2NO_2) - a class of molecules that generally act as temporary reservoirs of NO_x and serve to transport NO_x on regional and global scales. Reaction of peroxy radicals with NO generally acts to propagate the ozone production cycle (R1a), however, a minor channel of the reaction (R1b), which proceeds with the efficiency α (also known as the branching ratio), results in the formation of organic nitrates ($RONO_2$).

$$RO_2 + NO \rightarrow RO + NO_2 \qquad (1-\alpha) \qquad \text{(R1a)}$$

$$RO_2 + NO \rightarrow RONO_2 \qquad (\alpha) \qquad \text{(R1b)}$$

Calculations with box and chemical transport models (CTMs) have shown that organic nitrates play a significant role on the NO_x and O_3 budgets (e.g., Trainer et al., 1991; Chen et al., 1998; Horowitz et al., 1998; Liang et al., 1998; von Kuhlmann et al., 2004; Fiore et al., 2005; Horowitz et al., 2007; Wu et al., 2007; Paulot et al., 2012). In Chapter 3 I have shown that at NO_x concentrations typical of remote and rural environments, the formation of ΣANs is the dominant instantaneous NO_x sink even at modest concentrations of BVOC. However, the net impact on O_3 and NO_x depends on the extent to which ΣANs act as permanent versus temporary NO_x sink as has been shown in numerous models (e.g., von Kuhlmann et al., 2004; Fiore et al., 2005; Horowitz et al., 2007; Ito et al., 2009; Fiore et al., 2011; Paulot et al., 2012).

Here, I use observations of a suite of nitrogen oxides, organic molecules, and oxidants (OH and O_3) from the July 2008 NASA ARCTAS (Arctic Research of the Composition of the Troposphere from Aircraft and Satellites) campaign over the Canadian boreal forest, to examine the extent to which the organic nitrate products of BVOC oxidation control the lifetime of NO_x in the remote continental boundary layer. I then examine the role of chemical loss processes of

ΣANs including oxidation of isoprene nitrates and hydrolysis of ΣANs in aerosol. I find that the ozonolysis of isoprene nitrates is the largest gas-phase sink and I find suggestions that the particle phase hydrolysis of ΣANs, which produces HNO_3, may be both an important loss process for ΣANs and a significant source of HNO_3. The branching of ΣANs loss between these two channels, one of which returns NO_x to the pool of available free radicals and the other that removes NO_x from the atmosphere has important consequences for regional and global NO_x and O_3.

4.2 ARCTAS measurements

The NASA ARCTAS experiment was designed to study processes influencing Arctic chemistry and climate and has been described in detail previously by Jacob et al. (2010). In this analysis I use measurements from the summer portion of the campaign over the Canadian boreal forest (June-July 2008). These measurements were made aboard the DC-8 aircraft, which contained an extensive suite of gas and aerosol measurements.

NO_2, total peroxy nitrates (ΣPNs), and total organic nitrates (ΣANs) were measured aboard the DC-8 using Thermal Dissociation-Laser Induced Fluorescence (TD-LIF). The instrument has been described in detail elsewhere (Day et al., 2002; Wooldridge et al., 2010) and the specific configuration used during ARCTAS has been described in Chapter 2. Briefly, a two-cell TD-LIF with supersonic expansion (Thornton et al., 2000; Cleary et al., 2002; Day et al., 2002; Wooldridge et al., 2010) was deployed for ARCTAS. A 7 kHz, Q-switched, frequency doubled Nd:YAG laser is used to pump a tunable dye laser (pyrromethene 597 in isopropanol) tuned to a 585 nm absorption in the NO_2 spectrum. Prompt scatter is rejected using time gated detection and eliminate scattered light at < 700 nm using bandpass filters. Fluorescence is imaged onto a red sensitive photomultiplier tube and counts are recorded at 4 Hz. The dye laser is tuned on and off an isolated rovibronic feature in the NO_2 spectrum, spending 9 s on the peak of the NO_2 absorbance and 3 s in an off-line position in the continuum of the NO_2 absorption. The difference between the two signals is directly proportional to the NO_2 concentration. Calibration is preformed at least every two hours during a level flight leg using a 4.5 ppm NO_2 reference standard diluted to ~2-8 ppbv in zero air.

The sample flow was split in thirds with one third directed to detection cell 1, where ambient NO_2 was continuously measured. The remaining flow was equally split between the measurement of total peroxy nitrates (ΣPNs) and total organic nitrates (ΣANs). These molecules are detected by thermal conversion to NO_2 in heated quartz tubes. ΣPNs were converted to NO_2 at ~200 ^oC and ΣANs at ~375 ^oC , which is sufficient to dissociate ΣANs as well as any semivolatile aerosol phase organic nitrates (Rollins et al., 2010). The resulting NO_2 of both heated channels (NO_2 + ΣPNs or NO_2 + ΣPNs+ ΣANs) was measured in cell 2. The duty cycle of cell 2 was evenly split between the measurement of ΣPNs and of ΣANs and alternated between the two either every 12 s or every 24 s. The 9 s average from each on-line block was reported to the data archive that is publically available at http://www-air.larc.nasa.gov/cgi-bin/arcstat-c.

ΣPNs are calculated from the difference in signal between the ambient temperature and 200 ^oC channel and likewise, ΣANs are calculated from the difference in signal between the 375 ^oC (NO_2+ ΣPNs+ ΣANs) and the 200 ^oC (NO_2+ ΣPNs). The detection limit (defined as signal to noise of 2 for the 9 s average) of the ΣANs signal is directly related to the magnitude of the

NO_2+ ΣPNs (NP) signal and during ARCTAS was on average < 20 pptv for a 200 pptv NP signal. The ΣANs signal also requires interpolation of the NP signal, which is calculated using a weighted sum of a linear interpolation of the NP signal (weight ~1/3) and an interpolation of the ratio of NP to NO_2 signal scaled to the measured NO_2. The uncertainty in the ΣANs measurement depends both on the magnitude and the variability of the NP signal. On average, the NP signal varied by less than 20% on the timescale of the ΣANs measurements. An example time series of the ΣANs and ΣPNs data is shown in Fig. 4.1.

In the analysis below I use measurements only between 10 and 18 local sun time, which enables us to neglect the possible interference from $ClNO_2$ (Thaler et al., 2011).

In addition to the core measurement of ΣANs, described above, I use the measurements listed in Table 4.1 in the analysis. I use the merged data set from flights over the boreal forest of Canada that took place June 29-July 13, 2008 averaged to the 10 s time base (version 13).

4.3 ΣANs concentration and production

In the continental boundary layer over the boreal forest (0-2 km GPS altitude between 50° and 67.5°N) ΣANs were 20% (median) of NO_y in areas removed from recent anthropogenic or biomass burning influence (Fig. 4.2). These background conditions were defined as CO less than 180 ppbv and NO_x less than 200 pptv with remaining burning and anthropogenic influences removed by visual inspecting the HCN and CH_3CN concentrations. The mean concentrations of CO, CH_3CN, and HCN used in the analysis are lower than the means of the background ARCTAS measurements from Simpson et al. (2011). In this analysis I define NO_y as the sum of the measured individual components of NO_y (NO, NO_2, ΣPNs, ΣANs, gas phase nitric acid, and submicron aerosol nitrate). The observation that ΣANs are of order 20% of NO_y is consistent with almost all past measurements of ΣANs from TD-LIF in continental locations (Day et al., 2003; Rosen et al., 2004; Cleary et al., 2005; Perring et al., 2009a, 2010; Farmer et al., 2011), however, in this data set I find that the instantaneous production rate of ΣANs is larger than the HNO_3 production rate-a situation that has not been reported previously.

Using the measured VOCs, OH, HO_2, and NO concentrations (Table 4.1), I calculate the instantaneous production rate of ΣANs (P(ΣANs) Eq. 4.1) by assuming that peroxy radicals are in steady-state (Eq. 4.2- Eq. 4.3), resulting in Eq. 4.4:

$$P(\Sigma ANs) = \sum_i \alpha_i k_{RO_{2i}+NO}[RO_2]_i[NO] \tag{4.1}$$

$$\frac{d[RO_2]_i}{dt} = k_{OH+VOCi}[OH][VOC]_i - k_{RO_{2i}+NO}[RO_2]_i[NO] - k_{RO_{2i}+HO_2}[RO_2]_i[HO_2] - \sum_j k_{RO_{2i}+RO_{2j}}[RO_2]_i[RO_2]_j - k_{isom}[RO_2]_i \approx 0 \tag{4.2}$$

$$[RO_2]_i \approx \frac{k_{OH+VOCi}[OH][VOC]_i}{k_{RO_{2i}+NO}[NO] + k_{RO_{2i}+HO_2}[HO_2] + \sum_j k_{RO_{2i}+RO_{2j}}[RO_2]_j + k_{isom}} \tag{4.3}$$

$$P(\Sigma ANs) \approx \sum_i \gamma_i \alpha_i k_{OH+VOCi}[OH][VOC]_i \quad (4.4)$$

where

$$\gamma_i = \frac{k_{RO_{2i}+NO}[NO]}{k_{RO_{2i}+HO_2}[HO_2] + k_{RO_{2i}+RO_{2_j}}[RO_2] + k_{RO_{2i}+NO}[NO] + k_{isom}} \quad (4.5)$$

Here, k_{isom} refers to the rate of a unimolecular isomerization reaction of RO_2. This class of reactions has recently been shown to be important when the lifetime of RO_2 is long, such as in low NO_x conditions (Peeters et al., 2009; Peeters and Müller, 2010; Crounse et al., 2011, 2012a). γ (Eq. 4.5) represents the fraction of RO_2 that reacts with NO and it depends on the identity of the RO_2. I calculate a specific γ for monoterpenes (α- and β-pinene), isoprene, methacrolein, and methyl vinyl ketone. All other peroxy radicals (which, as shown below, account for only 4% of the ΣANs production) are assumed to behave like methyl vinyl ketone peroxy radicals. Each of these γ values are calculated using the RO_2+HO_2 rate calculated from the parameterization used in the Master Chemical Mechanism (MCM) v3.2 (Jenkin et al., 1997; Saunders et al., 2003) available at http://mcm.leeds.ac.uk/MCM. I use measured isomerization rates for isoprene peroxy radicals (Crounse et al., 2011) and methacrolein peroxy radicals (Crounse et al., 2012). Although there are theoretical predictions that peroxy radicals derived from monoterpenes undergo a fast ring closure reaction followed by addition of O_2, regenerating a peroxy radical (Vereecken and Peeters, 2004), there are no experimental constraints on the organic nitrate yield for this peroxy radical. I assume that the organic nitrate yield is the same as the parent and thus implicitly assume the isomerization reaction of monoterpene-derived RO_2 is unimportant. I also assume that the isomerization reaction is negligible for the remaining RO_2 species. All γ values use the same rate of reaction for RO_2+NO (from MCM v3.2) and for RO_2+RO_2 (the IUPAC CH_3O_2 + $C_2H_5O_2$ rate available at http://www.iupac-kinetic.ch.cam.ac.uk/ (Atkinson et al., 2006)). In these calculations, the data set that has been merged to the TOGA time base is used and when the measured NO is less than 0 ppt, it is assigned a value of 1 pptv. Due to the more complete data coverage, the LIF measurements of OH and HO_2 are used. Details regarding the VOCs, OH oxidation rates, branching ratios, and uncertainties regarding rate coefficients are described in Appendix B.

The instantaneous production of HNO_3 is calculated using the measured OH and NO_2. The rate constant from Mollner et al. (2010) with the temperature dependence from Henderson et al. (2012) is used.

The total calculated P(ΣANs), shown in Fig. 4.3, is similar to or greater than the calculated nitric acid production. Biogenic species account for the majority (96%) of P(ΣANs) (Fig. 4.4) with isoprene (53%), methyl vinyl ketone (12%), and α and β-pinene (30%) contributing the most production. Due to the rapid isomerization of the methacrolein peroxy radical, very few methacrolein nitrates are formed (< 1% of P(ΣANs)). This conclusion holds for the isoprene branching ratio of 11.7% from Paulot et al. (2009a) as shown in Fig. 4.3 and the lower value of 7% from Lockwood et al. (2010) (details in Appendix B). The time series of ΣANs and isoprene shown in Fig. 4.1 illustrates how increases in ΣANs roughly correspond to increases in the precursors (e.g., isoprene).

Despite this larger production rate of ΣANs than of HNO_3, the median concentration of HNO_3 (sum of gas phase HNO_3 and particulate NO_3^-) is greater than that of ΣANs (Fig. 4.2),

implying a shorter lifetime of ΣANs than of HNO_3. I note that the lifetime of ΣANs represents the loss of the nitrate functionality and thus will be longer than the average lifetime of individual nitrates because oxidation of some nitrates results in products that are more highly functionalized nitrates that are still ΣANs.

4.4 Lifetimes of HNO_3 and ΣANs

The lifetime and fate of ΣANs remains one of the outstanding questions about their chemistry and results in large uncertainties in global ozone budgets. For instance, recent modeling studies have found that the ozone response to increasing isoprene emissions (as predicted in a warmer climate) is highly sensitive to the fate of isoprene nitrates (e.g., Ito et al., 2009; Weaver et al., 2009). The measurements provide a constraint on the ratio of the ΣANs lifetime to the HNO_3 lifetime over the boreal forest.

The lifetime of HNO_3 in the boundary layer is primarily determined by deposition. Using measurements of boundary layer heights (~2 km) in Northern Saskatchewan in July 2002 (Shashkov et al., 2007) and a deposition velocity of 4 cm s^{-1}, I calculate a lifetime of ~14 h for HNO_3. Other losses, photolysis and oxidation by OH, are quite slow with median values of several weeks.

Since ΣANs are produced more rapidly than HNO_3, but are present in lower concentrations, the loss rate of ΣANs must be larger than the HNO_3 deposition rate of 2×10^{-5} s^{-1}. Since it is generally assumed that HNO_3 deposition occurs with unit efficiency at a mass transfer rate set by turbulence, a more rapid ΣANs removal rate implies a significant sink in addition to deposition, in other words, chemistry must be the primary sink of ΣANs. Compared to other aspects of the NO_y, HO_x and VOC chemistry, there has been limited research on products of ΣANs oxidation. Even for those nitrates whose oxidation products and yields have been measured, these measurements have occurred under conditions where the resulting peroxy radicals react primarily with NO and not with HO_2 or RO_2 (which are the expected reactions in the low NO_x conditions of the boreal forest). As recently pointed out by Elrod and co-workers (Darer et al., 2011; Hu et al., 2011), ΣANs may also be removed via hydrolysis in aerosol resulting in the formation of HNO_3.

4.4.1 Deposition

Deposition is likely a significant term in the ΣANs budget. The measured Henry's law coefficients of some of the more soluble individual $RONO_2$ (~10^3-10^5 M atm^{-1} (Shepson et al., 1996; Treves et al., 2000)) are orders of magnitude lower than that of HNO_3 (1×10^{14} M atm-1 at pH ~6.5 (Seinfeld and Pandis, 2006)). Still these measured Henry's law coefficients for hydroxy nitrates indicate that wet deposition is a significant loss process (Shepson et al., 1996; Treves et al., 2000) and a recent study indicates that foliar uptake of organic nitrates is possible (Lockwood et al., 2008). The only direct simultaneous measurements of ΣANs and HNO_3 deposition are those of Farmer and Cohen (2008) who estimated a ΣANs dry deposition velocity of 2.7 cm s^{-1} compared to 3.4 cm s^{-1} for HNO_3 above a ponderosa pine forest. Similar results have been obtained more recently at the same forest (K.-E. Min, private communication). Although the exact magnitude of the depositional loss likely depends on the specific composition of ΣANs, I assume that the result is similar for the boreal forest since it is also dominated by pine

trees. These results suggest an overall lifetime of ΣANs that is ~25% longer than that of HNO_3 implying the existence of other ΣANs loss processes.

4.4.2 Photolysis

Oxidation of both isoprene and monoterpenes produces hydroxy nitrates as the first generation products. These molecules account for at least 83% of the instantaneous production rate of ΣANs (Fig. 4.4). Although there are no direct measurements of the photolysis rates of these specific molecules, by analogy to other compounds it is estimated that photolysis is a negligible sink for them. Roberts and Fajer (1989) report that the cross section of nitrooxy ethanol is approximately a factor of three smaller than methyl nitrate (which has a summertime lifetime of greater than 24 days). Similarly, photolysis rates of alkyl nitrates (median 29% of the ΣANs) are on the order of days (Roberts and Fajer, 1989; Barnes et al., 1993; Talukdar et al., 1997a) and are thus too slow to be important. Nitrates containing a carbonyl functionality, in contrast, are thought to photolyze more rapidly (Roberts and Fajer, 1989; Barnes et al., 1993). The calculations suggest these are too small a fraction of the total to affect the overall lifetime. To estimate an upper limit, I assume that 12% of the nitrates (the methyl vinyl ketone contribution in Fig. 4.4) contain a carbonyl. Using the photolysis rate from Barnes et al. (1993) for nitroxy acetone on July 1 at noon at 40°N, this results in an overall photolysis rate for ΣANs of 3.9×10^{-6} s^{-1}, a rate that even when combined with deposition is too slow to account for the inferred ΣANs loss.

4.4.3 Oxidation

The overall gas-phase chemical removal rate of ΣANs can be represented as:

$$k_{ox-loss} = \sum_i k_{AN_i+OX}[OX]\frac{[AN_i]}{[\Sigma ANs]}\chi_i \quad (4.6)$$

where [OX] represents the concentration of oxidant (OH, O_3, or NO_3), [AN_i] represents the concentration of a specific nitrate, k_{ANi+OX} the rate constant of that oxidant with the specific nitrate, and χ the fraction of the reaction that results in loss of the nitrate functionality (referred to as NO_x recycling). To simplify the calculation, I neglect the formation of dinitrates, which would result in a small positive term in Eq. (4.6), and ignore oxidation by NO_3 since I use only daytime measurements.

I estimate the composition of ΣANs as a mixture of the small organic nitrates measured in the whole air samples and molecules that can be estimated from the instantaneous production rate of ΣANs (Fig. 4.4). The small nitrates have very long lifetimes and are a negligible term in the overall loss rate. I use oxidation rates of isoprene (assuming 60% δ-hydroxy isoprene nitrates and 40% β-hydroxy isoprene nitrates) and methyl vinyl ketone nitrates by OH based on Paulot et al. (2009a). The ozone oxidation rates measured by Lockwood et al. (2010) of the isoprene nitrates are isomer specific. I assume that the δ-hydroxy nitrates all react with the rate constant of the E-1,4 nitrate and bound the isoprene nitrate ozonolysis rate by assuming that all the β-hydroxy nitrates react with ozone either following the 1,2 isomer rate or the 2,1 isomer rate from Lockwood et al. (2010). This results in an ozonolysis rate ranging from 7.4×10^{-17} cm^3 $molecules^{-1}$ s^{-1} to 1.7×10^{-16} cm^3 $molecules^{-1}$ s^{-1}. Results using the branching ratio between the δ

and β hydroxy nitrate channels as determined by Lockwood et al. (2010) are included in Appendix C.

I am unaware of any experimental constraints on the oxidation rate of monoterpene nitrates by OH and I estimate an OH oxidation rate constant of 4.8×10^{-12} cm^3 $molecules^{-1}$ s^{-1} based on a weighting of the MCM v3.2 rates for α-pinene and β-pinene nitrates as described in Chapter 5. The monoterpene nitrates in the calculations are based on the production from the observed concentrations of α- and β-pinene. These nitrates will predominately be saturated molecules and thus ozonolysis of these nitrates should be too slow to be important.

The NO_x recycling following OH oxidation depends on the fate of the resulting nitroxy peroxy radical ($R(NO_3)O_2$), which may react with NO, HO_2, or other RO_2. I assume that reactions with HO_2 generate a more highly functionalized nitrate and that the NO_x recycling (the loss of the nitrate functionality) occurs with the same efficiency through both the $R(NO_3)O_2$+NO and $R(NO_3)O_2$+RO_2 channels. I use the same assumptions for the $R(NO_3)O_2$+HO_2 rate as in the calculation of γ in section 3, however, I assume that no isomerization reactions occur. I find that RO_2+RO_2 reactions account for at most 1 % of the RO_2 reactions. NO_x recycling from the RO_2+NO reaction have been constrained by laboratory experiments to be ~55% for isoprene nitrates and 100% for MVK nitrates (Paulot et al., 2009a). I am unaware of any measurements of NO_x recycling from monoterpene nitrates and assume a value of 100% as an upper limit. The contribution (as calculated below) from monoterpene nitrates to NO_x recycling is negligible making a more accurate estimate unnecessary.

NO_x recycling following ozonolysis of unsaturated nitrates (isoprene nitrates) depends on the initial branching of the ozonide to the two possible pairs of a carbonyl molecule and an energy-rich Criegee biradical and the subsequent fate of the Criegee biradical (stabilization or decomposition). To my knowledge, no experimental constraints on this process exist for any unsaturated organic nitrate. The MCM v3.2 assumes equal branching between the two possible carbonyl/Criegee biradical pairs; I calculate NO_x recycling (40%) using the MCM v3.2 products of the ozonolysis of isoprene nitrates, the assumption that a stabilized Criegee biradical reacts only with water, and the relative abundances of the different isoprene nitrate isomers from Paulot et al. (2009a) (ignoring the minor 3,4 and 2,1 isomers). Using the relative abundances of the different isoprene nitrate isomers from Lockwood et al. (2010) results in a NO_x recycling of 37%.

The calculation of the ΣANs loss rate can be summarized by expanding Eq. 4.6 to:

$$k_{ox-loss} = \sum_i k_{AN_i+OH}[OH]\frac{[AN_i]}{[\Sigma ANs]}\beta_i(1-F_{RO_{2i}+HO_2}) + \sum_i k_{AN_i+O_3}[O_3]\frac{[AN_i]}{[\Sigma ANs]}\delta_i \quad (4.7)$$

$$F_{RO_2+HO_2} = \frac{k_{RO_{2i}+HO_2}[HO_2]}{k_{RO_{2i}+NO}[NO] + k_{RO_{2i}+HO_2}[HO_2] + \sum_j k_{RO_{2i}+RO_{2j}}[RO_{2j}]} \quad (4.8)$$

Here, β represents the fraction of NO_x recycled following the reaction of the peroxy radical with RO_2 or NO, $F_{RO_2+HO_2}$ (Eq. 4.8) represents the fraction of the time that the peroxy radical reacts with HO_2 (and thus does not recycle NO_x), and δ represents the NO_x recycling from ozonolysis. Uncertainties regarding this calculation are described in Appendix C.

Using the assumptions above, I calculate a chemical ΣANs lifetime of ~10-22 h (Table 4.2) that ranges from slightly shorter to slightly longer than the estimated HNO_3 lifetime (~14

hours). In combination with deposition (~17.5 h for a 2 km boundary layer), a detailed representation of oxidative ΣANs loss results in a calculated ΣANs lifetime approximately equal to or shorter than the assumed lifetime of HNO_3. In these calculations, the majority of ΣANs loss occurs via isoprene nitrate ozonolysis, which has recently been reported to be much faster than previously assumed (Lockwood et al., 2010). Additional measurements of this rate and the products are important to constraining our understanding of ΣANs and their role in the NO_x budget.

4.4.4 Hydrolysis of particulate organic nitrates

4.4.4.1 Loss of ΣANs

I note that using the ARCTAS data I am unable to constrain the exact magnitude of the ΣANs loss rate. To do so would require knowledge of the photochemical age of the airmass and the history of ΣANs production, which is likely to have significant vertical gradients. Although I calculate a chemical ΣANs loss rate that is similar to the assumed loss rate of HNO_3, the recent suggestion that organic nitrates may undergo hydrolysis in aerosols to produce HNO_3 as a product (Sato, 2008; Darer et al., 2011; Hu et al., 2011) is also a viable hypothesis. Evidence for organic nitrates losses in ambient particles analyzed with IR spectroscopy is consistent with this mechanism (Day et al., 2010). This chemistry results in the depletion of ΣANs and an enhancement in HNO_3; both effects would contribute to the ratio of ΣANs to HNO_3 lifetimes I report here.

Bulk solution studies of hydrolysis of organic nitrates indicate that primary and secondary nitrates are stable at atmospherically relevant pH, but that the lifetime of tertiary hydroxy organic nitrates is surprisingly short (0.019-0.67 hours), even in neutral solutions (Darer et al., 2011; Hu et al., 2011). I estimate the loss of ΣANs to hydrolysis using absorptive partitioning theory to determine the fraction of the nitrate in the particle phase (Pankow, 1994):

$$K_p = \frac{C_a}{C_g M_{om}} = \frac{760 \cdot R \cdot T}{MW_{om} \cdot 10^6 \cdot \zeta \cdot p_{vap}} \quad (4.9)$$

Here C_a represents the concentration of the compound (an organic nitrate) in the condensed phase (μg m^{-3}), C_g the concentration of the organic nitrate in the gas phase (μg m^{-3}), M_{om} is the concentration of organic aerosol (μg m^{-3}). In the second equality, R is the universal gas constant (8.206×10^{-5} atm m^3 K^{-1} mol^{-1}), MW_{om} is the average molecular weight of the organic aerosol (assumed here to be 215 g mol^{-1} (Fry et al., 2009)), ζ is the activity coefficient (assumed to be 1), p_{vap} is the vapor pressure of the organic nitrate partitioning into the aerosol (torr), and 760 and 10^6 are unit conversion factors. I assume that only monoterpene nitrates partition into aerosol since the vapor pressures of first generation isoprene nitrates are generally too high (Rollins et al., 2009) and calculate an estimated bound on this partitioning using vapor pressures of 4×10^{-6} torr derived from chamber measurements of nitrate products of the NO_3 + β-pinene reaction (Fry et al., 2009) and of 9.6×10^{-7} torr from chamber measurements of the NO_3+limonene reaction (Fry et al., 2011). I use the AMS measurement of organic aerosol concentration. The fraction of the compound in the aerosol is then calculated using Eq. 4.10.

$$F_{aero} = \frac{C_a}{C_a + C_g} = \frac{K_p M_{om}}{1 + K_p M_{om}} \quad (4.10)$$

I then calculate the loss rate of ΣANs through hydrolysis ($k_{hyd\text{-}loss}$) using Eq. 4.11:

$$k_{hyd-loss} = \sum_i k_{hyd} F_{aero,i} F_{tertiary,i} \frac{[AN_i]}{[\Sigma ANs]} \quad (4.11)$$

where k_{hyd} represents the hydrolysis rate constant, F_{aero} the fraction of a given nitrate in the aerosol, and $F_{tertiary}$ the fraction that is tertiary nitrate. I set $F_{tertiary}$ at 75%, midway between the 63% for α-pinene nitrates and 92% for β-pinene nitrates from MCM v3.2. Darer et al. (2011) and Hu et al. (2011) reported a range of neutral hydrolysis lifetimes of 0.019-0.67 h for tertiary organic nitrates. In Table 4.3 I show the median calculated ΣANs loss rates assuming a vapor pressure of 4×10^{-6} torr and a hydrolysis lifetime of 0.67 hours (case A), the same vapor pressure with a 0.12 hour lifetime (case B) and at a vapor pressure of 9.6×10^{-7} torr with a lifetime of 0.67 hours (case C). This calculated loss rate ranges from being ~2.5 times larger than the oxidative loss rate of isoprene nitrates by OH to being greater than the oxidative loss rate of isoprene nitrates by O_3. These numbers correspond to a range of lifetimes for ΣANs to hydrolysis of ~7.5-42 h and an overall lifetime using the slower oxidation rate from Table 4.2 of ~6-14 h. I find no combination of reasonable assumptions where it is possible to neglect this contribution to the ΣANs loss.

4.4.4.2 Production of HNO_3

I am unable to put a numerical constraint on the hydrolysis loss of ΣANs and its corresponding influence on HNO_3 due to the chemical complexity of the system. In particular, this process depends on the composition of ΣANs and knowledge of the hydrolysis rate. In the calculation I have assumed an average composition of ΣANs based on the speciation of the calculated instantaneous production rate. By necessity, this entails that I am only considering first generation nitrates. It is likely that the ΣANs concentration includes contributions from higher generation nitrates, which likely have lower vapor pressures than their first generation counterparts. Thus, it is possible that tertiary nitrates derived from VOCs other than monoterpenes (e.g., isoprene) may partition to the aerosol and undergo hydrolysis. Furthermore, based on the data of Darer et al. (2011) and Hu et al. (2011) the hydrolysis rate appears to depend on the structure of the nitrate.

However, the range of rates from above include a range of the ΣANs source of HNO_3 that spans being just over half the size of the rate of OH+NO_2 to more than three times larger than that rate (Table 4.3). The variation of the ratio of HNO_3 to NO_2 with NO_x also supplies evidence that ΣANs are an HNO_3 source. In the boundary layer when the lifetime of HNO_3 is short, HNO_3 is in photochemical steady state and the ratio of HNO_3 to NO_2 should be proportional to the OH concentration (Day et al., 2008). I estimate the lifetime of HNO_3 with respect to deposition (τ_{dep} = 1/(v_{dep}/boundary layer height)) to be ~14 hours (assuming a deposition velocity (v_{dep}) of 4 cm s^{-1} and a boundary layer height of 2 km), a value short enough that HNO_3 should be in diurnal steady state. However, as NO_x decreases the ratio of HNO_3 to NO_2 increases while the OH concentration decreases (Fig. 4.5a). These higher HNO_3 to NO_2 ratios are associated with higher ΣANs concentrations (Fig. 4.5a) as well as with higher monoterpene concentrations (and thus presumably higher aerosol ΣANs concentration-not shown) consistent with a source of HNO_3 from ΣANs. This trend of increasing values as NO_x decreases is also the same trend as

the ratio of P(ΣANs) to P(HNO_3) (where P(HNO_3) = k_{OH+NO_2}[OH][NO_2]) as shown in Fig. 4.5b using results from the steady-state model in Chapter 3. The similarity in magnitude between the HNO_3 to NO_2 ratio and the P(ΣANs) to P(HNO_3) ratio is expected if the hydrolysis of ΣANs constitutes the major loss process of ΣANs. These results suggest that the ARCTAS HNO_3 concentration is consistent with a source of HNO_3 other than the reaction of OH with NO_2 and that this source may be the hydrolysis of ΣANs. There are similar hints of this source in a reinterpretation of data from previous experiments.

Previous measurements of ΣANs in a ponderosa pine forest have found evidence for a temperature dependent OH source (Day et al., 2008) and of elevated within-canopy OH (Farmer and Cohen, 2008). These interpretations are also consistent with a source of HNO_3 from fast ΣANs hydrolysis. The temperature dependence may be due to an increase in biogenic VOC emissions with temperature resulting in a larger ΣANs production and consequently a larger HNO_3 source. Likewise, the fast hydrolysis of ΣANs with low vapor pressures formed from sesquiterpenes and monoterpenes in the forest canopy would result in a within canopy source of HNO_3. The hydrolysis of ΣANs is consistent with OH measurements made in the same ponderosa pine forest a few years later that report an in-canopy OH gradient and an OH temperature dependence smaller than inferred in the previous studies (Mao et al., 2012). However, I note that these studies were conducted in different years and it is possible that the ecosystem has changed.

It is interesting to consider the ultimate fate of the NO_3^- possibly produced by the organic nitrate hydrolysis. In ~60% of the filtered data the molar ratio of sulfate to ammonium is greater than one-half, indicating that it is unfavorable for NO_3^- to be present in the aerosol and that ΣANs hydrolysis is possibly a source of gas phase HNO_3. However, this is a simplistic approximation to an extremely complex problem. Presumably, organic nitrates will partition into organic phase of aerosol. The thermodynamics of an aerosol that is an organic-inorganic mixture are much more complex (Zuend et al., 2011) than purely inorganic aerosols and are subject to uncertainties regarding the composition of aerosol and the interaction of ions with various functional groups present on organic species. Further studies on organic nitrate hydrolysis in aerosols are needed to better constrain the atmospheric impacts, however it appears that the hydrolysis of organic nitrates may contribute (quite significantly) to HNO_3 production.

These results suggest the need for significant work on constraining the possible hydrolysis loss of ΣANs. In particular, measurements of how the hydrolysis of organic nitrates differs in aerosol versus bulk solution, the aerosol liquid water content necessary for this reaction, and rates for monoterpene nitrates are needed.

4.5 Implications

As shown in Fig. 4.3, the calculated ΣANs production is in good agreement with the steady-state model results from Chapter 3 if I assume a branching ratio somewhere between 5% and 10% for ΣANs formation from the entire VOC mixture. For the ARCTAS data I calculate that the biogenic VOCs account for ~63% of the VOC reactivity (median value). Assuming that the biogenic VOCs are the only sources of ΣANs with an average branching ratio of 11% (similar to isoprene), this results in an overall branching ratio of ~7%. This suggests that the NO_x lifetime and ozone production efficiency in the boreal forest are similar to those calculated

in Chapter 3 and that the steady-state model provides a useful framework for understanding the NO_x budget under low NO_x conditions on the continents.

However, as discussed in Chapter 3, the net regional and global impact of ΣANs on NO_x lifetime and ozone production depends on the degree to which ΣANs serve as a permanent versus temporary NO_x sink. Modeling studies have found that different assumptions regarding NO_x recycling from isoprene nitrates result in large sensitivities in NO_x and O_3 (e.g., von Kuhlmann et al., 2004; Fiore et al., 2005; Horowitz et al., 2007; Wu et al., 2007) and that these uncertainties affect predictions of ozone in a future climate (e.g., Ito et al., 2009; Weaver et al., 2009). The analysis presented here suggests that ΣANs have a short atmospheric lifetime due to a combination of deposition and chemical loss, but I find the data is ambiguous about the relative fraction of ΣANs that react to release NO_x or to produce HNO_3. Furthermore, the exact fate of ΣANs loss is likely ecosystem dependent; for instance, ΣANs may have a significantly different impact on the NO_x budget in forests dominated by isoprene emissions versus in forests dominated by monoterpene emissions since first generation monoterpene nitrates have lower vapor pressures than first generation isoprene nitrates.

Due to the lumped treatment of ΣANs in most condensed chemical mechanisms, these mechanisms most likely are unable to reproduce the ARCTAS results, leading to problems in the calculation of NO_x lifetime and ozone production. For instance, some condensed mechanisms instantaneously convert isoprene nitrates to HNO_3, resulting in zero NO_x recycling. The ozonolysis of isoprene nitrates is also ignored in many mechanisms; this is incompatible with the results that the majority of NO_x recycling during ARCTAS results from ozonolysis. Lastly, many condensed mechanisms ignore monoterpene nitrates or lump them into a long lived nitrate. The results here suggest that, at least in the boreal forest, monoterpene nitrates are an important NO_x sink and that their particle phase hydrolysis may represent a source of HNO_3.

Finally, it is interesting to note that since the loss of ΣANs through hydrolysis depends on the specific isomer of the nitrate, there are interesting implications for the loss of monoterpene nitrates formed from OH versus from NO_3 chemistry. Based on the assumption that tertiary radicals are more stable than primary radicals and thus have a higher yield, the oxidation of α- or β-pinene and limonene by NO_3 is more likely to result in a primary nitrate and oxidation by OH is more likely to result in a tertiary nitrate. Thus, nitrates formed by OH oxidation may have a shorter atmospheric lifetime than those formed from NO_3 chemistry.

4.6 Conclusions

I present the first measurements of ΣANs in the remote boreal forest of Canada and show that ΣANs are present in significant concentrations. Using measurements of VOCs I calculate the instantaneous production rate of ΣANs and find that, as expected for a remote forested environment, biogenic species dominate the ΣANs production. I find that monoterpenes contribute ~30% to the production rate, implying a significant role for monoterpene nitrates in the NO_x budget; if the observations of α- and β-pinene underestimate the total source of monoterpenes (as is typical of observations in the boreal forest of Finland (e.g., Spirig et al., 2004; Räisänen et al., 2009; Hakola et al., 2012)) then monoterpenes play an even larger role. I also find that the instantaneous production rate of ΣANs is greater than that of gas phase HNO_3 production, despite a lower overall concentration. This implies that ΣANs have a shorter lifetime than HNO_3. I estimate that depositional loss of ΣANs is important, but insufficient to explain the

lifetime of ΣANs and therefore that chemical loss must be important. If I assume that the speciation of ΣANs is a combination of the long-lived, short chain alkyl nitrates measured in the whole air samples and the speciation of the instantaneous production rate, I calculate that the median loss rate of ΣANs to reaction with O_3 and OH is similar to the assumed deposition rate of HNO_3. Oxidation of isoprene nitrates, in particular by O_3, is primarily responsible for the fast loss rate.

I next investigate the possibility that particulate organic nitrates undergo rapid hydrolysis, and find that the ARCTAS data is consistent with hydrolysis of ΣANs contributing to HNO_3 production. Using assumptions regarding the ΣANs composition and literature values of vapor pressures and hydrolysis rates, I calculate the loss rate of ΣANs through hydrolysis for three different possibilities. Although, I am unable to constrain the magnitude of this source, all reasonable assumptions imply that it is a non-negligible loss. Furthermore, there is evidence of its existence in the variation of the HNO_3 to NO_2 ratio as a function of NO_x. This suggests that the chemical loss of ΣANs consists of two channels: one that recycles NO_x and one that removes it.

Species	Method	Reference
VOCs[a]	Whole air sampling	Blake et al. (2003)
VOCs[a]	Gas chromatography - mass spectrometry	Apel et al. (2003)
VOCs[a]	Proton transfer reaction mass spectrometry	Wisthaler et al. (2002)
CH_4	Tunable diode laser absorption spectroscopy	Sachse et al. (1987)
NO, O_3	Chemiluminescence	Weinheimer et al. (1994)
OH,HO_2	Laser Induced Fluorescence	Faloona et al. (2004)
	Chemical ionization mass spectrometry	Cantrell et al. (2003a)
HNO_3	Chemical ionization mass spectrometry	Crounse et al. (2006)
Submicron aerosol nitrate and organic aerosol	Aerosol mass spectrometry	DeCarlo et al. (2008)

[a]A full list of the VOCs from each measurement technique can be found in Appendix B.

Table 4.1 Species and measurement techniques used in this chapter in addition to the core measurement of ΣANs and NO_2.

	k_{AN+OX} [OX]	$[AN_i]/[\Sigma ANs]$	β or δ	$(1-F_{RO2+HO2})$	Loss rate (s^{-1})
Isoprene	6.2E-11 [OH]	0.38	0.55	0.24	2.57E-06
Isoprene	1.7E-16 [O_3] (7.4E-17[O_3])	0.38	0.40	N/A	2.06E-05 (8.95E-06)
MVK	0.56E-11 [OH]	0.09	1	0.27	1.06E-07
Monoterpenes	4.8E-12 [OH]	0.21	1	0.20	1.64E-07
				Total	2.66E-05 (1.27E-05)

Table 4.2 Median oxidation rates calculated using the assumptions from the text. Here k_{AN+OX} refers to the rate of reaction with the class of organic nitrates with either OH or O_3, β and δ refer to the NO_x recycling following reaction with OH or O_3 (respectively), and $(1-F_{RO_2+HO2})$ refers to the fraction of RO_2 reactions that lead to NO_x recycling (i.e., the fraction of the time RO_2 reacts with either NO or other RO_2). The two numbers listed for the isoprene + O_3 rate reflect the range in possible β-hydroxy isoprene nitrate ozonolysis rates.

	k_{hyd} (s^{-1})	p_{vap} (torr)	F_{aero}	[Monoterpene nitrates]/ [ΣANs]	$k_{hyd\text{-}loss}$ (s^{-1})	$k_{hyd\text{-}loss}$[ΣANs]/ (k_{OH+NO2}[OH][NO_2])
A	4.15E-04	4.00E-06	0.11	0.21	6.58E-06	0.58
B	2.30E-03	4.00E-06	0.11	0.21	3.68E-05	3.27
C	4.15E-04	9.60E-07	0.34	0.21	2.10E-05	1.97

Table 4.3 Median calculated loss rate of ΣANs due to hydrolysis in the particle phase assuming that only monoterpene nitrates may partition into the aerosol and hydrolyze. I consider three cases (A, B, and C) that span different vapor pressures and hydrolysis rates. Here, F_{aero} refers to the fraction of the nitrate that would be in the aerosol based on partitioning theory and observed loadings and $k_{hyd\text{-}loss}$ refers to the calculated median ΣANs loss rate. The last column shows the median of the ratio of this HNO_3 source to the source from the reaction of OH with NO_2.

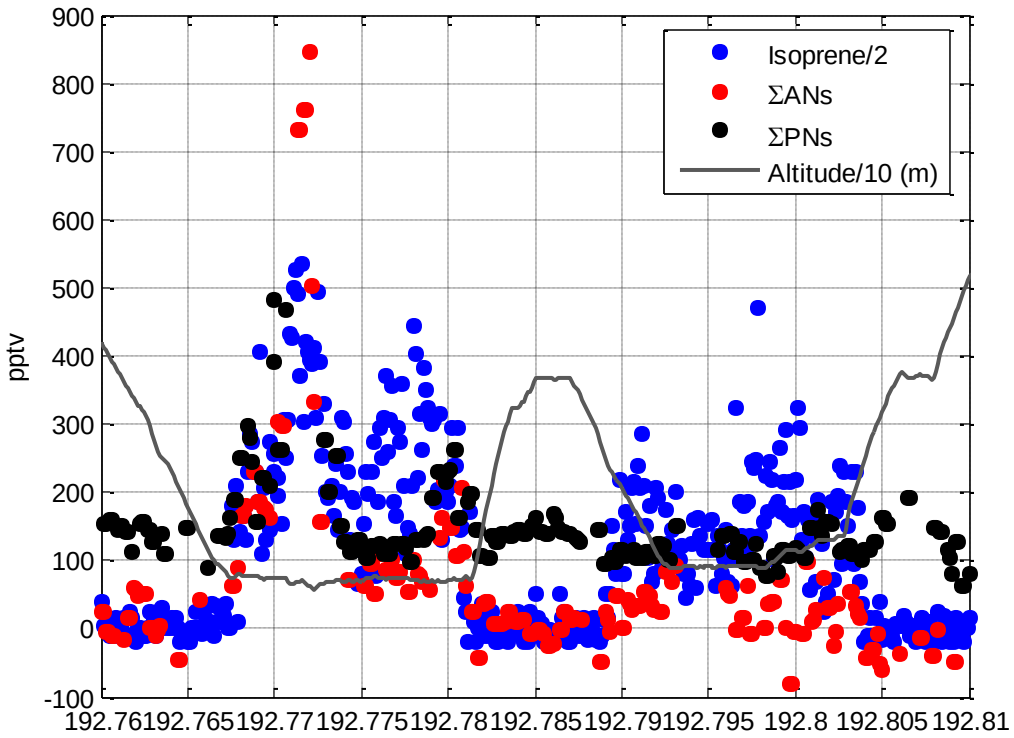

Figure 4.1 An example of the ΣANs, ΣPNs, and isoprene (from the PTRMS) concentrations. The solid line is the altitude of the plane. The data is from the 10 second merge, version 13.

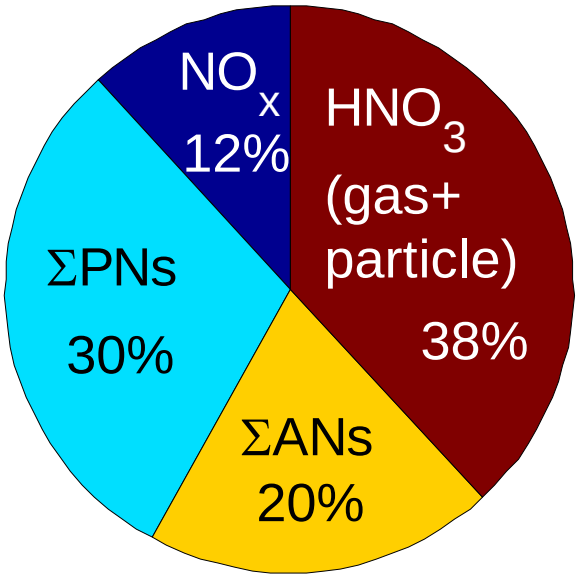

Figure 4.2 NO_y composition in the boundary layer over the remote boreal forest. Submicron particulate NO_3^- is generally ~17% (median) of the total HNO_3.

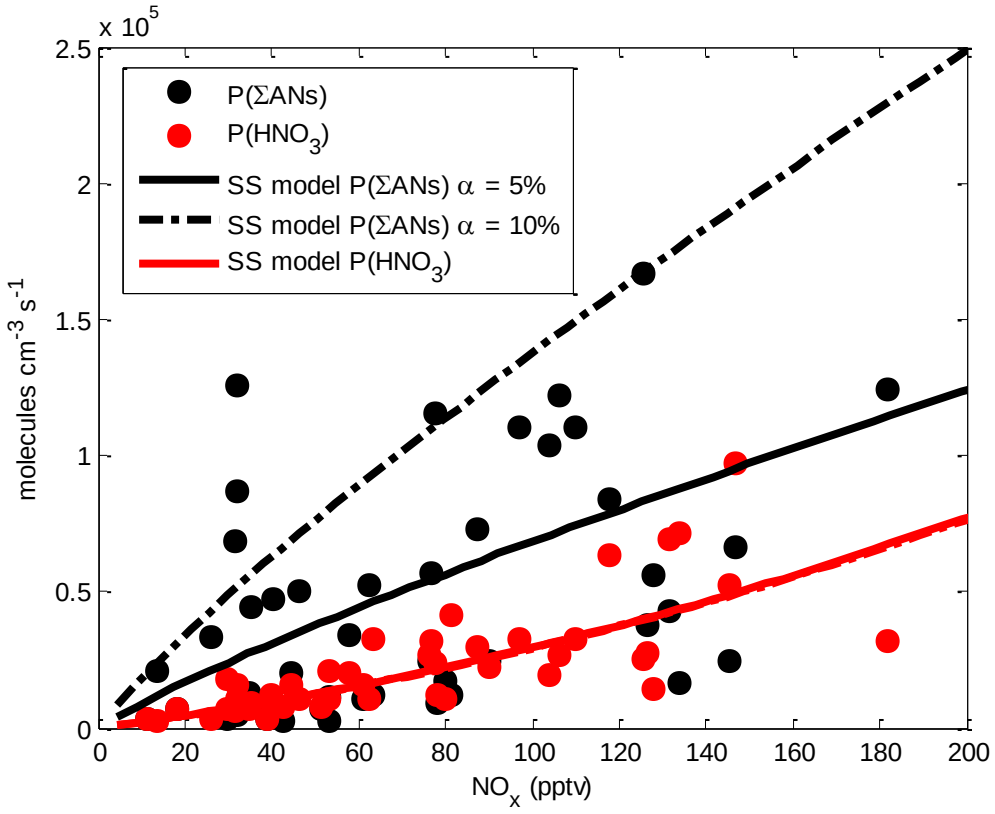

Figure 4.3 Calculated instantaneous production rates of HNO_3 (red) and ΣANs (black) as a function of NO_x. The points are calculated using in situ observations as described in Appendix A. The lines are calculations from the steady state model described in Chapter 3. The two lines shown assume branching ratios of 5% (solid black line) and 10% (dashed black line) for ΣANs production.

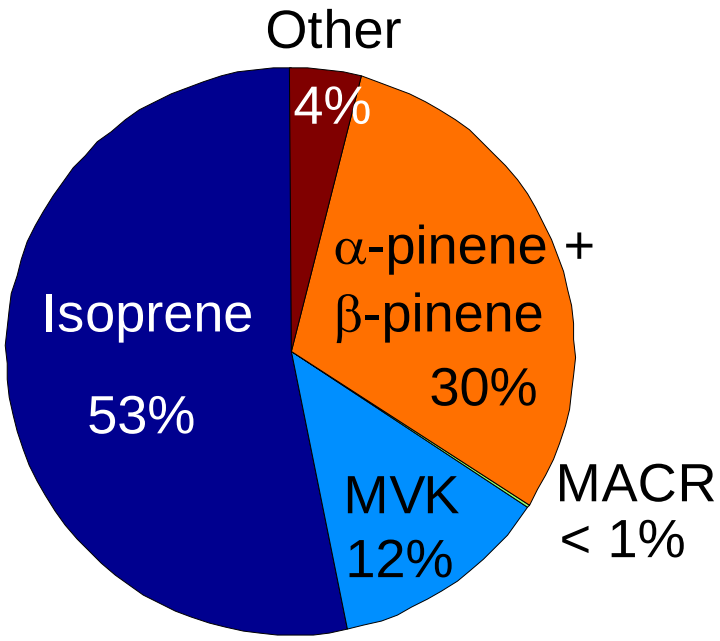

Figure 4.4 Sources of the instantaneous production rate of organic nitrates in the boundary layer over the remote boreal forest. Details of the calculation are described in Appendix B.

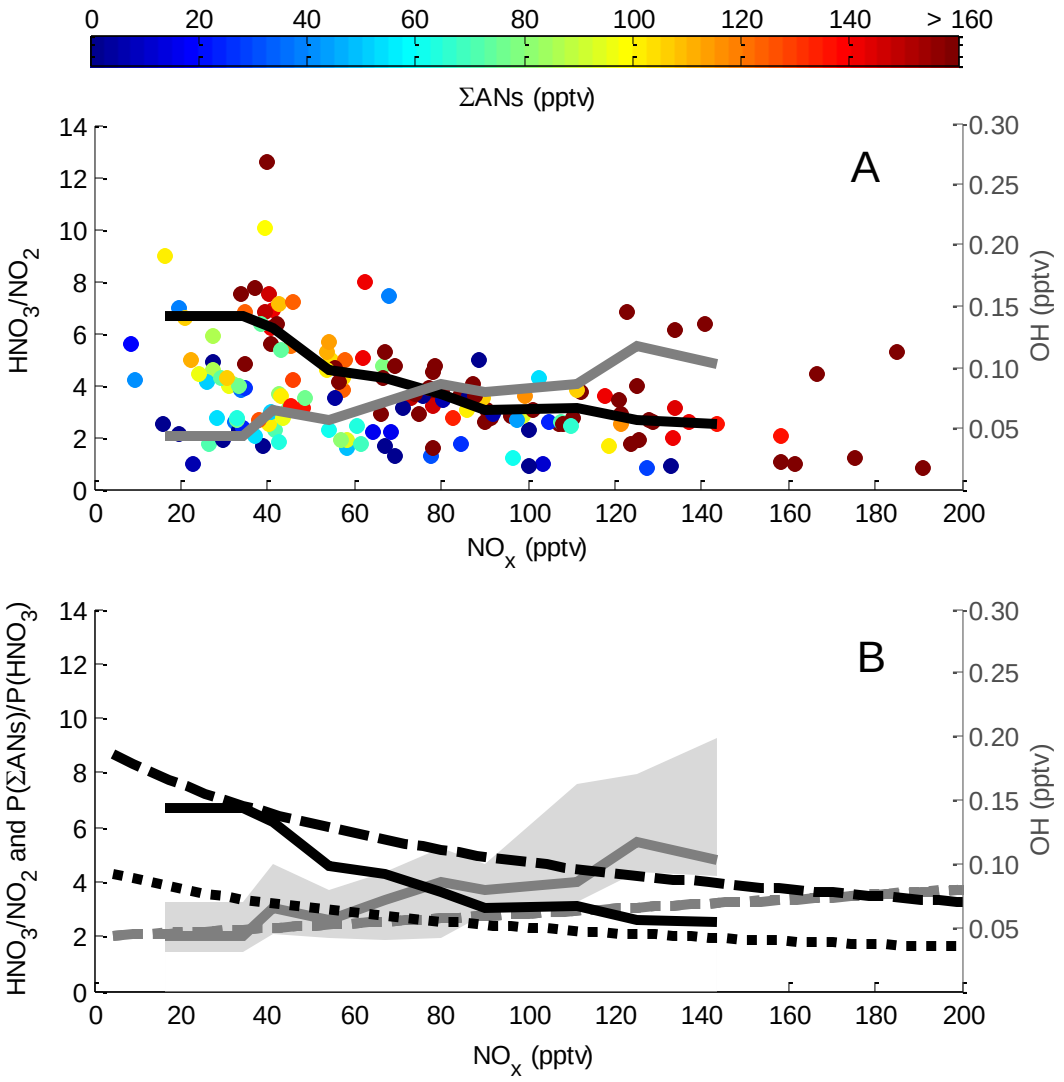

Figure 4.5 A) On the left y-axis is the ratio of HNO_3 (gas+particle) to NO_2 versus NO_x colored by ΣANs concentration. The solid lines are binned median values of points corresponding to ΣANs concentrations ≥ 100 pptv (55% of the data) for the ratio of HNO_3 to NO_2 (black line, left y-axis) and for OH concentration (grey line, right y-axis). **B)** Comparison between the ARCTAS measurements and predictions from the steady-state model described in Chapter 3. The solid lines are the same as in Fig. 5a with the shaded grey area representing the interquartile range of the OH concentration. The dashed and dotted black lines represent the steady state model predictions of the ration of ΣANs production to HNO_3 production for branching ratios of 10% and 5% respectively (left y-axis). The dashed grey line represents the steady-state model prediction of the OH concentration (right y-axis).

Chapter 5

On the role of monoterpene chemistry in the remote continental boundary layer

5.1 Introduction

Measurements of concentrations and fluxes indicate that monoterpenes are emitted to the atmosphere at rates large enough to affect OH concentrations and to contribute a large fraction of the secondary organic aerosol (SOA) mass in such diverse environments as the Amazon (e.g., Karl et al., 2007), the Mediterranean (e.g., Owen et al., 1997; Davison et al., 2009; Seco et al., 2011), pine forests of western North America (e.g., Bouvier-Brown et al., 2009; Kim et al., 2010), the boreal forest (e.g., Spirig et al., 2004; Räisänen et al., 2009; Hakola et al., 2012), and in urban regions of California's central valley (Rollins et al., 2012). While there is a growing body of laboratory and field measurements related to monoterpene SOA (e.g., Tunved et al., 2006; Williams et al., 2007; Fry et al., 2009; Hallquist et al., 2009; Rollins et al., 2009; Slowik et al., 2010; Fry et al., 2011), the gas phase chemistry of monoterpenes that must precede SOA formation has not been explored in detail with chemical transport models (CTMs). In part this is due to the uncertainties in isoprene chemistry that, until recently, were so large that they overwhelmed any uncertainties in modeling monoterpene chemistry. With substantial progress in understanding isoprene oxidation sequences (e.g., Paulot et al., 2009a, 2009b; Peeters and Müller, 2010), it is timely to consider the role of the gas phase chemistry of monoterpenes in more detail.

In the remote continental boundary layer, I have shown in Chapters 3 and 4 that total $RONO_2$ (ΣANs) formation is the primary reaction determining the lifetime of NO_x. Thus, over regions where monoterpene emissions are important to the total OH and NO_3 reactivity, the formation of monoterpene nitrates (MTNs) can be expected to affect the NO_x lifetime, which, in turn, will affect OH concentrations and the ozone production efficiency. In Chapter 4 I used observations of volatile organic compounds (VOCs), OH, and NO_x to calculate that the instantaneous production of ΣANs is more rapid than production of HNO_3 over the Canadian boreal forest and that a significant fraction of the ΣANs production rate is due to the oxidative chemistry of α and β-pinene. These are the two most abundant monoterpenes on the global scale and thus insights from the Canadian forests are likely of relevance to other locations. The analysis of observations described in Chapter 4 also indicates that the lifetime of ΣANs is shorter than that of HNO_3 over the boreal forest, and that this short lifetime is due to a combination of oxidation of ΣANs resulting in the return of NO_x to the atmosphere (NO_x recycling), deposition, and the hydrolysis of particulate ΣANs (forming HNO_3). Each of these loss processes have different implications for the NO_x budget since the first one recycles NO_x, converting a reservoir species back to the active radical pool while the latter two result in rapid removal of odd-nitrogen from the atmosphere.

In this chapter, I explore the consequences of MTNs chemistry for nitrogen oxides as well as the drivers of atmospheric oxidative chemistry (e.g., OH, O_3) using WRF-Chem (Weather Research and Forecasting model with Chemistry) (Grell et al., 2005), a regional

chemical transport model. To study this chemistry I have added an extended representation of organic nitrate chemistry to the chemical mechanism. I begin with a comparison between the model calculations and observations from the NASA ARCTAS (Arctic Research of the Composition of the Troposphere from Aircraft and Satellites) campaign (Jacob et al., 2010) over the Canadian boreal forest showing that the model with the expanded chemical mechanism captures the observed features of NO_y ($NO_y = NO + NO_2 + NO_3 + 2 \times N_2O_5 + HNO_3 + HONO +$ peroxy nitrates + ΣANs + …) and HO_x ($HO_x = OH + HO_2$) concentrations in this region. I then explore the relative contributions of OH and NO_3 chemistry to the production of MTNs and investigate how the total production impacts NO_y partitioning. To understand the range of possible roles for MTNs I examine their sinks, comparing model predictions for several atmospheric constituents in scenarios where oxidation of MTNs results in the release of NO_x to predictions where the ONO_2 functional group is retained as an organic nitrate.

5.2 Model description

5.2.1 Domain and emissions

I use WRF-Chem v3.2.1 (Grell et al., 2005) at 36 km x 36 km resolution over a 5364 km (East-West) by 3384 km (North-South) domain centered over Canada. I discard data from the outer 180 km of the domain to allow for relaxation of boundary conditions taken from MOZART-4 model (Emmons et al., 2010) using meteorology from GEOS-5 (available at http://www.acd.ucar.edu/wrf-chem/). Meteorological data is from the North American Regional Reanalysis and I run the model for six days prior to simulating the time period corresponding to the ARCTAS measurements over the Canadian boreal forest from June 29 to July 13, 2008. I do not aim to directly simulate the ARCTAS conditions, but rather to investigate the impacts of MTNs on NO_x and O_3 in the boreal forest. To that end, I do not include fire emissions in the model. Anthropogenic emissions are from RETRO (Reanalysis of Tropospheric composition) and EDGAR (Emissions Database for Global Atmospheric Research) using the global emissions preprocessor for WRF-Chem (Freitas et al., 2011) and biogenic emissions are from MEGAN (Guenther et al., 2006) available at http://www.acd.ucar.edu/wrf-chem/. In order to achieve approximate agreement with the ARCTAS observations of NO_x and biogenic volatile organic compounds (BVOCs), I have uniformly reduced isoprene emissions by 20% and have increased the soil NO_x, lumped α-pinene, and lumped limonene emission, each by a factor of two. These increases are within the uncertainties of the emission inventories (e. g., Guenther et al., 2012; Hudman et al., 2012)

5.2.2 Chemical mechanism

The chemical mechanism is based on the RACM2 mechanism (Goliff and Stockwell, 2010; Stockwell et al., 2010) which includes three organic nitrate species: two isoprene-derived nitrates and one lumped nitrate (ONIT). This lumped nitrate is long-lived (>100 h lifetime to oxidation by 1×10^6 molecules cm^{-3} of OH at 298 K), assumed to release NO_2 with 100% efficiency upon oxidation, and has a long lifetime to deposition (Henry's law constant of ~1 M atm^{-1}). In contrast, Henry's law coefficients for hydroxy nitrates have been measured to be on the order of 10^3-10^5 M atm^{-1} (Shepson et al., 1996; Treves et al., 2000). Monoterpene nitrates

are likely to be multifunctional nitrates (containing a nitrate and most likely a hydroxy or peroxide group) and are thus likely to have deposition rates that are much faster than the rate assumed for ONIT. As a ten carbon molecule, monoterpene nitrates will likely have a faster oxidation rate and return NO_2 to the atmosphere with less than 100% efficiency. Furthermore, some monoterpene nitrates will be unsaturated molecules that in addition to having a faster OH oxidation rate will also undergo ozonolysis. Thus, investigating the low NO_x, high BVOC chemistry of organic nitrates required an expansion of the organic nitrate chemistry. These reactions, including photolysis and dry deposition, are available in Appendix D.

Briefly, RACM2 mechanism includes two lumped species to represent low reactivity (lumped into the model species α-pinene) and high reactivity (lumped as limonene) monoterpenes. RACM2 includes an 18% yield of organic nitrate from the reaction of the lumped α-pinene peroxy radical with NO and a 0% yield for the reaction of the lumped limonene peroxy radical with NO. I increase the yield from limonene to 22% as reported in Leungsakul et al. (2005) and as is assumed in the Master Chemical Mechanism v3.2 available at http://mcm.leeds.ac.uk/MCM (Jenkin et al., 1997; Saunders et al., 2003) and introduce two monoterpene-derived nitrates, one unsaturated (UTONIT) and one saturated (TONIT). The lumped limonene peroxy radicals react with NO to form unsaturated nitrates, while lumped α-pinene peroxy radicals react with NO to yield both saturated and unsaturated nitrates with yields of 0.12 and 0.06 respectively. I note that this branching is not constrained by laboratory measurements; however changes to this branching should only be important if the NO_x recycling from monoterpene nitrate oxidation is high. Oxidation rates with OH are calculated using weighted averages of the MCM v3.2 rates of α-pinene and β-pinene (assuming a 50-50 mixture and ignoring the OH abstraction channels) for TONIT and from limonene for UTONIT. The ozonolysis rate of UTONIT is estimated using the EPA Estimation Program Interface (EPI) Suite v4.1 (available at http://www.epa.gov/opptintr/exposure/pubs/episuite.htm) (US EPA, 2011). In what I refer to as the BASE case, TONIT and UTONIT are converted by oxidation to a second generation monoterpene nitrate which behaves identically to HNO_3.

RACM2 assumes that the oxidation of monoterpenes by NO_3 results in the formation of two nitroxy-peroxy radicals, one which primarily decomposes recycling NO_x, and one which primarily forms a nitrate. I use the same split between these two radicals as RACM2, but rename them such that their products form MTNs (70% saturated and 30% unsaturated). The split of peroxy radicals for the lumped limonene is based on Spittler et al. (2006) who report an organic nitrate yield of 67%. Fry et al. (2011) recently reported a smaller organic nitrate yield (30%) from the reaction of NO_3 with limonene. The reason for the discrepancies between the two studies is unclear.

Assessing the impact of monoterpene chemistry on the NO_x budget also requires updating the isoprene chemistry scheme to be consistent with the recent laboratory and theoretical studies. The isoprene oxidation scheme follows Paulot et al. (2009a, 2009b). The formation of hydro-peroxy aldehydes (HPALD) from the isomerization reaction of isoprene peroxy radicals is included using the rate measured by Crounse et al. (2011). The fate of HPALD follows the assumptions of Peeters and Müller (2010). The isomerization of the non-acyl methacrolein peroxy radical is included using the rate and products from Crounse et al. (2012). Peroxy radical reactions with other peroxy radicals were determined following the protocol of Madronich and Calvert (1990) updated in some cases to Tyndall et al., (2001) and using updated reaction rates from IUPAC (Atkinson et al., 2006). Reactions of peroxy radicals with HO_2 were

determined using the product yields from Hasson et al. (2004). Full details regarding the isoprene chemistry can be found in Appendix D.

Recently, Xie et al. (2012) implemented a revised isoprene chemistry scheme in SAPRC-07 based on similar assumptions as ours. Xie et al. (2012) show that this scheme, as implemented in the US EPA CMAQ (Community Multiscale Air Quality) model results in significant improvement in the representation of chemistry over eastern US forests and they pay particular attention to the comparison of isoprene nitrates to ΣANs observed from aircraft (Perring et al., 2009a).

Although of minor importance in the remote boreal forest, the treatment of the organic nitrates that are primarily of anthropogenic origin also required extension due to similar arguments as those for monoterpenes (presented above). The extended organic nitrate chemistry includes four nitrates primarily of anthropogenic origin (aromatic-derived, multifunctional unsaturated, multifunctional saturated, and monofunctional saturated nitrates) which were partitioned from the lumped precursors following the procedure of Middleton et al. (1990) and using branching ratios from Arey et al. (2001) and the MCM v3.2. The yields of the nitrates are generally unchanged from RACM2, with the exception of the yield from the lumped species representing short lived alkanes, alcohols, esters, and alkynes. This yield, originally derived using the branching ratio parameterization from Carter and Atkinson (1989), was reduced (and the non-nitrate products correspondingly increased) to be consistent with the more recent parameterization from Arey et al. (2001). The oxidation, photolysis, and dry deposition of these nitrates are listed in Appendix D.

5.3 Comparison to ARCTAS observations

Comparisons of the vertical profiles from the surface to 600 mbar (~4.2 km pressure altitude) between the BASE model and the ARCTAS measurements for key species are shown in Fig. 5.1 for NO_y and HO_x species. In making these comparisons, I average the ARCTAS measurements to the WRF-Chem resolution, use the closest WRF-Chem output time (output is hourly), and sample the WRF-Chem model along the flight track. However, during one flight leg the aircraft sampled a plume high in biogenics that WRF-Chem predicts to be southeast of the aircraft. I use the WRF-Chem predictions from this plume and not the flight location in my comparison.

As shown in Fig. 5.1, both the mean values as well as the range of the values (the standard deviations) of the model compare well with the measurements for the different components of NO_y as well as OH, HO_2, and O_3. The mean value of the modeled total peroxy nitrates (ΣPNs) and O_3 are slightly lower, 6-24% and 10-20% respectively, than the measurements. The mean of the modeled NO, HO_2 and HNO_3 are slightly lower than the observations at 950 mbar (by ~18%, ~19%, and ~28% respectively) and higher above 900 mbar (~29-63%, ~13-23%, and ~29-58%) than the measurements. The standard deviations of the modeled values always include the mean measured value. I note that some of the discrepancies are due to differences between modeled and observed clouds as reflected in comparison of measured and modeled photolysis rates of NO_2 that are ~30% higher on average in WRF.

In Fig. 5.2 I show the measurement-model comparison for the major biogenic species. The increase in the measurements from 950 mbar to 850 mbar is not captured by the model and is likely due to errors in the WRF-Chem representation of the wind field. In the 950 mbar bin I

see good agreement between measured and modeled monoterpenes despite the fact that the only measured monoterpenes are only α and β-pinene and thus may underestimate the total monoterpene concentration. There is also slightly more isoprene in the model than in the measurements at the lowest altitude. The difference between the measured and modeled methacrolein (MACR) is similar in shape to the difference in measured and modeled isoprene - an indicator that the concentrations of OH and O_3 are represented reasonably accurately. However, the modeled methyl vinyl ketone (MVK) shows a different pattern that suggests the branching of MVK and MACR in either the OH oxidation or ozonolysis of isoprene is not described properly in the chemical mechanism.

In Figs. 5.3a and 5.3b I show a comparison of the WRF-Chem ΣANs production to the calculation of ΣAN production from the VOCs measured during ARCTAS (Chapter 4). The two different calculations show similar sources of ΣANs, however in WRF-Chem the contribution from monoterpenes is lower and the contribution from isoprene is larger than indicated by the measurements, consistent with the BVOC comparison shown in Fig. 5.2. The composition of ΣANs as calculated by WRF-Chem is shown in Fig. 5.4a along with the ARCTAS observations of the contribution of small alkyl nitrates measured in the whole air samples (Blake et al., 2003) to the total ΣANs measured by thermal dissociation-laser induced fluorescence (full details regarding this measurement during ARCTAS can be found in Chapter 4). As compared to the production rates, the importance of monoterpene and non-biogenic nitrates is enhanced and the importance of isoprene nitrates is decreased reflecting differences in loss rates of these ΣANs. During ARCTAS the small alkyl nitrates measured in whole air samples accounted for 26% (median – Fig. 5.4b) of the ΣANs measurement, slightly higher than the WRF-Chem prediction of 19%. These small differences in the long-lived nitrates are likely associated with the boundary conditions; they do not affect any of the conclusions about monoterpene chemistry.

5.4 Monoterpene nitrate abundance, formation, and fate

I assess the role of MTNs using a 24 h boundary layer average from the 15 days corresponding to the ARCTAS measurements (June 28-July 13, 2008) and use model output from areas located north of 49 ^{o}N and defined as forest or wooded tundra in the USGS land use categories, an area of 5.59×10^6 km^2. I define NO_x as $NO + NO_2 + NO_3 + 2 \times N_2O_5$. In addition to assuming that the oxidation of MTNs forms a nitrate that behaves identically to HNO_3 as in the BASE case, it is instructive to compare a simulation in which monoterpene-derived nitrates release NO_2 upon oxidation (referred to as RECYCLE). These two situations represent extremes and the likely situation is intermediate between them. However, since there are no experimental constraints on the NO_x recycling from MTNs the differences between the RECYCLE and BASE cases are useful in defining a range for the effects of MTNs.

5.4.1 Abundance

In the BASE case over most of the boreal forest, first generation MTNs account for ~20% of ΣANs and second generation MTNs account for ~10-15% (not shown). Together, the MTNs account for 30-40% of ΣANs over most of the domain and 60-80% over British Columbia (not shown). However, although the fractional contributions over British Columbia are large, the absolute concentrations are very small in this region (Fig. 5.5a). The remaining ΣANs are

primarily of biogenic origin (~90-95% of ΣANs are biogenic over most of the domain – not shown), a slightly smaller value than what was sampled along the flight track (Fig. 5.4a).

Monoterpene nitrates are a significant contribution to NO_y accounting for ~8-12% of NO_y over most of the domain (Fig. 5.5b), however in general they contribute less to NO_y (~6-8%) in areas where the absolute concentration is highest (Fig. 5.5a). These high concentrations are in southern Canada where the anthropogenic influence on total NO_y is larger. In the RECYCLE case the contribution of MTNs to NO_y has the same spatial distribution; however, the contribution to NO_y is reduced to ~4-8.5% over most of the domain.

5.4.2 Formation

Monoterpene nitrates may be formed as a result of either OH or NO_3 oxidation. Figure 5.6 shows the absolute production rates as a function of NO_x concentration. Each point in the figure represents an equal number of model boxes (208). Production is dominated by OH chemistry for NO_x concentrations < ~75 pptv and is dominated by NO_3 chemistry for higher concentrations of NO_x. Since these averages are weighted by mass, this split between NO_3 and OH production is not an artifact due to differences in boundary layer heights between day and night. Rather the high production rates are due to a sharp increase in NO_3 and in the NO_3 to OH ratio above 50 pptv NO_x (not shown). There are no significant differences between the BASE and the RECYCLE (not shown) cases in the absolute or fractional production of MTNs.

5.4.3 Fate

Figure 5.7a shows the fractional loss of MTNs to OH, photolysis, and deposition for the BASE case. In the BASE case I assume that upon oxidation, first generation MTNs are converted into a more highly functionalized nitrate that behaves identically to HNO_3. Since this oxidation step retains the nitrate functionality, it is not a loss of MTNs. The loss of MTNs is dominated deposition (due to the rapid depositional loss of the second generation MTNs) with a small contribution from the photolysis of both first and second generation MTNs. In contrast, for the RECYCLE case (Fig. 5.7b), oxidation (and thus the return of NO_x to the atmosphere) accounts for the majority (48%) of the MTNs loss. Although oxidation by OH is more important, ozonolysis accounts for roughly a third of the NO_x loss. Since most of the deposition loss in the BASE case is due to deposition of the second generation nitrate which is not formed in the RECYCLE case, deposition is a smaller loss process in the RECYCLE case (Fig. 5.7b) than in the BASE case (Fig. 5.7a), however it is still important accounting for ~17% of the loss. This is the most important difference between the BASE and RECYCLE calculations. The calculations show that the majority (93%) of the MTN loss removes NO_x from the atmosphere by deposition in the BASE case where as this permanent removal drops to 16% of the MTNs in the RECYCLE case.

The averaged MTNs loss rate is 8% greater in the RECYCLE case compared to the BASE case, however the averaged production rate is ~7.25% greater in the RECYCLE case as well. These differences are due to the changes in OH, O_3, and NO_x that are discussed in the next section. As a result of the slightly higher net MTNs loss in the RECYCLE case, the concentration of MTNs is higher in the BASE case. However, this is due to the presence of the second generation MTNs; the concentration of the first generation MTNs are slightly larger

(~5%) in the RECYCLE case. This is because the difference between the production of first generation MTNs and their loss through reaction with OH and O_3 (releasing NO_x in the RECYCLE case and generating second generation MTNs in the BASE case) is larger in the RECYCLE case.

5.5 MTNs and NO_x, NO_y, OH, and O_3

5.5.1 NO_x and NO_y

The lifetime of NO_x and the mechanism of NO_x removal are affected by MTNs chemistry, as shown in Fig. 5.8. In Fig. 5.8, I show these loss rates as a function of NO_x to illustrate how the partitioning of NO_x losses change as discussed in Chapter 3. The loss to HNO_3 is nearly identical for the BASE and RECYCLE cases and for clarity I only show the BASE case. Additionally, I have added symbols on the HNO_3 line representing the midpoint of each NO_x bin in the BASE case. Each bin contains the same number of model points. The net chemical loss (loss of NO_x – production from photolysis and oxidation) of NO_x to ΣANs (black lines) is larger than the loss to HNO_3 (blue line), except at the highest concentrations of NO_x in the RECYCLE case, consistent with the analysis presented in Chapter 3. The oxidation of MTNs in the RECYCLE case results in a ~8-14% increase in NO_x (mean of ~5 pptv and max of 25 pptv) (Fig 5.9a). The concentrations of ΣPNs changes by almost the same percentage (mean 8.5 pptv and max of 30 pptv) with the same spatial distribution (not shown). In the BASE case, the net NO_x loss to MTNs (red solid line in Fig. 5.8) is very similar to the net NO_x loss to HNO_3. In the RECYCLE case, the net NO_x loss to MTNs is smaller although it is always positive and greater than the loss to ΣPNs. MTN chemistry also affects the link between ΣPNs and NO_x. At high NO_x concentrations (> 75 pptv) in the RECYCLE case ΣPNs (grey dashed line in Fig. 5.8) act as a net NO_x sink, while at lower concentrations they are a net NO_x source (negative chemical loss). In the BASE case ΣPNs are primarily a net NO_x sink.

5.5.2 OH and O_3

The NO_x differences between the BASE and RECYCLE cases in turn affect the concentrations of O_3 and OH. Changes in OH follow the same spatial pattern as NO_x (Fig. 5.9a) and are about half as large – increases of ~3-6% (mean of 5.2×10^4 molecules cm^{-3} and max of 2.3×10^5 molecules cm^{-3}) in the RECYCLE case over the BASE case. Ozone also increases by up to 3% (Fig. 5.9b), which corresponds to a mean of 0.4 ppbv and a maximum of 1 ppbv. The spatial pattern of the ozone change is shifted slightly downwind from the NO_x and OH changes reflecting the slower kinetics of ozone production.

5.5.3 Mid-tropospheric effects

In addition to the boundary layer averages discussed above, I see changes between the RECYLE and BASE at 600 mbar for ΣPNs of ~4% and for O_3 of ~1.2% over the eastern part of the domain. NO_x changes by ~2.5-5% over most of the domain with the hot spots occurring in the northwest and the east. By altering the mid-tropospheric burden, as well as the boundary layer burden of peroxy nitrates, monoterpene nitrates act to change the export of nitrogen from

the continent thus affecting ozone and OH concentrations downwind. These changes, while different in magnitude and location, should be qualitatively similar to the effects of isoprene nitrate chemistry, which have been discussed in detail in previous global modeling studies (e.g., von Kuhlmann et al., 2004; Fiore et al., 2005; Ito et al., 2007, 2009; Fiore et al., 2011).

5.6 Hydrolysis of tertiary MTNs

Recent studies have shown that tertiary nitrates undergo rapid hydrolysis in aqueous solutions with the assumed product being HNO_3 (Darer et al., 2011; Hu et al., 2011) and thus a "permanent" loss of nitrogen from the atmosphere. In Chapter 4 I investigated the impact of particle phase hydrolysis as a loss of ΣANs and find evidence in the ARCTAS data that particle phase hydrolysis of MTNs is likely a significant loss process and an important source of HNO_3. Due to the limitations of the model representation of organic aerosol (and its water content), I do not attempt a calculation of this chemistry in WRF-Chem, but rather estimate its effect using the organic aerosol loadings observed during ARCTAS. The aircraft encountered two distinct regions of organic aerosol loading in the boundary layer during ARCTAS (excluding air masses with recent biomass burning or anthropogenic influences): a region with low loading (average of 1 μg m^{-3}) and a high loading (average of 6.6 μg m^{-3}). The area of high loading was correlated with higher concentrations of acetone, an oxidation product of some monoterpenes, consistent with previous observations of high SOA yields from monoterpene oxidation (e.g., Tunved et al., 2006; Fry et al., 2009; Hallquist et al., 2009; Slowik et al., 2010; Fry et al., 2011).

Although WRF-Chem predicts significantly less acetone (24 h average boundary layer maximum of ~500 pptv) than was measured during ARCTAS (boundary layer median ~2 ppbv) by proton transfer reaction mass spectrometry (Wisthaler et al., 2002), possibly indicating that monoterpene emissions and oxidation rates are underestimated or that the boundary conditions for acetone are too low, WRF-Chem does predict areas of higher acetone concentration that are correlated with higher monoterpene concentrations. I assume that in these areas of high acetone (≥ 250 pptv) the organic aerosol loading is 6.6 μg m^{-3} and elsewhere that it is 1 μg m^{-3}. I calculate a hydrolysis loss only for the first generation MTNs since presumably the formation of second generation MTNs would be greatly diminished if hydrolysis of MTNs results in HNO_3. I set up the calculation by assuming that there is sufficient liquid water content in the aerosol and using hydrolysis rates measured by Elrod and co-workers (Darer et al., 2011; Hu et al., 2011). Additionally, I assume that 75% of the MTNs formed from the reaction of OH with monoterpenes are tertiary with a vapor pressure of 4×10^{-6} torr and that NO_3 initiated oxidation results in nitrates whose lifetime to hydrolysis is long and can be ignored (based on Chapter 4). Using these ideas, I calculate a loss rate of MTNs and a corresponding production rate of HNO_3 averaged over the entire domain that ranges from 1.01 ppt hr^{-1} (hydrolysis rate of 4.15×10^{-4} s^{-1}) to 5.61 ppt hr^{-1} (hydrolysis rate of 2.3×10^{-3} s^{-1}). For comparison, the production rate of HNO_3 via reaction of NO_2 with OH in the domain is 3.14 ppt hr^{-1}.

This extra source of HNO_3 initially seems incompatible with the HNO_3 budget since WRF-Chem generally predicts larger concentrations of gas-phase HNO_3 (Fig. 5.1g) than indicated by the ARCTAS measurements. However, this measurement-model discrepancy is in part due to the higher OH concentrations predicted by WRF-Chem and the lower particle phase NO_3^- predicted by WRF-Chem, compared to the observations. An extra HNO_3 source at the low end of the range calculated here is compatible with the measurements and the model. The

measurement-model comparison of the ΣANs data also suggest a rate at the low end of the range: the oxidation and photolysis loss in the RECYCLE case averages 1.33 ppt hr^{-1} while the deposition loss in the BASE case averages 1.37 ppt hr^{-1}. Given the good agreement between the measurement and model concentrations, any extra loss would necessitate an increase in the source of ΣANs. It is reasonable to believe that the source of ΣANs may be larger; in particular, monoterpenes may be increased while still maintaining agreement between the measurements and the model.

5.7 Discussion

The 3-D CTM calculations presented here indicate that oxidation of monoterpenes is a major sink of NO_x and source of low vapor pressure MTNs and a likely source of HNO_3. The chemistry as parameterized here represents a range that brackets some of the key uncertainties while remaining consistent with the measurements from ARCTAS. Although there remain important issues to resolve concerning the gas and multiphase chemistry of monoterpenes and MTNs, I interpret the results of these calculations to indicate that this chemistry will be locally important wherever monoterpene emissions are a large fraction of VOC reactivity (which includes areas with conifer trees, but may include other ecosystems – and even some urban areas – as well). In addition to these local changes in the chemistry of the atmosphere, the depositional loss of monoterpene nitrates will have important impacts on soil nitrogen, and consequently, the carbon cycle.

To my knowledge, there has been no prior work specifically looking at how the chemistry of MTNs impacts the composition and oxidizing capacity of the troposphere. Past global modeling studies, however, have included the oxidation of monoterpenes and the formation of MTNs (Horowitz et al., 2007; Ito et al., 2007, 2009), but have investigated the impact of MTNs in conjunction with isoprene-derived nitrates. Nevertheless, the results of these studies imply that modeled concentrations of NO_x, OH, O_3, and ΣPNs are sensitive to the assumptions regarding the formation and fate of biogenic organic nitrates. The finding that the production of MTNs from NO_3 chemistry accounts for the majority of MTNs production at higher NO_x concentrations is similar to the results of Horowitz et al. (2007) for isoprene nitrates over the eastern United States and to the results of Pye et al. (2010) who found that the aerosol produced from monoterpenes and sesquiterpenes doubled over the southeastern United States when NO_3 oxidation of these species was included. Furthermore, a recent 1-D model study simulating a Northern Michigan forest calculated a nighttime production rate larger than the daytime production rate for the monoterpene-derived nitrates (Pratt et al., 2012). Together, these studies in conjunction with the work presented here indicate that the chemistry of MTNs must be included in order to accurately simulate SOA and tropospheric chemistry and composition.

Although my focus here was on the boreal forest of Canada where I had observations to test the calculations, similar results are likely wherever monoterpene emissions are abundant including the Mediterranean (e.g., Owen et al., 1997; Davison et al., 2009; Seco et al., 2011), the Pearl River Delta (e.g., Wang et al., 2011), and ponderosa pine forests (e.g., Bouvier-Brown et al., 2009; Kim et al., 2010). It is also likely that emissions of sesquiterpenes ($C_{15}H_{24}$), whose emissions are currently lumped into the monoterpenes, are important sinks of NO_x and sources of SOA. The oxidative chemistry of sesquiterpenes will likely have a different impact on the oxidative capacity of the atmosphere due to their higher reactivity and lower vapor pressures.

For example, a recent study using 2-methyl-1-alkenes as surrogates for terpenes found >22% yields of particle phase β-hydroxy organic nitrates with a 15 carbon alkene (Matsunaga and Ziemann, 2010). This large yield suggests that sesquiterpenes (and their nitrates) should have significant local impacts on both NO_y and SOA.

I do not investigate the global impacts here. However, based on Paulot et al. (2012) who showed that over the tropics the formation in isoprene nitrates results in a net chemical NO_x sink, while, over the oceans isoprene nitrates act as a net NO_x source, it can be expected that MTNs have similar effects on global chemistry. MTNs will act to increase the ozone burden if the NO_x is released in areas with a higher ozone production efficiency than that in which it was initially sequestered. This effect will depend on the details of the correct MTN chemistry, both directly through the reactions of MTNs and indirectly through their effect on NO_y partitioning, OH, and O_3. For example, the concentration of ΣPNs is higher in the RECYCLE case than in the BASE case. As a result, the transport of NO_x reservoirs from the continent to the oceans is larger in the RECYCLE than in the BASE case - a fact which will further amplify differences in downwind O_3.

5.8 Conclusions

Using the WRF-Chem model with an expanded organic nitrate representation, I am able to reproduce observations of a wide suite of chemicals, including ΣANs, observed during ARCTAS. I find monoterpene nitrates to be ~5-12% of NO_y over the boreal forest of Canada and I find that NO_3 chemistry is the most important production pathway for MTNs when NO_x is greater than ~75 pptv.

The fate of MTNs depends on the assumed oxidation products. In the BASE case where oxidation results in a more functionalized nitrate that behaves like HNO_3, deposition dominates the loss of MTNs. In this calculation MTN and HNO_3 formation are approximately equal sinks of NO_x. In the RECYCLE case where oxidation returns NO_x to the atmosphere, MTNs are still ~17% of the net NO_x removal and this sink is similar to or greater than the net chemical sink from peroxy nitrates. These calculations are likely lower bounds on the net NO_x sink represented by MTNs as particle phase hydrolysis of tertiary MTNs is likely an important loss process for MTNs as is hinted at by the ARCTAS observations (Chapter 4) and as suggested by laboratory measurements (Darer et al., 2011; Hu et al., 2011). I estimate that particle phase hydrolysis could be between ~60% and > 300% of the MTNs loss rate calculated using the WRF-Chem results as well as an additional source of HNO_3 that ranges from one-third as large to larger than the source from the reaction of NO_2 with OH.

A complete representation of monoterpene chemistry will strain the capabilities of modern CTMs. However, until there is a more thorough understanding of monoterpene oxidation and the appropriate means of representing their chemistry in a condensed chemical mechanism, I recommend that models treat the gas phase chemistry of monoterpenes in addition to their SOA chemistry. In parallel, evaluation of key parameters in the lab and consequences for ambient O_3, NO_x and OH should be explored both on local and global scales.

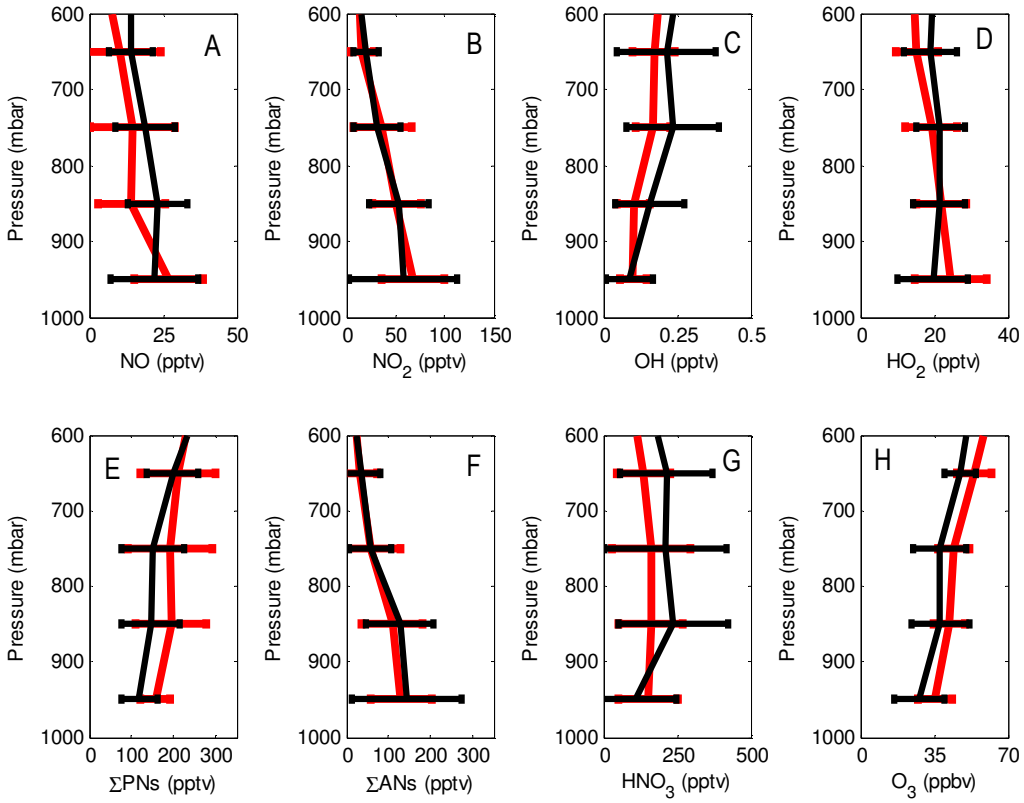

Figure 5.1 Mean concentrations binned by altitude of (red) ARCTAS observations and (black) WRF-Chem sampled along the flight track for **(a)** NO, **(b)** NO_2, **(c)** OH, **(d)** HO_2, **(e)** ΣPNs, **(f)** ΣANs, **(g)** HNO_3, and **(h)** O_3. ARCTAS observations are averaged to the resolution of WRF-Chem. Details regarding the measurements can be found in Browne et al. (2012). Measurements are from the NCAR chemiluminescence instrument for NO and O_3 (Weinheimer et al., 1994), the UC Berkeley Thermal Dissociation-Laser Induced Fluorescence (TD-LIF) instrument for NO_2, ΣPNs, and ΣANs (Thornton et al., 2000; Day et al., 2002; Wooldridge et al., 2010), the Pennsylvania State University LIF for OH and HO_2 (Faloona et al., 2004), and the California Institute of Technology Chemical Ionization Mass Spectrometer for HNO_3 (Crounse et al., 2006).

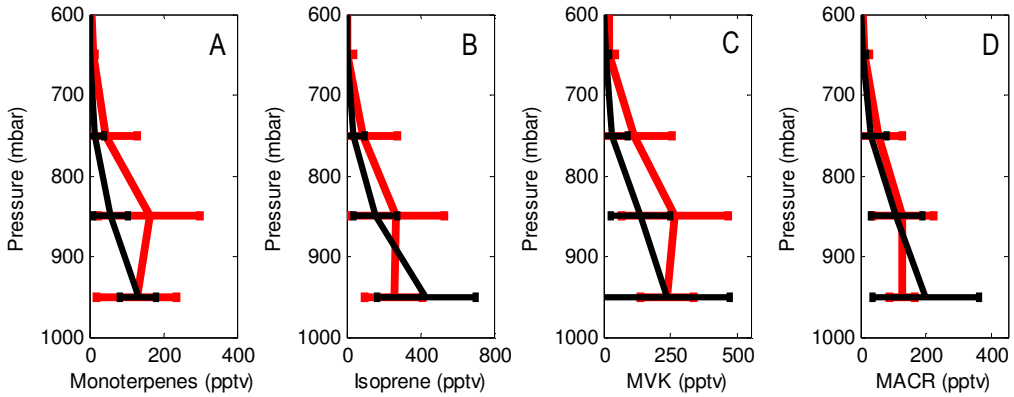

Figure 5.2 Same as Fig. 5.1 for **(a)** monoterpenes, **(b)** isoprene, **(c)** methyl vinyl ketone, and **(d)** methacrolein. The ARCTAS observations of monoterpenes only include α and β-pinene. Measurements are from the UC Irvine whole air samples for monoterpenes (Blake et al., 2003) and from the Trace Organic Gas Analyzer (TOGA) which uses gas chromatography-mass spectrometry for isoprene, MVK, and MACR (Apel et al., 2003).

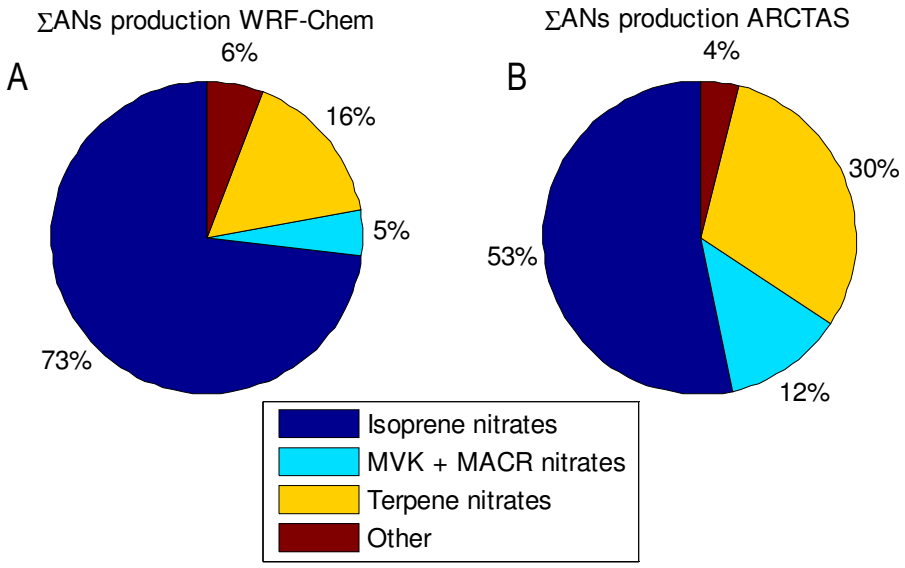

Figure 5.3 (a) Instantaneous ΣANs production rate as calculated by WRF-Chem along the ARCTAS flight track. **(b)** The calculated instantaneous ΣANs production based on the volatile organic compound precursors measured during ARCTAS. Details regarding this calculation can be found in Chapter 4.

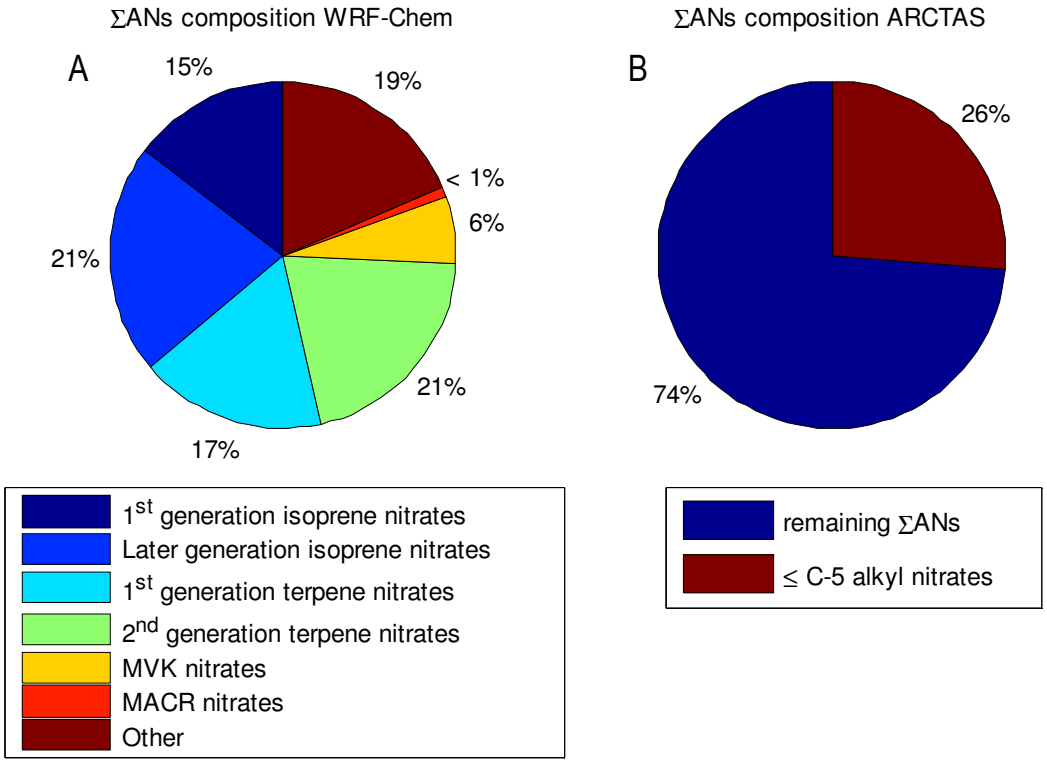

Figure 5.4 (a) The ΣANs composition predicted by WRF-Chem along the flight track. **(b)** The ΣANs composition during ARCTAS. The small nitrates were measured in the whole air samples and the total was measured using TD-LIF. Details are in Chapter 4.

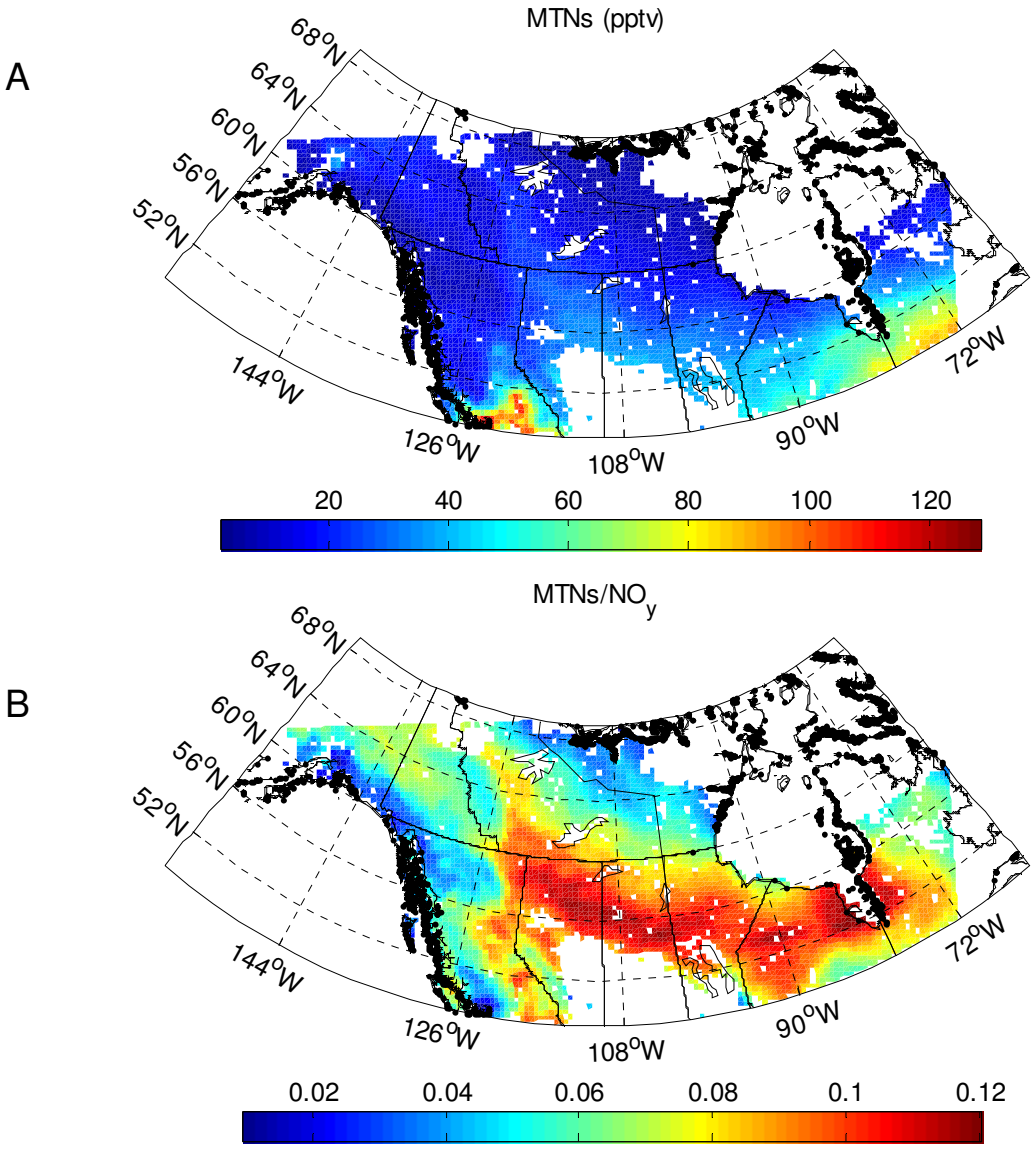

Figure 5.5 (a) Twenty-four hour, boundary layer averaged absolute concentration of MTNs in the BASE case. **(b)** Fractional contribution of MTNs to total oxidized nitrogen in the BASE case.

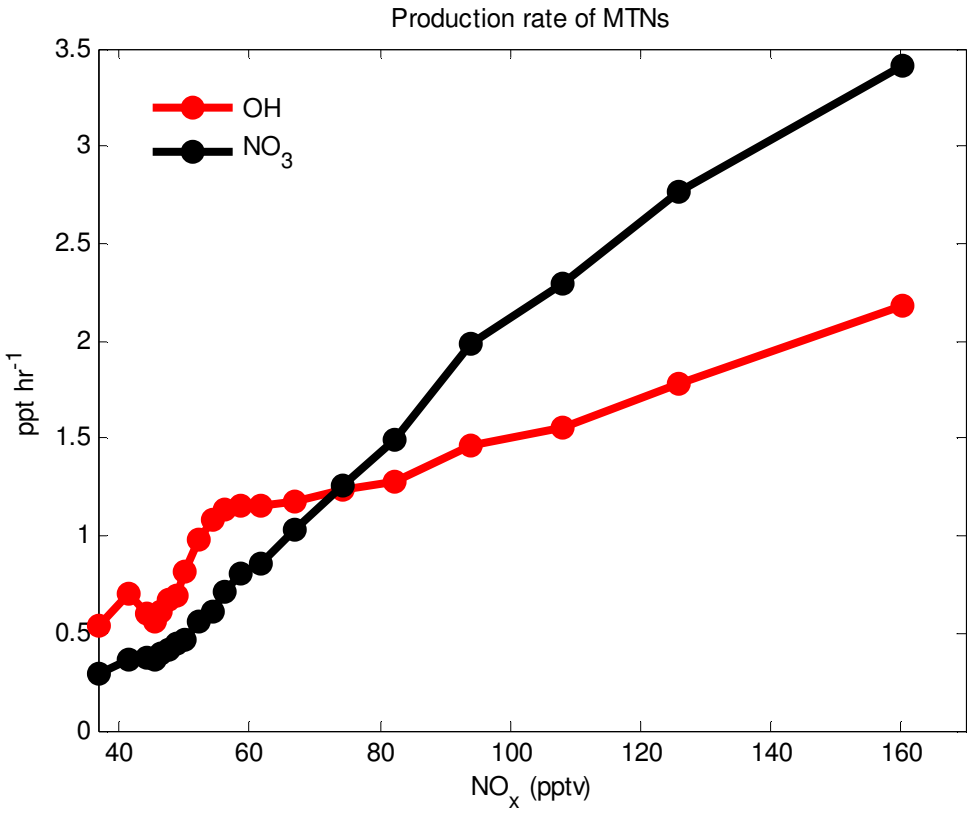

Figure 5.6 The 24 h, boundary layer average production rate of MTNs by OH chemistry (red line) and by NO_3 chemistry (black line) as a function of NO_x concentration. Each point represents the mean NO_x value in each bin. Each bin contains the same number of model grid points (208). Note that the bins are not evenly spaced.

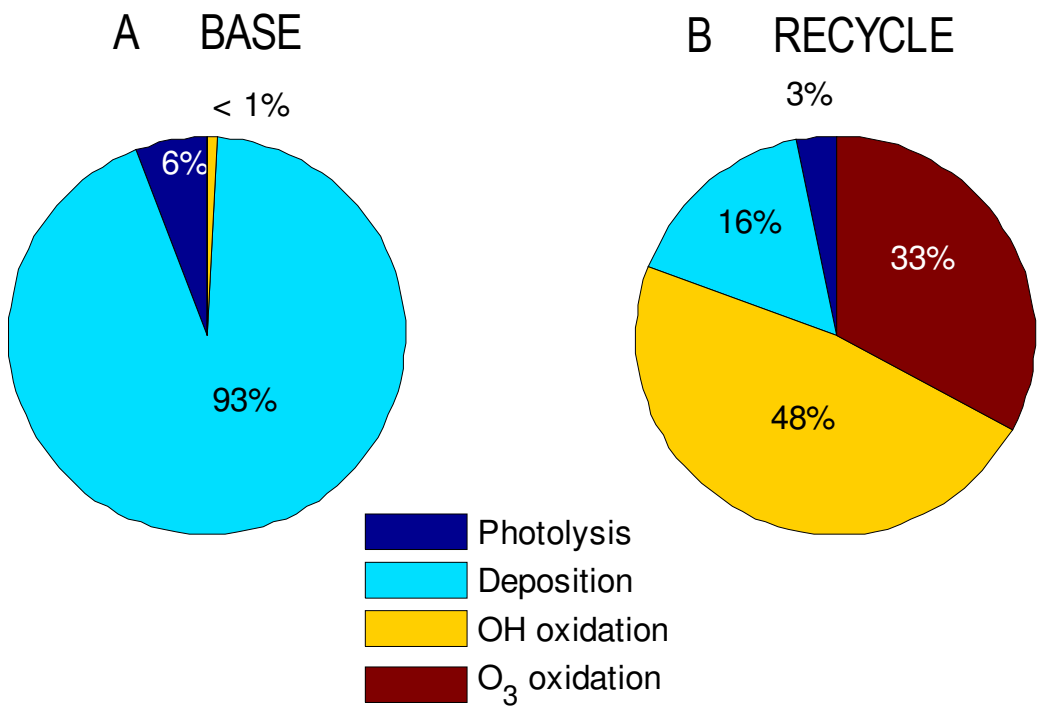

Figure 5.7 The partitioning of the 24 h, boundary layer averaged loss processes of MTNs in **(a)** the BASE case and **(b)** the RECYCLE case. The averaged total loss is 8% larger in the RECYCLE case compared to the BASE case. Loss of MTNs through oxidation by OH or O_3 and by photolysis results in the return of NO_x to the atmosphere. Loss of MTNs through deposition removes NO_x from the atmosphere and introduces it into the biosphere.

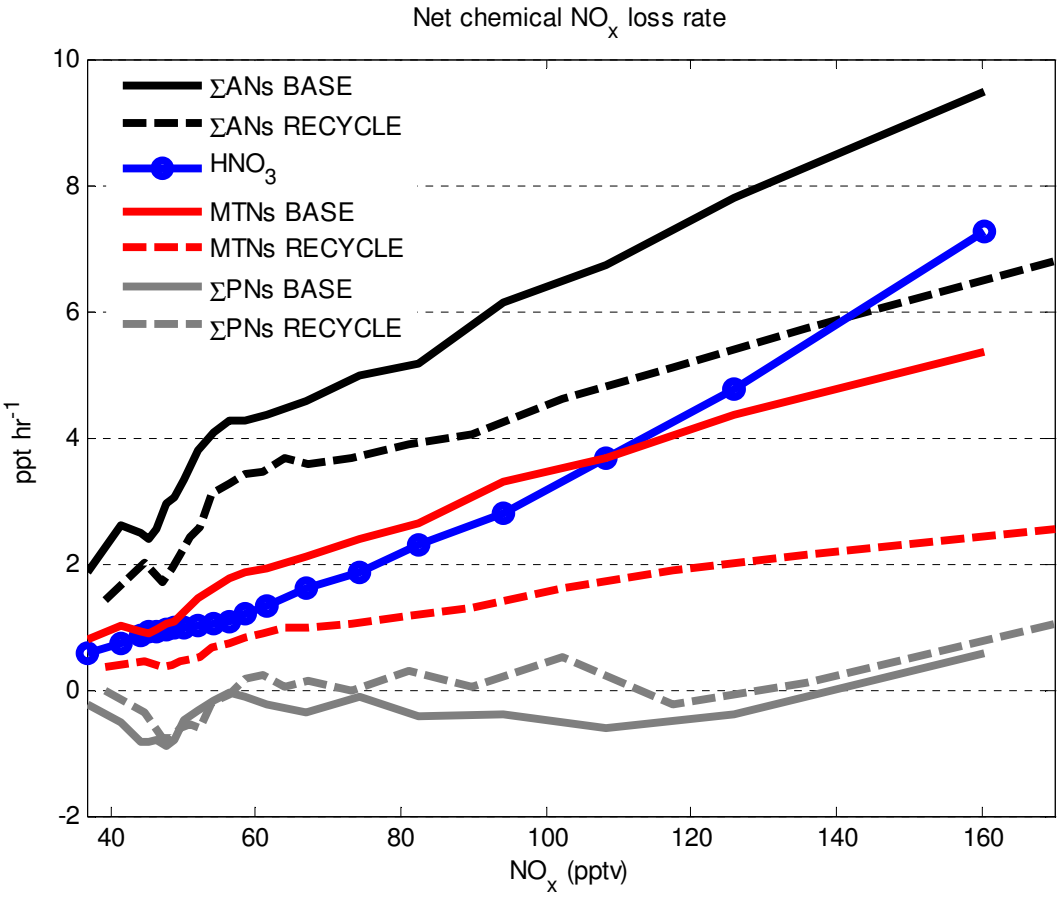

Figure 5.8 The 24 h, boundary layer averaged, net chemical NO_x loss partitioned by class of reaction as a function of NO_x. The loss to HNO_3 for the BASE and RECYCLE case are nearly identical and we show only the BASE case for clarity. The symbols on the HNO_3 curve represent the mean NO_x concentration of each bin. The NO_x bins contain equal numbers of model points.

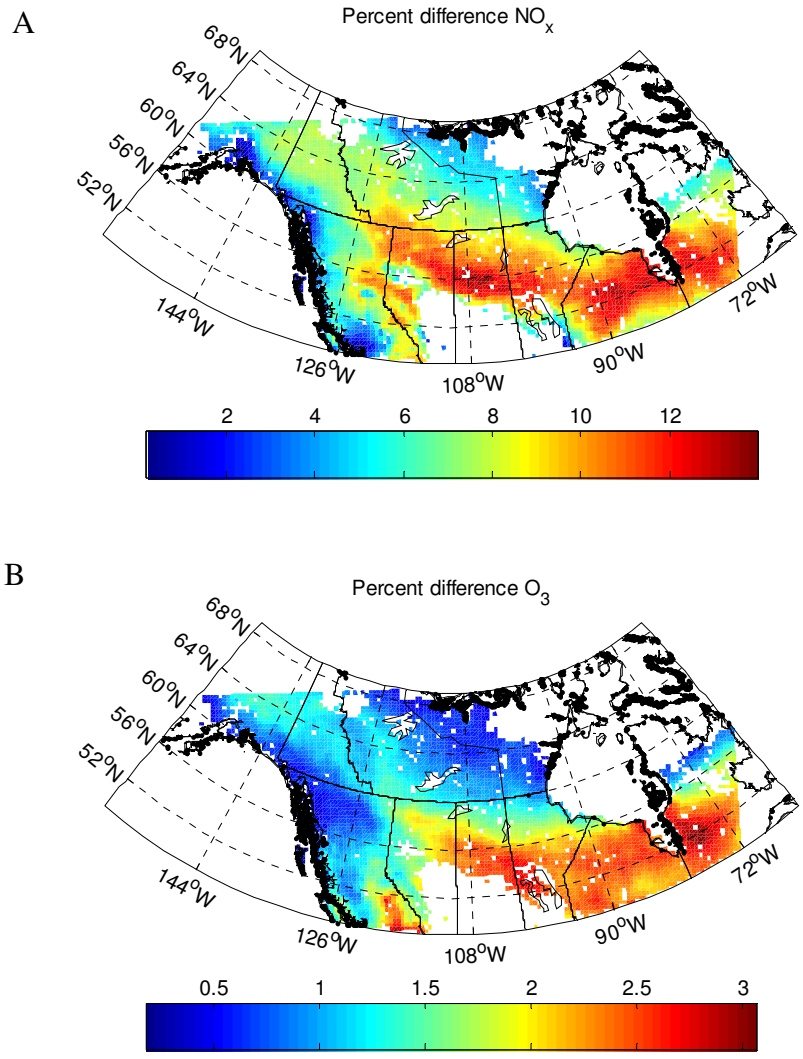

Figure 5.9 Percent differences ((RECYCLE-BASE)/BASE×100) between the RECYCLE and BASE cases for the 24 h, boundary layer averaged **(a)** NO_x and **(b)** O_3 concentrations.

References

Alvarado, M. J., Logan, J. A., Mao, J., Apel, E., Riemer, D., Blake, D., Cohen, R. C., Min, K.-E., Perring, A. E., Browne, E. C., Wooldridge, P. J., Diskin, G. S., Sachse, G. W., Fuelberg, H., Sessions, W. R., Harrigan, D. L., Huey, G., Liao, J., Case-Hanks, A., Jimenez, J. L., Cubison, M. J., Vay, S. A., Weinheimer, A. J., Knapp, D. J., Montzka, D. D., Flocke, F. M., Pollack, I. B., Wennberg, P. O., Kurten, A., Crounse, J., Clair, J. M. S., Wisthaler, A., Mikoviny, T., Yantosca, R. M., Carouge, C. C. and Le Sager, P.: Nitrogen oxides and PAN in plumes from boreal fires during ARCTAS-B and their impact on ozone: an integrated analysis of aircraft and satellite observations, Atmos. Chem. Phys., 10, 9739–9760, doi:10.5194/acp-10-9739-2010, 2010.

Apel, E. C., Hills, A. J., Lueb, R., Zindel, S., Eisele, S. and Riemer, D. D.: A fast-GC/MS system to measure C_2 to C_4 carbonyls and methanol aboard aircraft, J. Geophys. Res., 108, 8794, doi:10.1029/2002JD003199, 2003.

Archibald, A. T., Levine, J. G., Abraham, N. L., Cooke, M. C., Edwards, P. M., Heard, D. E., Jenkin, M. E., Karunaharan, A., Pike, R. C., Monks, P. S., Shallcross, D. E., Telford, P. J., Whalley, L. K. and Pyle, J. A.: Impacts of HO_x regeneration and recycling in the oxidation of isoprene: Consequences for the composition of past, present and future atmospheres, Geophys. Res. Lett., 38, L05804, doi:201110.1029/2010GL046520, 2011.

Arey, J., Aschmann, S. M., Kwok, E. S. C. and Atkinson, R.: Alkyl nitrate, hydroxyalkyl nitrate, and hydroxycarbonyl formation from the NO_x−air photooxidations of C5−C8 n-alkanes, J. Phys. Chem. A, 105, 1020–1027, doi:10.1021/jp003292z, 2001.

Aschmann, S. M., Arey, J. and Atkinson, R.: Products of the OH radical-initiated reactions of 2- and 3-hexyl nitrate, Atmos. Environ., 46, 264–270, doi:10.1016/j.atmosenv.2011.09.073, 2012.

Aschmann, S. M., Tuazon, E. C., Arey, J. and Atkinson, R.: Products of the OH radical-initiated reactions of 2-propyl nitrate, 3-methyl-2-butyl nitrate and 3-methyl-2-pentyl nitrate, Atmos. Environ., 45, 1695–1701, doi:10.1016/j.atmosenv.2010.12.061, 2011.

Atkinson, R. and Arey, J.: Atmospheric degradation of volatile organic compounds, Chem. Rev., 103, 4605–4638, doi:10.1021/cr0206420, 2003.

Atkinson, R., Aschmann, S. M., Carter, W. P. L., Winer, A. M. and Pitts, J. N.: Alkyl nitrate formation from the nitrogen oxide (NO_x)-air photooxidations of C2-C8 n-alkanes, J. Phys. Chem., 86, 4563–4569, doi:10.1021/j100220a022, 1982.

Atkinson, R., Baulch, D. L., Cox, R. A., Crowley, J. N., Hampson, R. F., Hynes, R. G., Jenkin, M. E., Rossi, M. J. and Troe, J.: Evaluated kinetic and photochemical data for atmospheric chemistry: Volume I - gas phase reactions of O_x, HO_x, NO_x and SO_x species, Atmos. Chem. Phys., 4, 1461–1738, doi:10.5194/acp-4-1461-2004, 2004.

Atkinson, R., Baulch, D. L., Cox, R. A., Crowley, J. N., Hampson, R. F., Hynes, R. G., Jenkin, M. E., Rossi, M. J., Troe, J. and IUPAC Subcommittee: Evaluated kinetic and photochemical

data for atmospheric chemistry: Volume II – gas phase reactions of organic species, Atmos. Chem. Phys., 6, 3625–4055, doi:10.5194/acp-6-3625-2006, 2006.

Atlas, E. L., Ridley, B. A. and Cantrell, C. A.: The Tropospheric Ozone Production about the Spring Equinox (TOPSE) Experiment: Introduction, J. Geophys. Res., 108, 8353, doi:10.1029/2002JD003172, 2003.

Bacak, A., Bardwell, M. W., Raventós-Duran, M. T., Percival, C. J., Hamer, P. D. and Shallcross, D. E.: Kinetics of the CH_3O_2 + NO_2 reaction: A temperature and pressure dependence study using chemical ionisation mass spectrometry, Chem. Phys. Lett., 419, 125–129, doi:10.1016/j.cplett.2005.11.070, 2006.

Barnes, I., Becker, K. H. and Zhu, T.: Near UV absorption spectra and photolysis products of difunctional organic nitrates: Possible importance as NO_x reservoirs, J. Atmos. Chem., 17, 353–373, doi:10.1007/BF00696854, 1993.

Beaver, M. R., Clair, J. M. S., Paulot, F., Spencer, K. M., Crounse, J. D., LaFranchi, B. W., Min, K. E., Pusede, S. E., Woolridge, P. J., Schade, G. W., Park, C., Cohen, R. C. and Wennberg, P. O.: Importance of biogenic precursors to the budget of organic nitrates during BEARPEX 2009: observations of multifunctional organic nitrates by CIMS and TD-LIF, Atmos. Chem. Phys. Discuss., 12, 319–349, doi:10.5194/acpd-12-319-2012, 2012.

Bertram, T. H., Cohen, R. C., Thorn III, W. J. and Chu, P. M.: Consistency of ozone and nitrogen oxides standards at tropospherically relevant mixing ratios, J. Air Waste Ma., 55, 1473–1479, doi:10.1080/10473289.2005.10464740, 2005a.

Bertram, T. H., Heckel, A., Richter, A., Burrows, J. P. and Cohen, R. C.: Satellite measurements of daily variations in soil NO_x emissions, Geophys. Res. Lett., 32, L24812, doi:200510.1029/2005GL024640, 2005b.

Bey, I., Jacob, D. J., Yantosca, R. M., Logan, J. A., Field, B. D., Fiore, A. M., Li, Q., Liu, H. Y., Mickley, L. J. and Schultz, M. G.: Global modeling of tropospheric chemistry with assimilated meteorology: Model description and evaluation, J. Geophys. Res., 106, PP. 23,073–23,095, doi:200110.1029/2001JD000807, 2001.

Blake, N. J., Blake, D. R., Simpson, I. J., Meinardi, S., Swanson, A. L., Lopez, J. P., Katzenstein, A. S., Barletta, B., Shirai, T., Atlas, E., Sachse, G., Avery, M., Vay, S., Fuelberg, H. E., Kiley, C. M., Kita, K. and Rowland, F. S.: NMHCs and halocarbons in Asian continental outflow during the Transport and Chemical Evolution over the Pacific (TRACE-P) field campaign: Comparison with PEM-West B, J. Geophys. Res., 108, 8806, doi:10.1029/2002JD003367, 2003.

Bonan, G. B. and Levis, S.: Quantifying carbon-nitrogen feedbacks in the Community Land Model (CLM4), Geophys. Res. Lett., 37, L07401, doi:201010.1029/2010GL042430, 2010.

Bouvier-Brown, N. C., Goldstein, A. H., Gilman, J. B., Kuster, W. C. and de Gouw, J. A.: In-situ ambient quantification of monoterpenes, sesquiterpenes, and related oxygenated compounds

during BEARPEX 2007: implications for gas- and particle-phase chemistry, Atmos. Chem. Phys., 9, 5505–5518, doi:10.5194/acp-9-5505-2009, 2009.

Bradshaw, J., Davis, D., Crawford, J., Chen, G., Shetter, R., Müller, M., Gregory, G., Sachse, G., Blake, D., Heikes, B., Singh, H., Mastromarino, J. and Sandholm, S.: Photofragmentation two-photon laser-induced fluorescence detection of NO_2 and NO: Comparison of measurements with model results based on airborne observations during PEM-Tropics A, Geophys. Res. Lett., 26, 471–474, doi:10.1029/1999GL900015, 1999.

Calvert, J. G., Atkinson, R., Becker, K. H., Kamens, R. K., Seinfeld, J. H., Wallington, T. J. and Yarwood, G.: The Mechanisms of Atmospheric Oxidation of Aromatic Hydrocarbons, Oxford University Press, Oxford ; New York., 2002.

Calvert, J. G., Atkinson, R., Kerr, J. A., Madronich, S. and Moortgat, G. K.: The Mechanisms of Atmospheric Oxidation of the Alkenes, Oxford University Press, New York., 2000.

Calvert, J. G., Derwent, R. G., Orlando, J. J., Tyndall, G. S. and Wallington, T. J.: Mechanisms of Atmospheric Oxidation of the Alkanes, Oxford University Press, Oxford ; New York., 2008.

Cantrell, C. A.: Technical Note: Review of methods for linear least-squares fitting of data and application to atmospheric chemistry problems, Atmos. Chem. Phys., 8, 5477–5487, doi:10.5194/acp-8-5477-2008, 2008.

Cantrell, C. A., Edwards, G. D., Stephens, S., Mauldin, R. L., Zondlo, M. A., Kosciuch, E., Eisele, F. L., Shetter, R. E., Lefer, B. L., Hall, S., Flocke, F., Weinheimer, A., Fried, A., Apel, E., Kondo, Y., Blake, D. R., Blake, N. J., Simpson, I. J., Bandy, A. R., Thornton, D. C., Heikes, B. G., Singh, H. B., Brune, W. H., Harder, H., Martinez, M., Jacob, D. J., Avery, M. A., Barrick, J. D., Sachse, G. W., Olson, J. R., Crawford, J. H. and Clarke, A. D.: Peroxy radical behavior during the Transport and Chemical Evolution over the Pacific (TRACE-P) campaign as measured aboard the NASA P-3B aircraft, J. Geophys. Res., 108, 8797, doi:10.1029/2003JD003674, 2003a.

Cantrell, C. A., Mauldin, L., Zondlo, M., Eisele, F., Kosciuch, E., Shetter, R., Lefer, B., Hall, S., Campos, T., Ridley, B., Walega, J., Fried, A., Wert, B., Flocke, F., Weinheimer, A., Hannigan, J., Coffey, M., Atlas, E., Stephens, S., Heikes, B., Snow, J., Blake, D., Blake, N., Katzenstein, A., Lopez, J., Browell, E. V., Dibb, J., Scheuer, E., Seid, G. and Talbot, R.: Steady state free radical budgets and ozone photochemistry during TOPSE, J. Geophys. Res., 108, 8361, doi:10.1029/2002JD002198, 2003b.

Carter, W. P. L. and Atkinson, R.: Alkyl nitrate formation from the atompsheric photoxidation of alkanes; a revised estimation method, J. Atmos. Chem., 8, 165–173, 1989.

Chen, X., Hulbert, D. and Shepson, P. B.: Measurement of the organic nitrate yield from OH reaction with isoprene, J. Geophys. Res., 103, PP. 25,563–25,568, doi:199810.1029/98JD01483, 1998.

Cleary, P. A., Murphy, J. G., Wooldridge, P. J., Day, D. A., Millet, D. B., McKay, M., Goldstein, A. H. and Cohen, R. C.: Observations of total alkyl nitrates within the Sacramento Urban Plume, Atmos. Chem. Phys. Discuss., 5, 4801–4843, doi:10.5194/acpd-5-4801-2005, 2005.

Cleary, P. A., Wooldridge, P. J. and Cohen, R. C.: Laser-induced fluorescence detection of atmospheric NO_2 with a commercial diode laser and a supersonic expansion, Appl. Optics, 41, 6950–6956, 2002.

Clemitshaw, K. C., Williams, J., Rattigan, O. V., Shallcross, D. E., Law, K. S. and Anthony Cox, R.: Gas-phase ultraviolet absorption cross-sections and atmospheric lifetimes of several C2-C5 alkyl nitrates, J. Photoch. Photobio. A, 102, 117–126, doi:10.1016/S1010-6030(96)04458-9, 1997.

Crawford, J., Davis, D., Chen, G., Bradshaw, J., Sandholm, S., Gregory, G., Sachse, G., Anderson, B., Collins, J., Blake, D., Singh, H., Heikes, B., Talbot, R. and Rodriguez, J.: Photostationary state analysis of the NO_2-NO system based on airborne observations from the western and central North Pacific, J. Geophys. Res., 101, 2053–2072, doi:10.1029/95JD02201, 1996.

Crounse, J. D., DeCarlo, P. F., Blake, D. R., Emmons, L. K., Campos, T. L., Apel, E. C., Clarke, A. D., Weinheimer, A. J., McCabe, D. C., Yokelson, R. J., Jimenez, J. L. and Wennberg, P. O.: Biomass burning and urban air pollution over the Central Mexican Plateau, Atmos. Chem. Phys., 9(14), 4929–4944, doi:10.5194/acp-9-4929-2009, 2009.

Crounse, J. D., Knap, H. C., Ørnsø, K. B., Jørgensen, S., Paulot, F., Kjaergaard, H. G. and Wennberg, P. O.: Atmospheric Fate of Methacrolein. 1. Peroxy Radical Isomerization Following Addition of OH and O_2, J. Phys. Chem. A, 116(24), 5756–5762, doi:10.1021/jp211560u, 2012.

Crounse, J. D., McKinney, K. A., Kwan, A. J. and Wennberg, P. O.: Measurement of gas-phase hydroperoxides by chemical ionization mass spectrometry, Anal. Chem., 78, 6726–6732, doi:10.1021/ac0604235, 2006.

Crounse, J. D., Paulot, F., Kjaergaard, H. G. and Wennberg, P. O.: Peroxy radical isomerization in the oxidation of isoprene, Phys. Chem. Chem. Phys., 13, 13607, doi:10.1039/c1cp21330j, 2011.

Dallmann, T. R. and Harley, R. A.: Evaluation of mobile source emission trends in the United States, J. Geophys. Res., 115, D14305, doi:201010.1029/2010JD013862, 2010.

Darer, A. I., Cole-Filipiak, N. C., O'Connor, A. E. and Elrod, M. J.: Formation and stability of atmospherically relevant isoprene-derived organosulfates and organonitrates, Environ. Sci. Technol., 45, 1895–1902, doi:10.1021/es103797z, 2011.

Davison, B., Taipale, R., Langford, B., Misztal, P., Fares, S., Matteucci, G., Loreto, F., Cape, J. N., Rinne, J. and Hewitt, C. N.: Concentrations and fluxes of biogenic volatile organic compounds above a Mediterranean macchia ecosystem in western Italy, Biogeosciences, 6, 1655–1670, doi:10.5194/bg-6-1655-2009, 2009.

Day, D. A., Dillon, M. B., Wooldridge, P. J., Thornton, J. A., Rosen, R. S., Wood, E. C. and Cohen, R. C.: On alkyl nitrates, O_3, and the "missing NO_y," J. Geophys. Res., 108, 4501, doi:200310.1029/2003JD003685, 2003.

Day, D. A., Farmer, D. K., Goldstein, A. H., Wooldridge, P. J., Minejima, C. and Cohen, R. C.: Observations of NO_x, ΣPNs, ΣANs, and HNO_3 at a rural site in the California Sierra Nevada Mountains: Summertime diurnal cycles, Atmos. Chem. Phys., 9, 4879–4896, doi:10.5194/acp-9-4879-2009, 2009.

Day, D. A., Liu, S., Russell, L. M. and Ziemann, P. J.: Organonitrate group concentrations in submicron particles with high nitrate and organic fractions in coastal southern California, Atmospheric Environment, 44, 1970–1979, doi:10.1016/j.atmosenv.2010.02.045, 2010.

Day, D. A., Wooldridge, P. J. and Cohen, R. C.: Observations of the effects of temperature on atmospheric HNO_3, ΣANs, ΣPNs, and NO_x: evidence for a temperature-dependent HO_x source, Atmos. Chem. Phys., 8, 1867–1879, doi:10.5194/acp-8-1867-2008, 2008.

Day, D. A., Wooldridge, P. J., Dillon, M. B., Thornton, J. A. and Cohen, R. C.: A thermal dissociation laser-induced fluorescence instrument for in situ detection of NO_2, peroxy nitrates, alkyl nitrates, and HNO_3, J. Geophys. Res., 107, 4046, doi:200210.1029/2001JD000779, 2002.

DeCarlo, P. F., Dunlea, E. J., Kimmel, J. R., Aiken, A. C., Sueper, D., Crounse, J., Wennberg, P. O., Emmons, L., Shinozuka, Y., Clarke, A., Zhou, J., Tomlinson, J., Collins, D. R., Knapp, D., Weinheimer, A. J., Montzka, D. D., Campos, T. and Jimenez, J. L.: Fast airborne aerosol size and chemistry measurements above Mexico City and Central Mexico during the MILAGRO campaign, Atmos. Chem. Phys., 8(14), 4027–4048, doi:10.5194/acp-8-4027-2008, 2008.

Derwent, R., Stevenson, D., Doherty, R., Collins, W., Sanderson, M. and Johnson, C.: Radiative forcing from surface NO_x emissions: spatial and seasonal variations, Climatic Change, 88, 385–401, doi:10.1007/s10584-007-9383-8, 2008.

Diskin, G. S., Podolske, J. R., Sachse, G. W. and Slate, T. A.: Open-path airborne tunable diode laser hygrometer, Proceedings of SPIE, 4817, 196–204, doi:doi:10.1117/12.453736, 2002.

Emmons, L. K., Walters, S., Hess, P. G., Lamarque, J.-F., Pfister, G. G., Fillmore, D., Granier, C., Guenther, A., Kinnison, D., Laepple, T., Orlando, J., Tie, X., Tyndall, G., Wiedinmyer, C., Baughcum, S. L. and Kloster, S.: Description and evaluation of the Model for Ozone and Related chemical Tracers, version 4 (MOZART-4), Geosci. Model Dev., 3, 43–67, doi:10.5194/gmd-3-43-2010, 2010.

Faloona, I. C., Tan, D., Lesher, R. L., Hazen, N. L., Frame, C. L., Simpas, J. B., Harder, H., Martinez, M., Di Carlo, P., Ren, X. and Brune, W. H.: A laser-induced fluorescence instrument for detecting tropospheric OH and HO_2: Characteristics and calibration, J. Atmos. Chem., 47, 139–167, doi:10.1023/B:JOCH.0000021036.53185.0e, 2004.

Farmer, D. K. and Cohen, R. C.: Observations of HNO_3, ΣAN, ΣPN and NO_2 fluxes: evidence for rapid HO_x chemistry within a pine forest canopy, Atmos. Chem. Phys., 8, 3899–3917, doi:10.5194/acp-8-3899-2008, 2008.

Farmer, D. K., Perring, A. E., Wooldridge, P. J., Blake, D. R., Baker, A., Meinardi, S., Huey, L. G., Tanner, D., Vargas, O. and Cohen, R. C.: Impact of organic nitrates on urban ozone production, Atmos. Chem. Phys., 11, 4085–4094, doi:10.5194/acp-11-4085-2011, 2011.

Fiore, A. M., Horowitz, L. W., Purves, D. W., II, H. L., Evans, M. J., Wang, Y., Li, Q. and Yantosca, R. M.: Evaluating the contribution of changes in isoprene emissions to surface ozone trends over the eastern United States, J. Geophys. Res., 110, D12303, doi:200510.1029/2004JD005485, 2005.

Fiore, A. M., Levy II, H. and Jaffe, D. A.: North American isoprene influence on intercontinental ozone pollution, Atmos. Chem. Phys., 11, 1697–1710, doi:10.5194/acp-11-1697-2011, 2011.

Freitas, S. R., Longo, K. M., Alonso, M. F., Pirre, M., Marecal, V., Grell., G., Stockler, R., Mello, R. F. and Sánchez Gácita, M.: PREP-CHEM-SRC – 1.0: a preprocessor of trace gas and aerosol emission fields for regional and global atmospheric chemistry models, Geosci. Model Dev., 4, 419–433, doi:10.5194/gmd-4-419-2011, 2011.

Fry, J. L., Kiendler-Scharr, A., Rollins, A. W., Brauers, T., Brown, S. S., Dorn, H.-P., Dubé, W. P., Fuchs, H., Mensah, A., Rohrer, F., Tillmann, R., Wahner, A., Wooldridge, P. J. and Cohen, R. C.: SOA from limonene: role of NO_3 in its generation and degradation, Atmos. Chem. Phys., 11, 3879–3894, doi:10.5194/acp-11-3879-2011, 2011.

Fry, J. L., Kiendler-Scharr, A., Rollins, A. W., Wooldridge, P. J., Brown, S. S., Fuchs, H., Dubé, W., Mensah, A., dal Maso, M., Tillmann, R., Dorn, H.-P., Brauers, T. and Cohen, R. C.: Organic nitrate and secondary organic aerosol yield from NO_3 oxidation of β-pinene evaluated using a gas-phase kinetics/aerosol partitioning model, Atmos. Chem. Phys., 9, 1431–1449, doi:10.5194/acp-9-1431-2009, 2009.

Fry, M. M., Naik, V., West, J. J., Schwarzkopf, M. D., Fiore, A. M., Collins, W. J., Dentener, F. J., Shindell, D. T., Atherton, C., Bergmann, D., Duncan, B. N., Hess, P., MacKenzie, I. A., Marmer, E., Schultz, M. G., Szopa, S., Wild, O. and Zeng, G.: The influence of ozone precursor emissions from four world regions on tropospheric composition and radiative climate forcing, J. Geophys. Res., 117, D07306, doi:201210.1029/2011JD017134, 2012.

Fuchs, H., Bohn, B., Hofzumahaus, A., Holland, F., Lu, K. D., Nehr, S., Rohrer, F. and Wahner, A.: Detection of HO_2 by laser-induced fluorescence: calibration and interferences from RO_2 radicals, Atmospheric Measurement Techniques, 4, 1209–1225, doi:10.5194/amt-4-1209-2011, 2011.

Fuglestvedt, J. S., Berntsen, T. K., Isaksen, I. S. A., Mao, H. T., Liang, X. Z. and Wang, W. C.: Climatic forcing of nitrogen oxides through changes in tropospheric ozone and methane; global 3D model studies, Atmos. Environ., 33, 961–977, doi:10.1016/S1352-2310(98)00217-9, 1999.

Galloway, J. N., Townsend, A. R., Erisman, J. W., Bekunda, M., Cai, Z., Freney, J. R., Martinelli, L. A., Seitzinger, S. P. and Sutton, M. A.: Transformation of the Nitrogen cycle: Recent trends, questions, and potential solutions, Science, 320, 889–892, doi:10.1126/science.1136674, 2008.

Ghude, S. D., Lal, D. M., Beig, G., A, R. van der and Sable, D.: Rain-induced soil NO_x emission from India during the onset of the summer monsoon: A satellite perspective, J. Geophys. Res., 115, D16304, doi:201010.1029/2009JD013367, 2010.

Gill, K. J. and Hites, R. A.: Rate constants for the gas-phase reactions of the hydroxyl radical with isoprene, α- and β-pinene, and limonene as a function of temperature, J. Phys. Chem. A, 106(11), 2538–2544, doi:10.1021/jp013532q, 2002.

Golden, D. M.: Evaluating data for atmospheric models, an example: $CH_3O_2 + NO_2 = CH_3O_2NO_2$, Int. J. Chem. Kinet., 37, 625–632, doi:10.1002/kin.20104, 2005.

Goliff, W. and Stockwell, W. R.: The Regional Atmospheric Chemistry Mechanism, Version 2 - a final frozen version at last, Atmospheric Chemical Mechanisms Conference, Davis, CA, USA, 2010.

Grell, G. A., Peckham, S. E., Schmitz, R., McKeen, S. A., Frost, G., Skamarock, W. C. and Eder, B.: Fully coupled "online" chemistry within the WRF model, Atmos. Environ., 39, 6957–6975, doi:10.1016/j.atmosenv.2005.04.027, 2005.

Guenther, A. B., Jiang, X., Heald, C. L., Sakulyanontvittaya, T., Duhl, T., Emmons, L. K. and Wang, X.: The Model of Emissions of Gases and Aerosols from Nature version 2.1 (MEGAN2.1): an extended and updated framework for modeling biogenic emissions, Geosci. Model Dev. Discuss., 5, 1503–1560, doi:10.5194/gmdd-5-1503-2012, 2012.

Guenther, A., Karl, T., Harley, P., Wiedinmyer, C., Palmer, P. I. and Geron, C.: Estimates of global terrestrial isoprene emissions using MEGAN (Model of Emissions of Gases and Aerosols from Nature), Atmos. Chem. Phys., 6, 3181–3210, doi:10.5194/acp-6-3181-2006, 2006.

Hakola, H., Hellén, H., Henriksson, M., Rinne, J. and Kulmala, M.: In situ measurements of volatile organic compounds in a boreal forest, Atmos. Chem. Phys. Discuss., 12, 15565–15596, doi:10.5194/acpd-12-15565-2012, 2012.

Hallquist, M., Wenger, J. C., Baltensperger, U., Rudich, Y., Simpson, D., Claeys, M., Dommen, J., Donahue, N. M., George, C., Goldstein, A. H., Hamilton, J. F., Herrmann, H., Hoffmann, T., Iinuma, Y., Jang, M., Jenkin, M. E., Jimenez, J. L., Kiendler-Scharr, A., Maenhaut, W., McFiggans, G., Mentel, T. F., Monod, A., Prévôt, A. S. H., Seinfeld, J. H., Surratt, J. D., Szmigielski, R. and Wildt, J.: The formation, properties and impact of secondary organic aerosol: current and emerging issues, Atmos. Chem. Phys., 9, 5155–5236, doi:10.5194/acp-9-5155-2009, 2009.

Hasson, A. S., Tyndall, G. S. and Orlando, J. J.: A product yield study of the reaction of HO_2 radicals with ethyl peroxy ($C_2H_5O_2$), acetyl peroxy ($CH_3C(O)O_2$), and acetonyl peroxy ($CH_3C(O)CH_2O_2$) radicals, J. Phys. Chem. A, 108, 5979–5989, doi:10.1021/jp048873t, 2004.

Henderson, B. H., Pinder, R. W., Crooks, J., Cohen, R. C., Carlton, A. G., Pye, H. O. T. and Vizuete, W.: Combining Bayesian methods and aircraft observations to constrain the HO + NO_2 reaction rate, Atmos. Chem. Phys., 12, 653–667, doi:10.5194/acp-12-653-2012, 2012.

Holland, E. A., Braswell, B. H., Lamarque, J.-F., Townsend, A., Sulzman, J., Müller, J.-F., Dentener, F., Brasseur, G., II, H. L., Penner, J. E. and Roelofs, G.-J.: Variations in the predicted spatial distribution of atmospheric nitrogen deposition and their impact on carbon uptake by terrestrial ecosystems, J. Geophys. Res., 102, 15,849–15,866, doi:199710.1029/96JD03164, 1997.

Horowitz, L. W., Fiore, A. M., Milly, G. P., Cohen, R. C., Perring, A., Wooldridge, P. J., Hess, P. G., Emmons, L. K. and Lamarque, J.-F.: Observational constraints on the chemistry of isoprene nitrates over the eastern United States, J. Geophys. Res., 112, D12S08, doi:200710.1029/2006JD007747, 2007.

Horowitz, L. W., Liang, J., Gardner, G. M. and Jacob, D. J.: Export of reactive nitrogen from North America during summertime: Sensitivity to hydrocarbon chemistry, J. Geophys. Res., 103, 13,451–13,476, doi:199810.1029/97JD03142, 1998.

Hu, K. S., Darer, A. I. and Elrod, M. J.: Thermodynamics and kinetics of the hydrolysis of atmospherically relevant organonitrates and organosulfates, Atmos. Chem. Phys., 11, 8307–8320, doi:10.5194/acp-11-8307-2011, 2011.

Hudman, R. C., Jacob, D. J., Turquety, S., Leibensperger, E. M., Murray, L. T., Wu, S., Gilliland, A. B., Avery, M., Bertram, T. H., Brune, W., Cohen, R. C., Dibb, J. E., Flocke, F. M., Fried, A., Holloway, J., Neuman, J. A., Orville, R., Perring, A., Ren, X., Sachse, G. W., Singh, H. B., Swanson, A. and Wooldridge, P. J.: Surface and lightning sources of nitrogen oxides over the United States: Magnitudes, chemical evolution, and outflow, J. Geophys. Res., 112, D12S05, doi:200710.1029/2006JD007912, 2007.

Hudman, R. C., Moore, N. E., Mebust, A. K., Martin, R. V., Russell, A. R., Valin, L. C. and Cohen, R. C.: Steps towards a mechanistic model of global soil nitric oxide emissions: implementation and space based-constraints, Atmos. Chem. Phys., 12, 7779–7795, doi:10.5194/acp-12-7779-2012, 2012.

Hudman, R. C., Russell, A. R., Valin, L. C. and Cohen, R. C.: Interannual variability in soil nitric oxide emissions over the United States as viewed from space, Atmos. Chem. Phys., 10, 9943–9952, doi:10.5194/acp-10-9943-2010, 2010.

Ito, A., Sillman, S. and Penner, J. E.: Effects of additional nonmethane volatile organic compounds, organic nitrates, and direct emissions of oxygenated organic species on global tropospheric chemistry, J. Geophys. Res., 112, D06309, doi:200710.1029/2005JD006556, 2007.

Ito, A., Sillman, S. and Penner, J. E.: Global chemical transport model study of ozone response to changes in chemical kinetics and biogenic volatile organic compounds emissions due to increasing temperatures: Sensitivities to isoprene nitrate chemistry and grid resolution, J. Geophys. Res., 114, D09301, doi:200910.1029/2008JD011254, 2009.

Jacob, D. J., Crawford, J. H., Maring, H., Clarke, A. D., Dibb, J. E., Emmons, L. K., Ferrare, R. A., Hostetler, C. A., Russell, P. B., Singh, H. B., Thompson, A. M., Shaw, G. E., McCauley, E., Pederson, J. R. and Fisher, J. A.: The Arctic Research of the Composition of the Troposphere from Aircraft and Satellites (ARCTAS) mission: Design, execution, and first results, Atmos. Chem. Phys., 10, 5191–5212, doi:10.5194/acp-10-5191-2010, 2010.

Jaeglé, L., Steinberger, L., Martin, R. V. and Chance, K.: Global partitioning of NOx sources using satellite observations: Relative roles of fossil fuel combustion, biomass burning and soil emissions, Faraday Discuss., 130, 407–423, doi:10.1039/b502128f, 2005.

Jenkin, M. E., Saunders, S. M. and Pilling, M. J.: The tropospheric degradation of volatile organic compounds: a protocol for mechanism development, Atmos. Environ., 31, 81–104, doi:10.1016/S1352-2310(96)00105-7, 1997.

Karl, T., Guenther, A., Yokelson, R. J., Greenberg, J., Potosnak, M., Blake, D. R. and Artaxo, P.: The tropical forest and fire emissions experiment: Emission, chemistry, and transport of biogenic volatile organic compounds in the lower atmosphere over Amazonia, J. Geophys. Res., 112, D18302, doi:10.1029/2007JD008539, 2007.

Kim, S., Huey, L. G., Stickel, R. E., Tanner, D. J., Crawford, J. H., Olson, J. R., Chen, G., Brune, W. H., Ren, X., Lesher, R., Wooldridge, P. J., Bertram, T. H., Perring, A., Cohen, R. C., Lefer, B. L., Shetter, R. E., Avery, M., Diskin, G. and Sokolik, I.: Measurement of HO_2NO_2 in the free troposphere during the intercontinental chemical transport experiment - North America 2004, J. Geophys. Res.-Atmos., 112, doi:10.1029/2006JD007676, 2007.

Kim, S., Karl, T., Guenther, A., Tyndall, G., Orlando, J., Harley, P., Rasmussen, R. and Apel, E.: Emissions and ambient distributions of Biogenic Volatile Organic Compounds (BVOC) in a ponderosa pine ecosystem: interpretation of PTR-MS mass spectra, Atmos. Chem. Phys., 10, 1759–1771, doi:10.5194/acp-10-1759-2010, 2010.

Kwok, E. S. C. and Atkinson, R.: Estimation of hydroxyl radical reaction rate constants for gas-phase organic compounds using a structure-reactivity relationship: An update, Atmospheric Environment, 29, 1685–1695, doi:10.1016/1352-2310(95)00069-B, 1995.

Lelieveld, J., Butler, T. M., Crowley, J. N., Dillon, T. J., Fischer, H., Ganzeveld, L., Harder, H., Lawrence, M. G., Martinez, M., Taraborrelli, D. and Williams, J.: Atmospheric oxidation capacity sustained by a tropical forest, Nature, 452, 737–740, doi:10.1038/nature06870, 2008.

Leungsakul, S., Jeffries, H. E. and Kamens, R. M.: A kinetic mechanism for predicting secondary aerosol formation from the reactions of d-limonene in the presence of oxides of nitrogen and natural sunlight, Atmospheric Environment, 39, 7063–7082, doi:10.1016/j.atmosenv.2005.08.024, 2005.

Li, Z., Nguyen, P., Fatima de Leon, M., Wang, J. H., Han, K. and He, G. Z.: Experimental and theoretical study of reaction of OH with 1,3-butadiene, J. Phys. Chem. A, 110, 2698–2708, doi:10.1021/jp0556557, 2006.

Liang, J., Horowitz, L. W., Jacob, D. J., Wang, Y., Fiore, A. M., Logan, J. A., Gardner, G. M. and Munger, J. W.: Seasonal budgets of reactive nitrogen species and ozone over the United States, and export fluxes to the global atmosphere, J. Geophys. Res., 103(D11), PP. 13,435–13,450, doi:199810.1029/97JD03126, 1998.

Lockwood, A. L., Filley, T. R., Rhodes, D. and Shepson, P. B.: Foliar uptake of atmospheric organic nitrates, Geophys. Res. Lett., 35, L15809, doi:200810.1029/2008GL034714, 2008.

Lockwood, A. L., Shepson, P. B., Fiddler, M. N. and Alaghmand, M.: Isoprene nitrates: preparation, separation, identification, yields, and atmospheric chemistry, Atmos. Chem. Phys., 10, 6169–6178, doi:10.5194/acp-10-6169-2010, 2010.

Madronich, S. and Calvert, J. G.: Permutation reactions of organic peroxy radicals in the troposphere, J. Geophys. Res., 95, 5697–5715, doi:10.1029/JD095iD05p05697, 1990.

Mao, J., Jacob, D. J., Evans, M. J., Olson, J. R., Ren, X., Brune, W. H., Clair, J. M. S., Crounse, J. D., Spencer, K. M., Beaver, M. R., Wennberg, P. O., Cubison, M. J., Jimenez, J. L., Fried, A., Weibring, P., Walega, J. G., Hall, S. R., Weinheimer, A. J., Cohen, R. C., Chen, G., Crawford, J. H., McNaughton, C., Clarke, A. D., Jaeglé, L., Fisher, J. A., Yantosca, R. M., Le Sager, P. and Carouge, C.: Chemistry of hydrogen oxide radicals (HO_x) in the Arctic troposphere in spring, Atmos. Chem. Phys., 10, 5823–5838, doi:10.5194/acp-10-5823-2010, 2010.

Mao, J., Ren, X., Brune, W. H., Van Duin, D. M., Cohen, R. C., Park, J.-H., Goldstein, A. H., Paulot, F., Beaver, M. R., Crounse, J. D., Wennberg, P. O., DiGangi, J. P., Henry, S. B., Keutsch, F. N., Park, C., Schade, G. W., Wolfe, G. M. and Thornton, J. A.: Insights into hydroxyl measurements and atmospheric oxidation in a California forest, Atmos. Chem. Phys. Discuss., 12, 6715–6744, doi:10.5194/acpd-12-6715-2012, 2012.

Martin, R. V., Sauvage, B., Folkins, I., Sioris, C. E., Boone, C., Bernath, P. and Ziemke, J.: Space-based constraints on the production of nitric oxide by lightning, J. Geophys. Res., 112, D09309, doi:10.1029/2006JD007831, 2007.

Matsunaga, A. and Ziemann, P. J.: Yields of β-hydroxynitrates, dihydroxynitrates, and trihydroxynitrates formed from OH radical-initiated reactions of 2-methyl-1-alkenes, PNAS, 107, 6664–6669, doi:10.1073/pnas.0910585107, 2010.

Mebust, A. K., Russell, A. R., Hudman, R. C., Valin, L. C. and Cohen, R. C.: Characterization of wildfire NO_x emissions using MODIS fire radiative power and OMI tropospheric NO_2 columns, Atmos. Chem. Phys., 11, 5839–5851, doi:10.5194/acp-11-5839-2011, 2011.

Mickley, L. J., Jacob, D. J. and Rind, D.: Uncertainty in preindustrial abundance of tropospheric ozone: Implications for radiative forcing calculations, J. Geophys. Res., 106, 3389–3399, 2001.

Middleton, P., Stockwell, W. R. and Carter, W. P. L.: Aggregation and analysis of volatile organic compound emissions for regional modeling, Atmospheric Environment. Part A. General Topics, 24, 1107–1133, doi:10.1016/0960-1686(90)90077-Z, 1990.

Mollner, A. K., Valluvadasan, S., Feng, L., Sprague, M. K., Okumura, M., Milligan, D. B., Bloss, W. J., Sander, S. P., Martien, P. T., Harley, R. A., McCoy, A. B. and Carter, W. P. L.: Rate of gas phase association of hydroxyl radical and nitrogen dioxide, Science, 330, 646–649, doi:10.1126/science.1193030, 2010.

Murphy, J. G., Day, D. A., Cleary, P. A., Wooldridge, P. J. and Cohen, R. C.: Observations of the diurnal and seasonal trends in nitrogen oxides in the western Sierra Nevada, Atmos. Chem. Phys., 6, 5321–5338, doi:10.5194/acp-6-5321-2006, 2006.

Murphy, J. G., Thornton, J. A., Wooldridge, P. J., Day, D. A., Rosen, R. S., Cantrell, C., Shetter, R. E., Lefer, B. and Cohen, R. C.: Measurements of the sum of HO_2NO_2 and $CH_3O_2NO_2$ in the remote troposphere, Atmos. Chem. Phys., 4, 377–384, doi:10.5194/acp-4-377-2004, 2004.

Nizkorodov, S. A., Crounse, J. D., Fry, J. L., Roehl, C. M. and Wennberg, P. O.: Near-IR photodissociation of peroxy acetyl nitrate, Atmos. Chem. Phys., 5, 385–392, doi:10.5194/acp-5-385-2005, 2005.

Novelli, P. C., Lang, P. M., Masarie, K. A., Hurst, D. F., Myers, R. and Elkins, J. W.: Molecular hydrogen in the troposphere: Global distribution and budget, J. Geophys. Res.-Atmos., 104, 30427–30444, doi:10.1029/1999JD900788, 1999.

Nozière, B., Barnes, I. and Becker, K.-H.: Product study and mechanisms of the reactions of α-pinene and of pinonaldehyde with OH radicals, J. Geophys. Res., 104, 23645–23,656, doi:10.1029/1999JD900778, 1999.

O'Brien, J. M., Czuba, E., Hastie, D. R., Francisco, J. S. and Shepson, P. B.: Determination of the Hydroxy Nitrate Yields from the Reaction of C2−C6 Alkenes with OH in the Presence of NO, J. Phys. Chem. A, 102, 8903–8908, doi:10.1021/jp982320z, 1998.

Owen, S., Boissard, C., Street, R. A., Duckham, S. C., Csiky, O. and Hewitt, C. N.: Screening of 18 Mediterranean plant species for volatile organic compound emissions, Atmos. Environ., 31, Supplement 1, 101–117, doi:10.1016/S1352-2310(97)00078-2, 1997.

Pankow, J. F.: An absorption model of gas/particle partitioning of organic compounds in the atmosphere, Atmospheric Environment, 28, 185–188, doi:10.1016/1352-2310(94)90093-0, 1994.

Paulot, F., Crounse, J. D., Kjaergaard, H. G., Kroll, J. H., Seinfeld, J. H. and Wennberg, P. O.: Isoprene photooxidation: new insights into the production of acids and organic nitrates, Atmos. Chem. Phys., 9, 1479–1501, doi:10.5194/acp-9-1479-2009, 2009a.

Paulot, F., Crounse, J. D., Kjaergaard, H. G., Kürten, A., Clair, S., M, J., Seinfeld, J. H. and Wennberg, P. O.: Unexpected Epoxide Formation in the Gas-Phase Photooxidation of Isoprene, Science, 325, 730–733, doi:10.1126/science.1172910, 2009b.

Paulot, F., Henze, D. K. and Wennberg, P. O.: Impact of the isoprene photochemical cascade on tropical ozone, Atmos. Chem. Phys., 12, 1307–1325, doi:10.5194/acp-12-1307-2012, 2012.

Peeters, J. and Müller, J.-F.: HO_x radical regeneration in isoprene oxidation via peroxy radical isomerisations. II: experimental evidence and global impact, Phys. Chem. Chem. Phys., 12, 14227, doi:10.1039/c0cp00811g, 2010.

Peeters, J., Nguyen, T. L. and Vereecken, L.: HO_x radical regeneration in the oxidation of isoprene, Phys. Chem. Chem. Phys., 11, 5935, doi:10.1039/b908511d, 2009.

Perring, A. E., Bertram, T. H., Farmer, D. K., Wooldridge, P. J., Dibb, J., Blake, N. J., Blake, D. R., Singh, H. B., Fuelberg, H., Diskin, G., Sachse, G. and Cohen, R. C.: The production and persistence of $\Sigma RONO_2$ in the Mexico City plume, Atmos. Chem. Phys., 10, 7215–7229, doi:10.5194/acp-10-7215-2010, 2010.

Perring, A. E., Bertram, T. H., Wooldridge, P. J., Fried, A., Heikes, B. G., Dibb, J., Crounse, J. D., Wennberg, P. O., Blake, N. J., Blake, D. R., Brune, W. H., Singh, H. B. and Cohen, R. C.: Airborne observations of total $RONO_2$: new constraints on the yield and lifetime of isoprene nitrates, Atmos. Chem. Phys., 9, 1451–1463, doi:10.5194/acp-9-1451-2009, 2009a.

Perring, A. E., Pusede, S. E. and Cohen, R. C.: An observational perspective on the atmospheric impacts of alkyl and multifunctional nitrates on ozone and secondary organic aerosol, Chem. Rev., in preparation, 2012.

Perring, A. E., Wisthaler, A., Graus, M., Wooldridge, P. J., Lockwood, A. L., Mielke, L. H., Shepson, P. B., Hansel, A. and Cohen, R. C.: A product study of the isoprene+NO_3 reaction, Atmos. Chem. Phys., 9, 4945–4956, doi:10.5194/acp-9-4945-2009, 2009b.

Pratt, K. A., Mielke, L. H., Shepson, P. B., Bryan, A. M., Steiner, A. L., Ortega, J., Daly, R., Helmig, D., Vogel, C. S., Griffith, S., Dusanter, S., Stevens, P. S. and Alaghmand, M.: Contributions of individual reactive biogenic volatile organic compounds to organic nitrates above a mixed forest, Atmos. Chem. Phys. Discuss., 12, 17031–17086, doi:10.5194/acpd-12-17031-2012, 2012.

Pye, H. O. T., Chan, A. W. H., Barkley, M. P. and Seinfeld, J. H.: Global modeling of organic aerosol: the importance of reactive nitrogen (NO_x and NO_3), Atmos. Chem. Phys., 10, 11261–11276, doi:10.5194/acp-10-11261-2010, 2010.

Räisänen, T., Ryyppö, A. and Kellomäki, S.: Monoterpene emission of a boreal Scots pine (Pinus sylvestris L.) forest, Agric. For. Meteorol., 149, 808–819, doi:10.1016/j.agrformet.2008.11.001, 2009.

Ren, X., Mao, J., Brune, W. H., Cantrell, C. A., Mauldin III, R. L., Hornbrook, R. S., Kosciuch, E., Olson, J. R., Crawford, J. H., Chen, G. and Singh, H. B.: Airborne intercomparison of HO_x measurements using laser-induced fluorescence and chemical ionization mass spectrometry during ARCTAS, Atmos. Meas. Tech., 5, 2025–2037, doi:10.5194/amtd-5-2529-2012, 2012.

Ren, X., Olson, J. R., Crawford, J. H., Brune, W. H., Mao, J., Long, R. B., Chen, Z., Chen, G., Avery, M. A., Sachse, G. W., Barrick, J. D., Diskin, G. S., Huey, L. G., Fried, A., Cohen, R. C., Heikes, B., Wennberg, P. O., Singh, H. B., Blake, D. R. and Shetter, R. E.: HO_x chemistry during INTEX-A 2004: Observation, model calculation, and comparison with previous studies, J. Geophys. Res., 113, D05310, doi:10.1029/2007JD009166, 2008.

Roberts, J. M. and Fajer, R. W.: UV absorption cross sections of organic nitrates of potential atmospheric importance and estimation of atmospheric lifetimes, Environ. Sci. Technol., 23, 945–951, doi:10.1021/es00066a003, 1989.

Rollins, A. W., Browne, E. C., Min, K.-E., Pusede, S. E., Wooldridge, P. J., Gentner, D. R., Goldstein, A. H., Liu, S., Day, D. A., Russell, L. M. and Cohen, R. C.: Evidence for NO</sub>x<sub> control over nighttime SOA formation, Science, in press, 2012.

Rollins, A. W., Kiendler-Scharr, A., Fry, J. L., Brauers, T., Brown, S. S., Dorn, H.-P., Dubé, W. P., Fuchs, H., Mensah, A., Mentel, T. F., Rohrer, F., Tillmann, R., Wegener, R., Wooldridge, P. J. and Cohen, R. C.: Isoprene oxidation by nitrate radical: alkyl nitrate and secondary organic aerosol yields, Atmos. Chem. Phys., 9, 6685–6703, doi:10.5194/acp-9-6685-2009, 2009.

Rollins, A. W., Smith, J. D., Wilson, K. R. and Cohen, R. C.: Real time in situ detection of organic nitrates in atmospheric aerosols, Environ. Sci. Technol., 44, 5540–5545, doi:10.1021/es100926x, 2010.

Rosen, R. S., Wood, E. C., Wooldridge, P. J., Thornton, J. A., Day, D. A., Kuster, W., Williams, E. J., Jobson, B. T. and Cohen, R. C.: Observations of total alkyl nitrates during Texas Air Quality Study 2000: Implications for O_3 and alkyl nitrate photochemistry, J. Geophys. Res., 109, D07303, doi:200410.1029/2003JD004227, 2004.

Russell, A. R., Valin, L. C., Bucsela, E. J., Wenig, M. O. and Cohen, R. C.: Space-based constraints on spatial and temporal patterns of NO_x emissions in California, 2005-2008, Environ. Sci. Technol., 44, 3608–3615, doi:10.1021/es903451j, 2010.

Russell, A. R., Valin, L. C. and Cohen, R. C.: Trends in OMI NO_2 observations over the US: Effects of emission control technology and the economic recession, Atmos. Chem. Phys. Discuss., 12, 15419–15452, doi:10.5194/acpd-12-15419-2012, 2012.

Sachse, G. W., Hill, G. F., Wade, L. O. and Perry, M. G.: Fast-response, high-precision carbon monoxide sensor using a tunable diode laser absorption technique, J. Geophys. Res., 92, 2071–2081, doi:10.1029/JD092iD02p02071, 1987.

Sander, S. P., Abbatt, J., Barker, J. R., Burkholder, J. B., Friedl, R. R., Golden, D. M., Huie, R. E., Kolb, C. E., Kurylo, M. J., Moortgat, G. K., Orkin, V. L. and Wine, P. H.: Chemical kinetics and photochemical data for use in atmospheric studies, Evaluation No. 17, JPL Publication 10-6, Jet Propulsion Laboratory, Pasadena, 2011 http://jpldataeval.jpl.nasa.gov, 2011.

Sander, S. P., Finlayson-Pitts,, J., Friedl, R. R., Golden, D. M., Huie, R. E., Keller-Rudek, H., Kolb, C. E., Kurylo, M. J., Molina, M. J., Moortgat, G. K., Orkin, V. L., Ravishankara, A. R. and

Wine, P. H.: Chemical kinetics and photochemical data for use in atmospheric studies, Evaluation No. 15, JPL Publication 06-2, Jet Propulsion Laboratory, Pasadena, 2006 http://jpldataeval.jpl.nasa.gov, 2006.

Sato, K.: Detection of nitrooxypolyols in secondary organic aerosol formed from the photooxidation of conjugated dienes under high-NOx conditions, Atmospheric Environment, 42(28), 6851–6861, doi:10.1016/j.atmosenv.2008.05.010, 2008.

Saunders, S. M., Jenkin, M. E., Derwent, R. G. and Pilling, M. J.: Protocol for the development of the Master Chemical Mechanism, MCM v3 (Part A): tropospheric degradation of non-aromatic volatile organic compounds, Atmos. Chem. Phys., 3, 161–180, doi:10.5194/acp-3-161-2003, 2003.

Schumann, U. and Huntrieser, H.: The global lightning-induced nitrogen oxides source, Atmos. Chem. Phys., 7, 3823–3907, doi:10.5194/acp-7-3823-2007, 2007.

Seco, R., Peñuelas, J., Filella, I., Llusià, J., Molowny-Horas, R., Schallhart, S., Metzger, A., Müller, M. and Hansel, A.: Contrasting winter and summer VOC mixing ratios at a forest site in the Western Mediterranean Basin: the effect of local biogenic emissions, Atmos. Chem. Phys., 11, 13161–13179, doi:10.5194/acp-11-13161-2011, 2011.

Seinfeld, J. H. and Pandis, S. N.: Atmospheric chemistry and physics: from air pollution to climate change, 2nd ed., Wiley, Hoboken, N.J., 2006.

Shashkov, A., Higuchi, K. and Chan, D.: Aircraft vertical profiling of variation of CO_2 over a Canadian Boreal Forest Site: a role of advection in the changes in the atmospheric boundary layer CO_2 content, Tellus Ser. B-Chem. Phys. Meteorol., 59, 234–243, doi:10.1111/j.1600-0889.2006.00237.x, 2007.

Shepson, P. B., Mackay, E. and Muthuramu, K.: Henry's law constants and removal processes for several atmospheric β-hydroxy alkyl nitrates, Environ. Sci. Technol., 30, 3618–3623, doi:10.1021/es960538y, 1996.

Shetter, R. E. and Müller, M.: Photolysis frequency measurements using actinic flux spectroradiometry during the PEM-Tropics mission: Instrumentation description and some results, J. Geophys. Res., 104, 5647–5661, doi:10.1029/98JD01381, 1999.

Sillman, S. and Samson, P. J.: Impact of temperature on oxidant photochemistry in urban, polluted rural and remote environments, J. Geophys. Res., 100, 11,497–11,508, doi:199510.1029/94JD02146, 1995.

Simpson, I. J., Akagi, S. K., Barletta, B., Blake, N. J., Choi, Y., Diskin, G. S., Fried, A., Fuelberg, H. E., Meinardi, S., Rowland, F. S., Vay, S. A., Weinheimer, A. J., Wennberg, P. O., Wiebring, P., Wisthaler, A., Yang, M., Yokelson, R. J. and Blake, D. R.: Boreal forest fire emissions in fresh Canadian smoke plumes: C1-C10 volatile organic compounds (VOCs), CO2, CO, NO2, NO, HCN and CH3CN, Atmos. Chem. Phys., 11(13), 6445–6463, doi:10.5194/acp-11-6445-2011, 2011.

Slowik, J. G., Stroud, C., Bottenheim, J. W., Brickell, P. C., Chang, R. Y.-W., Liggio, J., Makar, P. A., Martin, R. V., Moran, M. D., Shantz, N. C., Sjostedt, S. J., van Donkelaar, A., Vlasenko, A., Wiebe, H. A., Xia, A. G., Zhang, J., Leaitch, W. R. and Abbatt, J. P. D.: Characterization of a large biogenic secondary organic aerosol event from eastern Canadian forests, Atmos. Chem. Phys., 10, 2825–2845, doi:10.5194/acp-10-2825-2010, 2010.

Slusher, D. L., Huey, L. G., Tanner, D. J., Chen, G., Davis, D. D., Buhr, M., Nowak, J. B., Eisele, F. L., Kosciuch, E., Mauldin, R. L., Lefer, B. L., Shetter, R. E. and Dibb, J. E.: Measurements of pernitric acid at the South Pole during ISCAT 2000, Geophys. Res. Lett., 29, 2011, doi:10.1029/2002GL015703, 2002.

Slusher, D. L., Huey, L. G., Tanner, D. J., Flocke, F. M. and Roberts, J. M.: A thermal dissociation–chemical ionization mass spectrometry (TD-CIMS) technique for the simultaneous measurement of peroxyacyl nitrates and dinitrogen pentoxide, J. Geophys. Res., 109, D19315, doi:10.1029/2004JD004670, 2004.

Spencer, K. M., McCabe, D. C., Crounse, J. D., Olson, J. R., Crawford, J. H., Weinheimer, A. J., Knapp, D. J., Montzka, D. D., Cantrell, C. A., Hornbrook, R. S., Mauldin III, R. L. and Wennberg, P. O.: Inferring ozone production in an urban atmosphere using measurements of peroxynitric acid, Atmos. Chem. Phys., 9, 3697–3707, doi:10.5194/acp-9-3697-2009, 2009.

Spirig, C., Guenther, A., Greenberg, J. P., Calanca, P. and Tarvainen, V.: Tethered balloon measurements of biogenic volatile organic compounds at a Boreal forest site, Atmos. Chem. Phys., 4, 215–229, doi:10.5194/acp-4-215-2004, 2004.

Spittler, M., Barnes, I., Bejan, I., Brockmann, K. J., Benter, T. and Wirtz, K.: Reactions of NO_3 radicals with limonene and α-pinene: Product and SOA formation, Atmospheric Environment, 40, Supplement 1, 116–127, doi:10.1016/j.atmosenv.2005.09.093, 2006.

St. Clair, J. M., McCabe, D. C., Crounse, J. D., Steiner, U. and Wennberg, P. O.: Chemical ionization tandem mass spectrometer for the in situ measurement of methyl hydrogen peroxide, Rev. Sci. Instrum., 81, 094102, doi:doi:10.1063/1.3480552, 2010.

Stavrakou, T., Peeters, J. and Muller, J.-F.: Improved global modelling of HO_x recycling in isoprene oxidation: Evaluation against the GABRIEL and INTEX-A aircraft campaign measurements, Atmos. Chem. Phys., 10, 9863–9878, doi:10.5194/acp-10-9863-2010, 2010.

Stockwell, W. R., Goliff, W. S. and Lawson, C. V.: RACM Developments, Atmospheric Chemical Mechanisms Conference, Davis, CA, USA, 2010.

Stone, D., Evans, M. J., Edwards, P. M., Commane, R., Ingham, T., Rickard, A. R., Brookes, D. M., Hopkins, J., Leigh, R. J., Lewis, A. C., Monks, P. S., Oram, D., Reeves, C. E., Stewart, D. and Heard, D. E.: Isoprene oxidation mechanisms: measurements and modelling of OH and HO_2 over a South-East Asian tropical rainforest during the OP3 field campaign, Atmos. Chem. Phys., 11, 6749–6771, doi:10.5194/acp-11-6749-2011, 2011.

Talukdar, R. K., Burkholder, J. B., Hunter, M., Gilles, M. K., Roberts, J. M. and Ravishankara, A. R.: Atmospheric fate of several alkyl nitrates Part 2: UV absorption cross-sections and photodissociation quantum yields, J. Chem. Soc.-Faraday Trans., 93, 2797–2805, doi:10.1039/a701781b, 1997a.

Talukdar, R. K., Herndon, S. C., Burkholder, J. B., Roberts, J. M. and Ravishankara, A. R.: Atmospheric fate of several alkyl nitrates Part 1 Rate coefficients of the reactions of alkyl nitrates with isotopically labelled hydroxyl radicals, J. Chem. Soc.-Faraday Trans., 93, 2787, doi:10.1039/a701780d, 1997b.

Taraborrelli, D., Lawrence, M. G., Crowley, J. N., Dillon, T. J., Gromov, S., Groß, C. B. M., Vereecken, L. and Lelieveld, J.: Hydroxyl radical buffered by isoprene oxidation over tropical forests, Nature Geosci., 5, 190–193, doi:10.1038/ngeo1405, 2012.

Thaler, R. D., Mielke, L. H. and Osthoff, H. D.: Quantification of nitryl chloride at part per trillion mixing ratios by thermal dissociation cavity ring-down spectroscopy, Anal. Chem., 83, 2761–2766, doi:10.1021/ac200055z, 2011.

Thompson, A. M., Singh, H. B., Stewart, R. W., Kucsera, T. L. and Kondo, Y.: A Monte Carlo study of upper tropospheric reactive nitrogen during the Pacific Exploratory Mission in the Western Pacific Ocean (PEM-West B), J. Geophys. Res., 102, 28,437–28,446, doi:10.1029/97JD02555, 1997.

Thornberry, T., Carroll, M. A., Keeler, G. J., Sillman, S., Bertman, S. B., Pippin, M. R., Ostling, K., Grossenbacher, J. W., Shepson, P. B., Cooper, O. R., Moody, J. L. and Stockwell, W. R.: Observations of reactive oxidized nitrogen and speciation of NO_y during the PROPHET summer 1998 intensive, J. Geophys. Res., 106, 24,359–24,386, doi:200110.1029/2000JD900760, 2001.

Thornton, J. A., Wooldridge, P. J. and Cohen, R. C.: Atmospheric NO_2: In situ Laser-Induced Fluorescence detection at parts per trillion mixing ratios, Anal. Chem., 72, 528–539, doi:10.1021/ac9908905, 2000.

Thornton, J. A., Wooldridge, P. J., Cohen, R. C., Martinez, M., Harder, H., Brune, W. H., Williams, E. J., Roberts, J. M., Fehsenfeld, F. C., Hall, S. R., Shetter, R. E., Wert, B. P. and Fried, A.: Ozone production rates as a function of NO_x abundances and HO_x production rates in the Nashville urban plume, J. Geophys. Res.-Atmos., 107, 4146, doi:10.1029/2001JD000932, 2002.

Thornton, P. E., Doney, S. C., Lindsay, K., Moore, J. K., Mahowald, N., Randerson, J. T., Fung, I., Lamarque, J.-F., Feddema, J. J. and Lee, Y.-H.: Carbon-nitrogen interactions regulate climate-carbon cycle feedbacks: results from an atmosphere-ocean general circulation model, Biogeosciences, 6, 2099–2120, doi:10.5194/bg-6-2099-2009, 2009.

Thornton, P. E., Lamarque, J.-F., Rosenbloom, N. A. and Mahowald, N. M.: Influence of carbon-nitrogen cycle coupling on land model response to CO_2 fertilization and climate variability, Global Biogeochem. Cycles, 21, GB4018, doi:200710.1029/2006GB002868, 2007.

Trainer, M., Buhr, M. P., Curran, C. M., Fehsenfeld, F. C., Hsie, E. Y., Liu, S. C., Norton, R. B., Parrish, D. D., Williams, E. J., Gandrud, B. W., Ridley, B. A., Shetter, J. D., Allwine, E. J. and Westberg, H. H.: Observations and modeling of the reactive nitrogen photochemistry at a rural site, J. Geophys. Res., 96, 3045–3063, doi:199110.1029/90JD02395, 1991.

Treves, K., Shragina, L. and Rudich, Y.: Henry's law constants of some β-, γ-, and δ-hydroxy alkyl nitrates of atmospheric interest, Environ. Sci. Technol., 34, 1197–1203, doi:10.1021/es990558a, 2000.

Tunved, P., Hansson, H.-C., Kerminen, V.-M., Ström, J., Maso, M. D., Lihavainen, H., Viisanen, Y., Aalto, P. P., Komppula, M. and Kulmala, M.: High natural aerosol loading over boreal forests, Science, 312, 261–263, doi:10.1126/science.1123052, 2006.

Tyndall, G. S., Cox, R. A., Granier, C., Lesclaux, R., Moortgat, G. K., Pilling, M. J., Ravishankara, A. R. and Wallington, T. J.: Atmospheric chemistry of small organic peroxy radicals, J. Geophys. Res., 106, 12157–12,182, doi:10.1029/2000JD900746, 2001.

US EPA: Estimation programs interface Suite for Microsoft Windows v4.1,, 2011.

Vaida, V.: Spectroscopy of photoreactive systems: Implications for atmospheric chemistry, J. Phys. Chem. A, 113, 5–18, doi:10.1021/jp806365r, 2009.

Valin, L. C., Russell, A. R., Hudman, R. C. and Cohen, R. C.: Effects of model resolution on the interpretation of satellite NO_2 observations, Atmos. Chem. Phys., 11, 11647–11655, doi:10.5194/acp-11-11647-2011, 2011.

van der A, R. J., Eskes, H. J., Boersma, K. F., Noije, T. P. C. van, Roozendael, M. V., Smedt, I. D., Peters, D. H. M. U. and Meijer, E. W.: Trends, seasonal variability and dominant NO_x source derived from a ten year record of NO_2 measured from space, J. Geophys. Res., 113, D04302, doi:200810.1029/2007JD009021, 2008.

Vereecken, L. and Peeters, J.: Nontraditional (per)oxy ring-closure paths in the atmospheric oxidation of isoprene and monoterpenes, J. Phys. Chem. A, 108, 5197–5204, doi:10.1021/jp049219g, 2004.

von Kuhlmann, R., Lawrence, M. G., Pöschl, U. and Crutzen, P. J.: Sensitivities in global scale modeling of isoprene, Atmos. Chem. Phys., 4, 1–17, doi:10.5194/acp-4-1-2004, 2004.

Wang, X., Situ, S., Guenther, A., Chen, F., Wu, Z., Xia, B. and Wang, T.: Spatiotemporal variability of biogenic terpenoid emissions in Pearl River Delta, China, with high-resolution land-cover and meteorological data, Tellus B, 63, 241–254, doi:10.1111/j.1600-0889.2010.00523.x, 2011.

Weaver, C. P., Cooter, E., Gilliam, R., Gilliland, A., Grambsch, A., Grano, D., Hemming, B., Hunt, S. W., Nolte, C., Winner, D. A., Liang, X.-Z., Zhu, J., Caughey, M., Kunkel, K., Lin, J.-T., Tao, Z., Williams, A., Wuebbles, D. J., Adams, P. J., Dawson, J. P., Amar, P., He, S., Avise, J., Chen, J., Cohen, R. C., Goldstein, A. H., Harley, R. A., Steiner, A. L., Tonse, S., Guenther, A.,

Lamarque, J.-F., Wiedinmyer, C., Gustafson, W. I., Leung, L. R., Hogrefe, C., Huang, H.-C., Jacob, D. J., Mickley, L. J., Wu, S., Kinney, P. L., Lamb, B., Larkin, N. K., McKenzie, D., Liao, K.-J., Manomaiphiboon, K., Russell, A. G., Tagaris, E., Lynn, B. H., Mass, C., Salathé, E., O'neill, S. M., Pandis, S. N., Racherla, P. N., Rosenzweig, C. and Woo, J.-H.: A preliminary synthesis of modeled climate change impacts on U.S. regional ozone concentrations, Bulletin of the American Meteorological Society, 90, 1843–1863, doi:10.1175/2009BAMS2568.1, 2009.

Weinheimer, A. J., Walega, J. G., Ridley, B. A., Gary, B. L., Blake, D. R., Blake, N. J., Rowland, F. S., Sachse, G. W., Anderson, B. E. and Collins, J. E.: Meridional distributions of NO_x, NO_y, and other species in the lower stratosphere and upper troposphere during AASE II, Geophys. Res. Lett., 21, 2583–2586, doi:10.1029/94GL01897, 1994.

Wennberg, P. O., Salawitch, R. J., Donaldson, D. J., Hanisco, T. F., Lanzendorf, E. J., Perkins, K. K., Lloyd, S. A., Vaida, V., Gao, R. S., Hintsa, E. J., Cohen, R. C., Swartz, W. H., Kusterer, T. L. and Anderson, D. E.: Twilight observations suggest unknown sources of HO_x, Geophys. Res. Lett., 26, 1373–1376, doi:10.1029/1999GL900255, 1999.

Wesely, M. L.: Parameterization of surface resistances to gaseous dry deposition in regional-scale numerical models, Atmos. Environ., 23, 1293–1304, 1989.

Whalley, L. K., Edwards, P. M., Furneaux, K. L., Goddard, A., Ingham, T., Evans, M. J., Stone, D., Hopkins, J. R., Jones, C. E., Karunaharan, A., Lee, J. D., Lewis, A. C., Monks, P. S., Moller, S. J. and Heard, D. E.: Quantifying the magnitude of a missing hydroxyl radical source in a tropical rainforest, Atmos. Chem. Phys., 11, 7223–7233, doi:10.5194/acp-11-7223-2011, 2011.

Wiedinmyer, C., Quayle, B., Geron, C., Belote, A., McKenzie, D., Zhang, X., O'Neill, S. and Wynne, K. K.: Estimating emissions from fires in North America for air quality modeling, Atmos. Environ., 40, 3419–3432, doi:10.1016/j.atmosenv.2006.02.010, 2006.

Wild, O., Prather, M. J. and Akimoto, H.: Indirect long-term global radiative cooling from NO_x emissions, Geophys. Res. Lett., 28, 1719–1722, doi:200110.1029/2000GL012573, 2001.

Wild, O., Zhu, X. and Prather, M. J.: Fast-J: Accurate simulation of in- and below-cloud photolysis in tropospheric chemical models, Journal of Atmospheric Chemistry, 37, 245–282, doi:10.1023/A:1006415919030, 2000.

Williams, B. J., Goldstein, A. H., Millet, D. B., Holzinger, R., Kreisberg, N. M., Hering, S. V., White, A. B., Worsnop, D. R., Allan, J. D. and Jimenez, J. L.: Chemical speciation of organic aerosol during the International Consortium for Atmospheric Research on Transport and Transformation 2004: Results from in situ measurements, J. Geophys. Res., 112, D10S26, doi:10.1029/2006JD007601, 2007.

Wisthaler, A., Hansel, A., Dickerson, R. R. and Crutzen, P. J.: Organic trace gas measurements by PTR-MS during INDOEX 1999, J. Geophys. Res., 107, 8024, doi:10.1029/2001JD000576, 2002.

Wooldridge, P. J., Perring, A. E., Bertram, T. H., Flocke, F. M., Roberts, J. M., Singh, H. B., Huey, L. G., Thornton, J. A., Wolfe, G. M., Murphy, J. G., Fry, J. L., Rollins, A. W., LaFranchi, B. W. and Cohen, R. C.: Total Peroxy Nitrates (ΣPNs) in the atmosphere: the Thermal Dissociation-Laser Induced Fluorescence (TD-LIF) technique and comparisons to speciated PAN measurements, Atmos. Meas. Tech., 3, 593–607, doi:10.5194/amt-3-593-2010, 2010.

Wu, S., Mickley, L. J., Jacob, D. J., Logan, J. A., Yantosca, R. M. and Rind, D.: Why are there large differences between models in global budgets of tropospheric ozone?, J. Geophys. Res., 112, D05302, doi:200710.1029/2006JD007801, 2007.

Xie, Y., Paulot, F., Carter, W. P. L., Nolte, C. G., Luecken, D. J., Hutzell, W. T., Wennberg, P. O., Cohen, R. C. and Pinder, R. W.: Understanding the impact of isoprene nitrates on regional air quality using recent advances in isoprene photooxidation, , in prep., 2012.

Zuend, A., Marcolli, C., Booth, A. M., Lienhard, D. M., Soonsin, V., Krieger, U. K., Topping, D. O., McFiggans, G., Peter, T. and Seinfeld, J. H.: New and extended parameterization of the thermodynamic model AIOMFAC: calculation of activity coefficients for organic-inorganic mixtures containing carboxyl, hydroxyl, carbonyl, ether, ester, alkenyl, alkyl, and aromatic functional groups, Atmos. Chem. Phys., 11, 9155–9206, doi:10.5194/acp-11-9155-2011, 2011.

Appendix A

Effective branching ratio

The effective branching ratio is a measure of the average branching ratio for the VOC composition contributing to ozone production. For the steady state model, I calculate the effective α value using Eq. (A1):

$$\alpha_{eff} = \frac{\alpha k_{RO_2+NO}[RO_2]}{k_{CH_3O_2+NO}[CH_3O_2] + k_{RO_2+NO}[RO_2]} \quad \text{(A1)}$$

Here RO_2 refers to the lumped peroxy radical from Table 1. This is equivalent to

$$\alpha_{eff} = \frac{P(RONO_2)}{P(O_3) + P(RONO_2) - k_{HO_2+NO}[HO_2][NO]} \quad \text{(A2)}$$

where

$$P(O_3) = k_{HO_2+NO}[HO_2][NO] + \sum_i (1-\alpha_i) k_{RO_{2i}+NO}[RO_{2i}][NO] + k_{CH_3O_2+NO}[CH_3O_2][NO] \quad \text{(A3)}$$

$$P(RONO_2) = \sum_i \alpha_i k_{RO_{2i}+NO}[RO_{2i}][NO] \quad \text{(A4)}$$

Here I have generalized the production of O_3 and $RONO_2$ to account for situations of multiple peroxy radicals with an $RONO_2$ formation channel.

Unlike α, α_{eff} changes as a function of NO_x due to the dependence of α_{eff} on the ratio of RO_2 to CH_3O_2. This ratio decreases as NO_x decreases because RO_2+RO_2 reactions that form CH_3O_2, the loss of RO_{2b} by isomerization, and the importance of RO_2+HO_2 reactions (which are faster for RO_2 than for CH_3O_2) all increase in importance at low NO_x. As a result, α_{eff} decreases as NO_x decreases. This decrease is steepest under low NO_x conditions where, due to the high RO_2 concentrations, RO_2+RO_2 reactions are most important. As shown in Table 3, the increase in α_{eff} from 10 pptv to 100 pptv (~20-25% increases) is about twice the increase from 100 pptv to 500 pptv NO_x (~8-12% increase).

This definition of effective branching ratio differs slightly from that used by elsewhere in the literature (e.g., Rosen et al., 2004; Cleary et al., 2005; Perring et al., 2010; Farmer et al., 2011) where the effective branching ratio is approximated as

$$\alpha_{eff} \approx \frac{2}{P(O_3)/P(RONO_2)} \approx \frac{2}{\Delta[O_x]/\Delta[\Sigma ANs]} \quad \text{(A5)}$$

where $P(O_3)$ and $P(RONO_2)$ refer to the production rate of ozone and $RONO_2$ respectively. The second equality using concentrations holds under conditions where loss rates are small. This derivation relies on the assumption that HO_2 and RO_2 radicals are present in near equal concentrations (i.e., that each RO generates a carbonyl and an HO_2) and is equal to Eq. (A2) when this assumption is valid. This assumption is appropriate under high NO_x conditions where this derivation has been used previously, but is invalid under low NO_x conditions where RO_2 concentrations are larger than HO_2 concentrations.

Appendix B

ΣANs production calculation

B.1 Calculation of ΣANs production

In the calculation of the ΣANs production rate I use the VOCs, branching ratios, and OH reaction rates listed in Table A1. I do not attempt to estimate the concentration of any unmeasured VOCs.

B.2 Uncertainties in the calculation of ΣANs production

The calculated production of ΣANs is sensitive to the assumptions about reaction rates, branching ratios, and that the VOC measurements are representative of the entire VOC mix. I have investigated several possibilities (outlined in Table A2) and find that the conclusion is robust. Table A2 shows the median value of the ratio of the instantaneous production of ΣANs to HNO_3 for 7 different possibilities (including the base case that was presented in the text). In the unique RO_2+RO_2 rate case I take the rate of RO_2+RO_2 reactions from MCM v3.2 RO_2+CH_3O_2 rates for methyl vinyl ketone, methacrolein, isoprene, and monoterpenes. The methyl vinyl ketone and isoprene rates are weighted by the initial branching of the different peroxy radicals. The monoterpene rate is calculated assuming an even split between α and β pinene and weighting the different peroxy radicals. No significant difference is observed using these rates.

In the base calculation I use LIF OH measurement. It has recently been shown that this measurement may have an interference in environments with high biogenic emissions (Mao et al., 2012). This should have a minor effect on the calculation since any change in OH will affect both P(ΣANs) and P(HNO_3). Nevertheless, I test this possibility using the OH measurement from the chemical ionization mass spectrometry instrument (Cantrell et al., 2003a)-the HO_x CIMS OH case. These measurements agreed well during the campaign (Ren et al., 2012). I see a slight decrease in the ratio of P(ΣANs) to P(HNO_3), however this can be attributed to the discrepancy in data coverage between the two instruments; if I restrict the LIF OH to the same points with CIMS OH coverage, I calculate the same median ratio.

Recently it has been reported that some LIF HO_2 measurements may suffer from a positive interference from the conversion of RO_2 to HO_2 in the instrument (Fuchs et al., 2011). This should increase the production of ΣANs relative to HNO_3 due to an increase in the fraction of RO_2 that reacts with NO. By decreasing the HO_2 by 40% ([HO_2]×0.6) case, I find this to be true. Using the HO_x CIMS HO_2 measurement decreases the P(ΣANs) to P(HNO_3) ratio to less than one, however this is in part due to the more spare data coverage: using the same data with the LIF HO2 results in a median ratio one. Furthermore, the mean of the P(ΣANs) to P(HNO_3) ratio using the HO_x CIMS HO_2 measurement is 1.3 and overall, I conclude that the result is robust with respect to measurement uncertainties.

Recent measurements of the isoprene nitrate branching ratio range from 7% to 12% (Paulot et al., 2009a; Lockwood et al., 2010). In the base calculation I use the branching ratio of

11.7% reported by Paulot et al. (2009a). In the 7% IN case below, I use the yield of 7% measured by Lockwood et al. (2010) and find that although the contribution from isoprene decreases, P(ΣANs) is still larger than P(HNO_3).

It is also likely that there are VOCs contributing to organic nitrate production that were not measured during ARCTAS, and thus the base calculation is biased low. For instance, only the monoterpenes α-pinene and β-pinene are measured. Measurements from the boreal forest in Finland indicate substantial contributions from other monoterpenes as well as contributions from sesquiterpenes (e.g., Spirig et al., 2004; Räisänen et al., 2009; Hakola et al., 2012). As expected, if I double the production from monoterpenes to account for unmeasured species, I see increases in both the ratio of P(ΣANs) to P(HNO_3) and a large increase in the fraction of P(ΣANs) from monoterpenes.

In low NO_x environments it is possible that RO_2 is present in higher concentrations than HO_2, which would decrease the ΣANs production. However, I find that increasing the RO_2 concentration by an order of magnitude has a negligible effect on the calculation. Even if this increase is coupled with a doubling of the RO_2+RO_2 rate (not shown), there is no significant effect. Overall, I conclude that although there is uncertainty in the absolute numbers, the production of ΣANs is, on average, fast than the production of HNO_3.

VOC	α	OH reaction rate	VOC	α	OH reaction rate
Alkanes			Alkenes		
methane[a]	0.001[e]	2.45E-12×exp(-1775/T)[k]	ethene[b]	0.0086[h]	k_o=1.0E-28×(T/300) $^{-4.5}$ k_∞=7.5E-12×(T/300)$^{-0.85}$ F_c=0.6 N=1[k**]
ethane[b]	0.009[e]	7.66E-12×exp(-1020/T)[k]	propene[b]	0.015[h]	k_o =8E-27×(T/300)$^{-3.5}$ k_∞ =3.0E-11×(T/300)$^{-1}$ F=0.5 N=0.75-1.27×log(F_c)[l**]
propane[b]	0.036[f]	8.7E-12×exp(-615/T)[k]	1-butene[b]	0.039[e]	6.6E-12×exp(465/T)[l]
n-butane[c]	0.077[f]	9.8E-12×exp(-425/T)[l]	methylpropene[b]	0.012[e]	9.4E-12×exp(505/T)[l]
n-pentane[c]	0.129[f]	1.81E-11×exp(-452/T)[m]	trans-2-butene[b]	0.034[h]	1.0E-11×exp(553/T)[l]
i-butane[c]	0.027[e]	7.0E-12×exp(-350/T)[m]	cis-2-butene[b]	0.034[h]	1.1E-11×exp(485/T)[l]
i-pentane[c]	0.075[e]	1.01E-11×exp(-296/T)[m]	butandiene[b]	0.065[e]	1.58E-11×exp(436/T)[n]
2,3-dimethylbutane[b]	0.061[e]	1.25E-11×exp(-212/T)[m]			
2-methylpentane and 3-methylpentane[b]	0.11[e]	1.77E-11×exp(-362/T)[m*]	Aromatics		
hexane[b]	0.141[g]	1.98E-11×exp(-394/T)[m]	benzene[d]	0.029[e]	2.3E-12×exp(-190/T)[l]
heptane[b]	0.178[g]	2.76E-11×exp(-430/T)[m]	propyl-benzene[b]	0.093[e]	5.8E-12[p]
			toluene[d]	0.08[e]	1.8E-12×exp(340/T)[l]
Isoprene and derivatives			2-ethyltoluene[b]	0.106[e]	1.19E-11[p]
isoprene[c]	0.117[i]	2.7E-11×exp(390/T)[l]	3-ethyltoluene[b]	0.094[e]	1.86E-11[p]
methacrolein[c]	0.0705[i]	8.0E-12×exp(380/T)[l]	4-ethyltoluene[b]	0.137[e]	1.18E-11[p]
methyl vinyl ketone[c]	0.11[i]	2.6E-12×exp(610/T)[l]	o-xylene[c]	0.081[e]	1.36E-11[p]
			m-xylene and p-xylene[b]	0.085[e]	2.31E-11[p]
Monoterpenes			ethylbenzene[b]	0.072[e]	7.0E-12[p]
α-pinene[b]	0.18[j]	1.2E-11×exp(440/T)[l]	1,3,5-trimethylbenzene[b]	0.127[e]	5.67E-11[p]
β-pinene[b]	0.18[j]	1.47E-11×exp(467/T)[o]	1,2,4-trimethylbenzene[b]	0.105[e]	3.25E-11[p]
			1,2,3-trimethylbenzene[b]	0.119[e]	3.27E-11[p]
OVOC					
butanone[c]	0.015[e]	1.5E-12×exp(-90/T)[l]			
butanal[c]	0.013[e]	6.0e-12×exp(410/T)[l]			

[a]Tunable diode laser absorption spectroscopy [b]Whole air sampling [c]Gas chromatography - mass spectrometry [d]Proton transfer reaction mass spectrometry [e]MCM v3.2, may involve weighting by isomers [f]Atkinson et al. (1982) [g]Arey et al. (2001) [h]O'Brien et al. (1998) [i]Paulot et al. (2009a) [j]Nozière et al. (1999) [k]Sander et al. (2006) [l]Atkinson et al. (2006) [m]Calvert et al. (2008) [n]Li et al. (2006) [o]Gill and Hites (2002) [p]Calvert et al. (2002) [*]rate for 2-methylpentane [**]k= k_∞ k_oM/(k_oM+k_∞)×$F_c^{1/j}$, j=1+[1log(k_oM/k_∞)/N]^2, log = $\log_{10}$

Table B1 VOC parameters used in the calculation of the instantaneous production rate of ΣANs.

Case	P(ΣANs)/ P(HNO3)	% Isoprene	% MVK	% MACR	% Monoterpenes	% Other
Base	1.34	53	12	<1	30	4
Unique RO_2+RO_2 rate	1.29	52	13	<1	31	4
HO_x CIMS OH	1.05	59	18	<1	20	4
[HO_2]×0.6	1.89	53	12	<1	30	4
HO_x CIMS HO_2	0.95	56	35	<1	13	6
7% IN	1.1	40	16	<1	38	5
2*Monoterpenes	1.67	41	10	<1	46	3
[RO_2]×10	1.27	53	13	<1	30	4

Table B2 The median value of the P(ΣANs) to P(HNO_3) ratio and the speciation of P(ΣANs) for different assumptions regarding RO_2 reaction rates, OH and HO_2 concentrations, and VOC concentrations as described in Appendix B.

Appendix C

Uncertainties in the calculation of the ΣANs oxidation rate

The calculated oxidation rate of ΣANs is sensitive to uncertainties including: the assumption that the instantaneous production represents the composition, possible interferences in HO_x measurements, reaction rate uncertainties, and assumptions regarding NO_x recycling.

The two most likely deviations from my assumption that the production in Fig. 4.4 represents the composition are: nitrates produced from unmeasured BVOCS (likely monoterpenes and sesquiterpenes) and the presence of higher generation isoprene and monoterpene nitrates. In order for theses nitrates to increase the ΣANs loss rate, their loss rate must, on a per molecule basis, be faster than the isoprene nitrate loss, which implies that these nitrates are unsaturated. In Chapter 5 I estimate the oxidation rates of unsaturated monoterpene nitrates 7.29×10^{-11} cm^3 $molecules^{-1}$ s^{-1} for OH oxidation and 1.67×10^{-16} cm^3 $molecules^{-1}$ s^{-1} for ozonolysis, similar to the isoprene nitrate oxidation rates. Thus, if the monoterpene nitrates had a larger NO_x recycling than the isoprene nitrates, then they would increase the ΣANs loss. NO_x recycling from monoterpene nitrates is difficult to estimate given the magnitude of different monoterpene structures and the variability of emission factors between trees. Furthermore, since the ozonolysis of the nitrates will dominate the loss process, NO_x recycling through this channel will be most important.

To estimate the effect of this complex problem I use results from the WRF-Chem model run over the boreal forest of Canada for the ARCTAS time period. This model uses a chemical mechanism with a comprehensive treatment of ΣANs including 11 isoprene-derived nitrates and two monoterpene-derived nitrates (one unsaturated and one saturated) as described in Chapter 5. Sampled along the flight track, the WRF-Chem model predicts a ΣANs oxidative loss rate of 2.3×10^{-5} s^{-1} (median), a number similar to the estimate here, which suggests that these effects have only a small influence on the calculation.

Since the ozonolysis of isoprene nitrates accounts for the majority of the ΣANs loss rate, the possible interferences in the HO_x measurements (OH and HO_2) and uncertainties in the RO_2 reaction rates have a negligible effect on the calculated loss.

The largest uncertainty comes from uncertainty regarding the yields of the various isoprene nitrate isomers, the ozonolysis rates, and the magnitude of the NO_x recycling from isoprene nitrate ozonolysis. If I use the split between the δ-hydroxy and β-hydroxy nitrates from Lockwood et al. (2010) (~17% and ~83% respectively) and the distribution of ΣANs production calculated using the small isoprene nitrate formation yield, I calculate an overall ΣANs loss rate of 1.1×10^{-5} s^{-1} assuming the slower β-hydroxy rate and 3.0×10^{-5} s^{-1} if I assume the faster rate-rates that are similar to those in Table 2. I note that I have weighted the ozonolysis rates using the initial production yields of the β-hydroxy and δ-hydroxy nitrates. Given that these nitrates have (potentially) different atmospheric lifetimes (at 2×10^6 molecules cm^{-3} OH and 30 ppbv O_3 δ-hydroxy nitrates have a lifetime of ~1.2 h and the β-hydroxy nitrates of ~0.97-2.6 h using the OH rate constants from Paulot et al. (2009a)), it is likely that the reaction rate of the ΣANs measured will favor the less reactive nitrates and the calculation may be high.

In my derivation of the NO_x recycling I follow the assumptions of MCM v3.2, which includes the assumption of equal branching between the two possible carbonyl/Criegee biradical pairs. However, the exact branching depends on nature and number of the substituents on the alkene (Calvert et al., 2000). Overall, my calculations suggest that further experimental constraints on the relative yields of the β-hydroxy versus δ-hydroxy isoprene nitrates, their ozonolysis rates, and their ozonolysis products are needed.

Appendix D

Expanded organic nitrate chemistry

Abbreviation	Name	Abbreviation	Name
ACD	acetaldehyde	DIBOO	Dibble peroxy radical (see Paulot et al. (2009a))
ACO3	acetyl peroxy radical	DONIT	unsaturated, mulitfunctional organic nitrates
ACT	acetone	ETHLN	ethanal nitrate
ACTP	peroxy radical from acetone	ETHP	peroxy radicals from ethane
ADCN	aromatic-NO3 adduct	GLY	glyoxal
ALD	C-3 and higher aldehydes	GLYC	glycoaldehyde
AONIT	aromatic-derived organic nitrates	HAC	hydroxy acetone
API	α -pinene and other cyclic terpenes with one double bond	HC3P	peroxy radicals from alkanes, alcohols, esters, and alkynes with OH rate constants less than 3.4 $\times 10^{-12}$ cm^3 s^{-1} at 298 K, 1 atm
APIP	peroxy radical from API	HC5P	peroxy radicals from alkanes, alcohols, esters, and alkynes with OH rate constants between 3.4 $\times 10^{-12}$ cm^3 s^{-1} and 6.8×10^{-12} cm^3 s^{-1} at 298 K, 1 atm
BAL2	peroxy radicals from BALD	HC8P	peroxy radicals from alkanes, alcohols, esters, and alkynes with OH rate constants greater than 6.8 $\times 10^{-12}$ cm^3 s^{-1} at 298 K, 1 atm
BALD	benzaldehyde and other aromatic aldehydes	HKET	hydroxy ketone
BENP	peroxy radicals from benzene	HONIT	2nd generation monoterpene nitrate
CHO	phenoxy radical from cresol and other hydroxy substituted aromatics	HPALD	C-5 hydroperoxyaldhyde
DCB1	unsaturated dicarbonyls	IAP	hydroxy ketone/aldehyde peroxide from isoprene chemistry
DCB2	unsaturated dicarbonyls	IEPOX	isoprene-derived dihydroxy epoxide
DCB3	unsaturated dicarbonyls	ISO	isoprene
DHMOB	multi-hydroxy ketone/aldehyde from isoprene chemistry	ISOP	peroxy radical from ISOP

Table D1 Chemical species in expanded organic nitrate chemistry.

Abbreviation	Name	Abbreviation	Name
ISOPNB	β-hydroxy isoprene nitrate	OLI	internal alkene
ISOPNBO2	peroxy radical from ISOPNB	OLIP	peroxy radical from OLI
ISOPND	δ-hydroxy isoprene nitrate	OLND	NO_3-alkene adduct that primarily decomposes
ISOPNDO2	peroxy radical from ISOPND	OLNN	NO_3-alkene adduct that primarily retains the NO_3 functional group
KET	ketone	OLT	terminal alkene
KETP	peroxy radical from KET	OLTP	peroxy radical from OLT
IEPOXOO	peroxy radical from IEPOX	ONIT	monofunctional organic nitrate
IMONIT	multifunctional organic nitrate from isoprene chemistry	UHCAP	acyl peroxy radical from UHC
ISHP	hydroxy hydro peroxides	UHCP	peroxy radical from UHC
ISNP	peroxide from isoprene nitrate peroxy radicals	UTONIT	unsaturated first generation monoterpene organic nitrate
LIM	limonene and other cyclic diene-terpenes	VRP	peroxide from MVK peroxy radical
LIMP	peroxy radical from LIM	XO2	accounts for additional NO to NO_2 conversions in peroxy radical reactions
MACP	acyl peroxy radicals from MACR	XYLP	peroxy radicals from m and p-xylene
MACR	methacrolein	XYOP	peroxy radicals from o-xylene
MACRN	methacrolein nitrate	OP2	> C-1 organic peroxides
MACRO2	peroxy radicals from MACR	ORA1	formic acid
MAHP	methyl acrylic acid	ORA2	acetic and higher acids
MCTO	alkoxy radicals from methyl catechol oxidation	PER1	peroxy intermediate from toluene oxidation
MEK	methyl ethyl ketone	PER2	peroxy intermediate from toluene oxidation
MGLY	methyl glyoxal	PROPNN	propanone nitrate
MO2	methyl peroxy radical	PYAC	pyruvic acid
MOBA	organic acids	ROH	C-3 and higher alcohols
MOBAOO	peroxy radical from MOBA	TOLND	NO_3-alkene adduct from monoterpenes that primarily decomposes
MOH	methanol	TOLNN	NO_3-alkene adduct from monoterpenes that primarily retains the NO_3 functional group
MONIT	multifunctional organic nitrate	TOLP	peroxy radicals from toluene
MPAN	methacryloyl peroxy nitrate	TONIT	saturated first generation monoterpene organic nitrate
MVK	methyl vinyl ketone	UALD	unsaturated aldehydes
MVKN	methyl vinyl ketone nitrate	UHC	multifunctional alkene from isoprene chemistry
MVKP	peroxy radical from MVK		

Table D1 (continued) Chemical species in expanded organic nitrate chemistry.

Species	H* (M atm^{-1})	-ΔH/R (K)	f0	Reference
ISON, ETHLN, ISOPND, ISOPNB, TONIT, IMONIT, UTONIT, MACRN, MVKN	17000	9200	0	Ito et al. (2007) for biogenic hydroxy nitrates
MAHP, VRP, IAP, ISNP	340	6000	0.1	Ito et al. (2007) for organic peroxides
MONIT, PROPNN, DONIT, AONIT, ONIT	1.13	5487	0	WRF-Chem ONIT
ISHP, HONIT	2.69×10^{13}	8684	0	WRF-Chem HNO_3
IEPOX	75400	6615	1	WRF-Chem H_2O_2

Table D2 Dry deposition parameters for additional isoprene chemistry and organic nitrate species. H* is the Henry's law coefficient and f0 is the reactivity factor as defined in Wesely (1989).

Reactants		Products	Rate	Notes
APIP + NO	→	0.82 HO2 + 0.43 ALD + 0.82 NO2 + 0.44 KET + 0.12 TONIT + 0.06 UTONIT + 0.23 HCHO + 0.11 ACT + 0.07 ORA1	4.00×10^{-12}	RACM2 renamed
LIMP + NO	→	0.22 UTONIT + 0.686 HO2 + 0.491 UALD + 0.231 HCHO + 0.058 HAC + 0.78 NO2 + 0.289 OLI + 0.289 KET	4.00×10^{-12}	MCM products
API + NO3	→	0.10 TOLNN + 0.90 TOLND	1.19×10^{-12} ×exp(490.0/T)	RACM2 renamed
LIM + NO3	→	0.71 TOLNN + 0.29 TOLND	1.22×10^{-11}	RACM2 renamed
TOLNN + NO	→	TONIT + NO2 + HO2	4.00×10^{-12}	RACM2 renamed
TOLNN + HO2	→	0.7 TONIT + 0.3 UTONIT	1.66×10^{-13} ×exp(1300.0/T)	RACM2 renamed
TOLNN + MO2	→	HCHO + 2.0 HO2 + 0.7 TONIT + 0.3 UTONIT	1.60×10^{-13} ×exp(708.0/T)	RACM2 renamed
TOLNN + ACO3	→	0.7 TONIT + 0.3 UTONIT + MO2 + HO2	8.85×10^{-13} ×exp(765.0/T)	RACM2 renamed
TOLNN + NO3	→	0.7 TONIT + 0.3 UTONIT + NO2 + HO2	1.20×10^{-12}	RACM2 renamed
TOLNN + TOLNN	→	1.4 TONIT + 0.6 UTONIT + HO2	7.00×10^{-14}×exp(1000.0/T)	RACM2 renamed
TOLNN + OLND	→	0.202 HCHO + 0.64 ALD + 0.149 KET + 0.50 HO2 + 0.50 NO2 + 0.7 TONIT + 0.3 UTONIT + 0.5 MONIT	4.25×10^{-14}×exp(1000.0/T)	RACM2 renamed
TOLNN + OLNN	→	MONIT + 0.7 TONIT + 0.3 UTONIT + HO2	7.00×10^{-14}×exp(1000.0/T)	RACM2 renamed
TOLND + NO	→	0.287 HCHO + 1.24 ALD + 0.464 KET + 2.0 NO2	4.00×10^{-12}	RACM2 renamed
TOLND + HO2	→	0.7 TONIT + 0.3 UTONIT	1.66×10^{-13} ×exp(1300.0/T)	RACM2 renamed
TOLND + MO2	→	0.965 HCHO + 0.500 HO2 + 0.930 ALD + 0.348 KET + 0.500 NO2 + 0.250 MOH + 0.25 ROH + 0.350 TONIT + 0.15 UTONIT	9.68×10^{-14} ×exp(708.0/T)	RACM2 renamed
TOLND + ACO3	→	0.287 HCHO + 1.24 ALD + 0.464 KET + 0.500 MO2 + 0.500 ORA2 + NO2	5.37×10^{-13} ×exp(765.0/T)	RACM2 renamed
TOLND + NO3	→	0.287 HCHO + 1.24 ALD + 0.464 KET + 2.00 NO2	1.20×10^{-12}	RACM2 renamed
TOLND + TOLND	→	0.504 HCHO + 1.21 ALD + 0.285 KET + 0.7 TONIT + 0.3 UTONIT + NO2	2.96×10^{-14}×exp(1000.0/T)	RACM2 renamed
TOLND + OLND	→	0.504 HCHO + 1.21 ALD + 0.285 KET + NO2 + 0.35 TONIT + 0.15 UTONIT + 0.5 MONIT	2.96×10^{-14}×exp(1000.0/T)	RACM2 renamed
TOLND + OLNN	→	0.202 HCHO + 0.64 ALD + 0.149 KET + 0.50 HO2 + 0.50 NO2 + MONIT + 0.35 TONIT + 0.15 UTONIT	4.25×10^{-14}×exp(1000.0/T)	RACM2 renamed

Table D3 Monoterpene reactions added to/revised from RACM2.

Reactants	Products	Rate	Notes
TOLNN + TOLND	→ 0.202 HCHO + 0.640 ALD + 0.149 KET + 0.500 HO2 + 0.500 NO2 + 1.05 TONIT + 0.45 UTONIT	$4.25\times10^{-14}\times\exp(1000.0/T)$	RACM2 renamed
TONIT + hv	→ KET + NO2	J(onitOH3)	MCM tert-butyl nitrate photolysis cross-section, divided by 3 due to the hydroxy group (Roberts and Fajer, 1989)[#]
TONIT + HO	→ HONIT	4.8×10^{-12}	Assuming a 50-50 α,β-pinene mixture and using the MCM nitrates formed from the OH addition to the double bond
UTONIT + hv	→ UALD + NO2	J(onitOH3)	MCM tert-butyl nitrate photolysis cross-section, divided by 3 due to the hydroxy group (Roberts and Fajer, 1989)[#]
UTONIT + HO	→ HONIT	7.29×10^{-11}	Average of MCM limonene nitrate rates
UTONIT + O3	→ HONIT	1.67×10^{-16}	EPA EPI v4.1 rates weighted by MCM isomers
HONIT + hv	→ HKET + NO2	J(onitOH3)	MCM tert-butyl nitrate photolysis cross-section, divided by 3 due to the hydroxy group (Roberts and Fajer, 1989)[#]
HO + HONIT	→ NO3 + HKET	$k_0=2.4\times10^{-14}\times\exp(460/T)$ $k_1=2.7\times10^{-17}\times\exp(2199/T)$ $k_2=6.5\times10^{-34}\times\exp(1335/T)\times M$ $rate=k_0+k_2/(1+k_2./k_1)$	same as RACM2 HNO_3

[#] Cross sections are calculated using the Fast-JX cross-section generator (Wild et al., 2000).

Table D3 (continued) Monoterpene reactions added to/revised from RACM2.

Reactants		Products	Rate	Notes
HC3P + NO	→	0.063 ONIT + 0.002 MONIT + 0.132 ALD + 0.165 ACT + 0.504 ACD + 0.207 HO2 + 0.131 MO2 + 0.500 ETHP + 0.089 XO2 + 0.935 NO2 + 0.042 MEK	4.00×10^{-12}	RACM2 renamed
HC5P + NO	→	0.018 HCHO + 0.203 ALD + 0.039 KET + 0.438 HO2 + 0.051 MO2 + 0.231 ETHP + 0.435 XO2 + 0.114 ONIT + 0.022 MONIT + 0.864 NO2 + 0.033 MEK + 0.217 ACT + 0.045 ACD + 0.272 HKET	4.00×10^{-12}	RACM2 renamed
HC8P + NO	→	0.163 ALD + 0.698 KET + 0.145 ETHP + 0.197 ONIT + 0.803 NO2 + 0.658 HO2 + 0.452 XO2	4.00×10^{-12}	RACM2 renamed and nitrate yield re-scaled based on Arey et al. (2001)
OLTP + NO	→	0.44 ALD + 0.78 HCHO + 0.78 HO2 + 0.97 NO2 + 0.13 MEK + 0.012 ACD + 0.06 ACT + 0.03 MONIT	4.00×10^{-12}	RACM2 renamed
OLIP + NO	→	0.83 HO2 + 0.68 ALD + 0.09 KET + 0.95 NO2 + 0.035 MONIT + 0.015 DONIT + 0.81 ACD + 0.02 HKET + 0.20 ACT	4.00×10^{-12}	RACM2 renamed
BENP + NO	→	0.082 AONIT + 0.918 HO2 + 0.459 DCB2 + 0.918 NO2 + 0.459 DCB3 + 0.918 GLY	$2.54\times10^{-12}\times\exp(360.0/T)$	RACM2 renamed
TOLP + NO	→	0.95 DCB2 + 0.95 NO2 + 0.95 HO2 + 0.05 AONIT	$2.70\times10^{-12}\times\exp(360.0/T)$	RACM2 renamed
PER1 + NO	→	0.95 DCB1 + 0.95 NO2 + 0.95 MGLY + 0.95 HO2 + 0.050 AONIT + 0.95 BALD	$2.70\times10^{-12}\times\exp(360.0/T)$	RACM2 renamed
XYLP + NO	→	0.95 DCB3 + 0.95 NO2 + 0.95 HO2 + 0.05 AONIT	$2.70\times10^{-12}\times\exp(360.0/T)$	RACM2 renamed
PER2 + NO	→	0.95 DCB1 + 0.95 NO2 + 0.95 MGLY + 0.95 HO2 + 0.050 AONIT + 1.05 DCB3	$2.70\times10^{-12}\times\exp(360.0/T)$	RACM2 renamed
XYOP + NO	→	0.95 HO2 + 0.350 GLY + 0.600 MGLY + 0.700 DCB1 + 0.073 DCB2 + 0.177 DCB3 + 0.05 AONIT + 0.95 NO2	$2.70\times10^{-12}\times\exp(360.0/T)$	RACM2 renamed
KETP + NO	→	0.531 MGLY + 0.452 ALD + 0.226 ACO3 + 0.757 HO2 + 0.157 XO2 + 0.983 NO2 + 0.017 MONIT	4.00×10^{-12}	Added nitrate
OLNN + NO	→	MONIT + NO2 + HO2	4.00×10^{-12}	RACM2 renamed
BAL2 + NO2	→	AONIT	2.00×10^{-11}	RACM2 renamed
CHO + NO2	→	AONIT	2.00×10^{-11}	RACM2 renamed

Table D4 Non-biogenic organic nitrates added to RACM2.

Reactants		Products	Rate	Notes
MCTO + NO2	→	AONIT	2.08×10^{-12}	RACM2 renamed
ADCN + HO2	→	AONIT	$3.75\times10^{-13}\times\exp(980.0/T)$	RACM2 renamed
OLNN + HO2	→	MONIT	$1.66\times10^{-13}\times\exp(1300.0/T)$	RACM2 renamed
OLND + HO2	→	MONIT	$1.66\times10^{-13}\times\exp(1300.0/T)$	RACM2 renamed
OLNN + MO2	→	HCHO + 2.0 HO2 + MONIT	$1.60\times10^{-13}\times\exp(708.0/T)$	RACM2 renamed
OLND + MO2	→	0.965 HCHO + 0.500 HO2 + 0.930 ALD + 0.348 KET + 0.500 NO2 + 0.250 MOH + 0.25 ROH + 0.500 MONIT	$9.68\times10^{-14}\times\exp(708.0/T)$	RACM2 renamed
ADCN + MO2	→	HCHO + HO2 + 0.7 OP2 + 0.7 GLY + 0.7 NO2 + 0.3 AONIT	3.56×10^{-14}	RACM2 renamed
OLNN + ACO3	→	MONIT + MO2 + HO2	$8.85\times10^{-13}\times\exp(765.0/T)$	RACM2 renamed
ADCN + ACO3	→	MO2 + HO2 + 0.7 OP2 + 0.7 GLY + 0.7 NO2 + 0.3 AONIT	$7.40\times10^{-13}\times\exp(708.0/T)$	RACM2 renamed
OLNN + NO3	→	MONIT + NO2 + HO2	1.20×10^{-12}	RACM2 renamed
OLNN + OLNN	→	2.00 MONIT + HO2	$7.00\times10^{-14}\times\exp(1000.0/T)$	RACM2 renamed
OLNN + OLND	→	0.202 HCHO + 0.640 ALD + 0.149 KET + 0.500 HO2 + 0.500 NO2 + 1.50 MONIT	$4.25\times10^{-14}\times\exp(1000.0/T)$	RACM2 renamed
OLND + OLND	→	0.504 HCHO + 1.21 ALD + 0.285 KET + MONIT + NO2	$2.96\times10^{-14}\times\exp(1000.0/T)$	RACM2 renamed
AONIT + hv	→	KET + NO2	J(onitOH3)	MCM tert-butyl nitrate photolysis cross-section, divided by 3 due to the hydroxy group (Roberts and Fajer, 1989)[#]
DONIT + hv	→	UALD + NO2	J(onitOH1)	MCM n-propyl nitrate photolysis cross-section, divided by 3 due to the hydroxy group (Roberts and Fajer, 1989)[#]
MONIT + hv	→	KET + NO2	J(onitOH1)	Same as above
AONIT + HO	→	DCB2 + NO2	7.3×10^{-11}	MCM rate for major peroxy radical formed from benzene
DONIT + HO	→	UALD + NO2	4.1×10^{-11}	MCM weighted average based on butadiene nitrates
MONIT + HO	→	HKET + NO2	1.79×10^{-12}	Rate is from MCM hydroxy nitrate from 2-butene

[#] Cross sections are calculated using the Fast-JX cross-section generator (Wild et al., 2000).
MCM - (Jenkin et al., 1997; Saunders et al., 2003)

Table D4 (continued) Non-biogenic organic nitrates added to RACM2.

Reactants		Products	Rate	Notes
ISO + HO	→	ISOP	$3.1\times10^{-11}\times\exp(350.0/T)$	Rate from Sander et al. (2011)
ISOP + NO	→	0.4 MVK + 0.26 MACR + 0.883 NO2 + 0.07 ISOPND + 0.047 ISOPNB + 0.66 HCHO + 0.143 UHC + 0.08 DIBOO + 0.803 HO2	$2.7\times10^{-12}\times\exp(360.0/T)$	Products from Paulot et al. (2009a), rate from MCM
ISOP + HO2	→	0.88 ISHP + 0.12 HO + 0.047 MACR + 0.073 MVK + 0.12 HO2 + 0.12 HCHO	$7.4\times10^{-13}\times\exp(700.0/T)$	Paulot et al. (2009b)
ISOP	→	HPALD + HO2	$4.12\times10^{8}\times\exp(-7700.0/T)$	Products from Peeters and Müller (2010), rate from Crounse et al. (2011)
ISOPND + hv	→	ISOP + NO2	J(onit1)	MCM n-propyl nitrate photolysis cross-section#
ISOPND + HO	→	ISOPNDO2	$1.77\times10^{-11}\times\exp(500.0/T)$	Paulot et al. (2009a) products and rate with temperature dependence of RACM2 internal alkene
ISOPND + O3	→	0.266 PROPNN + 0.017 ORA2 + 0.249 GLYC + 0.075 H2O2 + 0.89 HO + 0.445 HO2 + 0.214 CO + 0.214 HCHO + 0.445 NO2 + 0.271 ETHLN + 0.018 IMONIT + 0.445 MGLY + 0.289 HAC + 0.231 GLY	$9.03\times10^{-16}\times\exp(-845.0/T)$	Products based on MCM, rate from Lockwood et al. (2010) with temperature dependence of RACM2 internal alkene
ISOPNDO2 + NO	→	0.15 PROPNN + 0.44 HAC + 0.07 MVKN + 0.13 ETHLN + 0.31 ORA1 + 0.31 NO3 + 0.72 HCHO + 0.15 GLYC + 1.34 NO2 + 0.35 HO2 + 0.34 HKET	$2.7\times10^{-12}\times\exp(360.0/T)$	Paulot et al. (2009a) products and MCM rate
ISOPNDO2 + HO2	→	ISNP	$2.06\times10^{-13}\times\exp(1300.0/T)$	MCM rate
ISOPNDO2 + MO2	→	1.506 HCHO + 0.949 HO2 + 0.3 IMONIT + 0.055 MVKN + 0.309 HAC + 0.093 ETHLN + 0.216 ORA1 + 0.235 HKET + 0.101 PROPNN + 0.101 GLYC + 0.216 NO3 + 0.235 NO2	7.5×10^{-14}	Madronich and Calvert (1990) RO_2 products and rate*
ISOPNDO2 + ACO3	→	0.078 MVKN + 0.442 HAC + 0.133 ETHLN + 0.309 ORA1 + 0.336 HKET + 0.144 PROPNN + 0.144 GLYC + 0.723 HCHO + 0.355 HO2 + 0.309 NO3 + MO2 + CO2 + 0.336 NO2	$9.53\times10^{-14}\times\exp(500.0/T)$	Madronich and Calvert (1990) RO_2 products and rate*

Table D5 Reactions of isoprene and related species added to RACM2.

Reactants		Products	Rate	Notes
ISOPNDO2 + NO3	→	0.078 MVKN + 0.442 HAC + 0.133 ETHLN + 0.309 ORA1 + 0.336 HKET + 0.144 PROPNN + 0.144 GLYC + 0.723 HCHO + 0.355 HO2 + 0.309 NO3 + 1.336 NO2	2.3×10^{-12}	Jenkin et al. (1997) RO_2+NO_3 products with MCM rate
ISOPNB + hv	→	ISOP + NO2	J(onitOH3)	MCM tert-butyl nitrate photolysis cross-section, divided by 3 due to the hydroxy group (Roberts and Fajer, 1989)[#]
ISOPNB + HO	→	ISOPNBO2	$2.43\times10^{-12}\times\exp(500.00/T)$	Paulot et al. (2009a) products and rate with temperature dependence of RACM2 terminal alkene
ISOPNB + O3	→	0.541 HCHO + 0.506 CO + 0.526 HO + 0.327 NO2 + 0.179 HAC + 0.102 H2O2 + 0.349 MACRN + 0.112 IMONIT + 0.128 CO2 + 0.327 HO2 + 0.068 ORA1 + 0.212 MVKN + 0.148 MGLY	$5.04\times10^{-14}\times\exp(-1800/T)$	Products based on MCM, rate from Lockwood et al. (2010) with temperature dependence of RACM2 terminal alkene
ISOPNBO2 + NO	→	0.6 GLYC + 0.6 HAC + 0.4 HCHO + 0.4 HO2 + 0.26 MACRN + 0.14 MVKN + 1.6 NO2	$2.7\times10^{-12}\times\exp(360.0/T)$	Paulot et al. (2009a) products, MCM rate
ISOPNBO2 + HO2	→	ISNP	$2.06\times10^{-13}\times\exp(1300.0/T)$	MCM
ISOPNBO2 + MO2	→	0.128 MACRN + 0.16 MOH + 0.101 MVKN + 0.801 HO2 + 1.069 HCHO + 0.343 HAC + 0.343 GLYC + 0.343 NO2 + 0.428 IMONIT	6.7×10^{-13}	Madronich and Calvert (1990) RO_2 products and rate*, RO follows same fate as in the NO reaction
ISOPNBO2 + ACO3	→	0.064 IMONIT + 0.23 MACRN + 0.144 MVKN + 0.374 HCHO + 0.562 HAC + 0.562 GLYC + 0.562 NO2 + 0.936 CO2 + 0.936 MO2 + 0.374 HO2 + 0.064 ORA2	$8.16\times10^{-13}\times\exp(500.0/T)$	Madronich and Calvert (1990)/Tyndall et al. (2001) products and rate*
ISOPNBO2 + NO3	→	0.256 MACRN + 0.144 MVKN + 0.6 HAC + 0.6 GLYC + 0.4 HCHO + 0.4 HO2 + 1.6 NO2	2.3×10^{-12}	Jenkin et al. (1997) RO_2+NO_3 products with MCM rate
HPALD + hv	→	1.0 HO + HO2 + 0.5 HAC + 0.5 MGLY + 0.25 GLYC + 0.25 GLY + HCHO	J(hpald)	Peeters and Müller (2010)
HPALD + HO	→	HO	4.6×10^{-11}	Peeters and Müller (2010)
IEPOX + HO	→	IEPOXOO	$5.78\times10^{-11}\times\exp(-400.0/T)$	Paulot et al. (2009b)

Table D5 (continued) Reactions of isoprene and related species added to RACM2.

Reactants		Products	Rate	Notes
IEPOXOO + NO	→	0.725 HAC + 0.275 GLYC + 0.275 GLY + 0.275 MGLY + 0.125 HO + 0.825 HO2 + 0.2 CO2 + 0.375 HCHO + 0.074 ORA1 + 0.251 CO + NO2	2.7×10^{-12} ×exp(360.0/T)	MCM
IEPOXOO + HO2	→	0.725 HAC + 0.275 GLYC + 0.275 GLY + 0.275 MGLY + 1.125 HO + 0.825 HO2 + 0.2 CO2 + 0.375 HCHO + 0.074 ORA1 + 0.251 CO	7.4×10^{-13} ×exp(700.0/T)	Paulot et al. (2009b)
IEPOXOO + NO3	→	0.725 HAC + 0.275 GLYC + 0.275 GLY + 0.275 MGLY + 0.125 HO + 0.825 HO2 + 0.2 CO2 + 0.375 HCHO + 0.074 ORA1 + 0.251 CO + NO2	2.3×10^{-12}	MCM
ISHP + hv	→	HO + 0.202 UHC + 0.108 DIBOO + 0.44 MVK + 0.25 MACR + 0.69 HCHO + 0.892 HO2	J(ch3o2h)	MCM CH_3OOH cross section [#]
ISHP + HO	→	IEPOX + HO	1.9×10^{-11} ×exp(390.0/T)	Paulot et al. (2009b)
ISHP + HO	→	0.7 ISOP + 0.3 UHC + 0.3 HO	3.8×10^{-12} ×exp(200.0/T)	Paulot et al. (2009b)
PROPNN + hv	→	NO2 + ACO3 + HCHO	J(noa)	MCM nitroxy acetone cross section[#]
PROPNN + HO	→	NO2 + MGLY	1.0×10^{-12}	Paulot et al. (2009a)
ETHLN + hv	→	HO2 + CO + HCHO + NO2	J(noa)	MCM nitroxy acetone cross section[#]
ETHLN + HO	→	HCHO + CO2 + NO2	1.0×10^{-11}	Paulot et al. (2009a)
IMONIT + hv	→	HKET + NO2	J(onitOH1)	MCM n-propyl nitrate photolysis cross-section, divided by 3 due to the hydroxy group (Roberts and Fajer, 1989)[#]
IMONIT + HO	→	HKET + NO2	7.2×10^{-12}	MCM weighted average
ISNP + hv	→	HO + 0.686 HO2 + 0.298 PROPNN + 0.612 GLYC + 0.632 HAC + 0.318 ETHLN + 0.314 NO2 + 0.07 MVKN + 0.07 HCHO	J(ch3o2h)	MCM CH_3OOH cross section [#]
ISNP + HO	→	0.460 ISOPNDO2 + 0.097 ISOPNBO2 + 0.443 IMONIT + 0.443 HO	1.67×10^{-11} ×exp(200.0/T)	Calculated using Kwok and Atkinson (1995) with temperature dependence and products of CH_3OOH from Sander et al. (2011)
UHC + hv	→	0.5 UHCAP + 1.24 HO2 + 0.26 ACO3 + 0.74 CO + 0.26 GLYC + 0.24 HAC	J(macr)	IUPAC cross section

Table D5 (continued) Reactions of isoprene and related species added to RACM2.

Reactants		Products	Rate	Notes
UHC + HO	→	0.74 UHCP + 0.26 UHCAP	1.1×10^{-10}	Paulot et al. (2009a)
UHC + O3	→	0.503 MGLY + 0.89 HO + 0.89 CO + 0.659 HO2 + 0.231 HCHO + 0.018 MOH + 0.018 CO2 + 0.271 GLYC + 0.076 H2O2 + 0.266 HAC + 0.266 GLY + 0.231 ACO3	4.0×10^{-17}	Rate from Jenkin et al. (1997) lowered by a factor of 10 due to the aldehyde
UHC + NO3	→	HNO3 + UHCAP	$5.95\times10^{-12}\times\exp(-1860/T)$	Jenkin et al. (1997) RO_2+NO_3 products with MCM rate
UHCP + NO	→	0.39 DHMOB + 0.32 GLYC + 0.32 MGLY + 0.29 HAC + 0.29 GLY + HO2 + NO2	$2.7\times10^{-12}\times\exp(360.0/T)$	Paulot et al. (2009a) products, MCM rate
UHCP + HO2	→	0.652 IAP + 0.136 DHMOB + 0.212 MGLY + 0.212 GLYC + 0.348 HO + 0.348 HO2	$2.06\times10^{-13}\times\exp(1300.0/T)$	Hasson et al. (2004) products, MCM rate
UHCP + MO2	→	0.573 DHMOB + HCHO + 1.4 HO2 + 0.222 GLYC + 0.222 MGLY + 0.205 HAC + 0.205 GLY	8.24×10^{-14}	Madronich and Calvert (1990) RO_2 products and rate*
UHCP + ACO3	→	MO2 + CO2 + 0.39 DHMOB + 0.32 GLYC + 0.32 MGLY + 0.29 HAC + 0.29 GLY + HO2	$1.04\times10^{-13}\times\exp(500.0/T)$	Madronich and Calvert (1990) RO_2 products and rate*
UHCP + NO3	→	NO2 + 0.39 DHMOB + 0.317 GLYC + 0.317 MGLY + 0.293 GLY + 0.293 HAC + HO2	2.3×10^{-12}	Jenkin et al. (1997) RO_2+NO_3 products with MCM rate
UHCAP + NO	→	NO2 + 0.65 MOBA + 0.35 ALD + 0.35 CO + HO2	$7.5\times10^{-12}\times\exp(290.0/T)$	Paulot et al. (2009a) products, MCM rate
UHCAP + HO2	→	0.4 IAP + 0.2 ORA2 + 0.2 O3 + 0.4 HO + 0.26 MOBA + 0.14 ALD + 0.14 CO	$5.2\times10^{-13}\times\exp(980.0/T)$	Hasson et al. (2004) branching MCM rate
UHCAP + MO2	→	0.1 ORA2 + HCHO + 1.8 HO2 + 0.585 MOBA + 0.315 ALD + 0.315 CO	$8.83\times10^{-13}\times\exp(500.0/T)$	Tyndall et al. (2001)
UHCAP + ACO3	→	MO2 + CO2 + HO2 + 0.65 MOBA + 0.35 ALD + 0.35 CO	$2.9\times10^{-12}\times\exp(500.0/T)$	Tyndall et al. (2001)
UHCAP + NO3	→	NO2 + HO2 + 0.65 MOBA + 0.35 ALD + 0.35 CO	4.0×10^{-12}	MCM
UHCAP + NO2	→	MPAN	TROE(9.0×10^{-28} , 8.9, 7.7×10^{-12} , 0.2, T, M)	Sander et al. (2011) rate for PPN
IAP + HO	→	0.165 UHCAP + 0.495 UHCP + 0.34 DIBOO	$2.7\times10^{-11}\times\exp(200.0/T)$	Calculated using Kwok and Atkinson (1995) with temperature dependence and products of CH_3OOH from Sander et al. (2011)

Table D5 (continued) Reactions of isoprene and related species added to RACM2.

Reactants		Products	Rate	Notes
IAP + hv	→	HO + 0.107 MOBA + 0.058 ALD + 0.058 CO + 0.193 DHMOB + 0.335 GLYC + 0.335 MGLY + 0.307 HAC + 0.307 GLY + HO2	J(ch3o2h)	MCM CH_3OOH cross section [#]
DIBOO + NO	→	NO2 + HO2 + 0.52 GLYC + 0.52 MGLY + 0.48 GLY + 0.48 HAC	2.7×10^{-12} ×exp(360.0/T)	Paulot et al. (2009a) products, MCM rate
DIBOO + HO2	→	0.33 IAP + 0.67 HO + 0.67 HO2 + 0.348 GLYC + 0.348 MGLY + 0.322 GLY + 0.322 HAC	2.06×10^{-13} ×exp(1300.0/T)	Hasson et al. (2004) branching MCM rate
DIBOO + MO2	→	0.396 DHMOB + 0.88 HCHO + 0.364 GLYC + 0.364 MGLY + 1.208 HO2 + 0.12 MOH + 0.24 GLY + 0.24 HAC	4.6×10^{-13}	Madronich and Calvert (1990) RO_2 products and rate*
DIBOO + ACO3	→	0.52 GLYC + 0.52 MGLY + 0.952 HO2 + 0.952 MO2 + 0.952 CO2 + 0.432 GLY + 0.432 HAC + 0.048 ORA2 + 0.048 DHMOB	5.8×10^{-13} ×exp(500.0/T)	Tyndall et al. (2001)
DIBOO + NO3	→	NO2 + HO2 + 0.52 GLYC + 0.52 MGLY + 0.48 GLY + 0.48 HAC	2.3×10^{-12}	Jenkin et al. (1997) RO_2+NO_3 products with MCM rate
MOBA + hv	→	0.53 PYAC + 0.48 GLY + 1.52 HO2 + 2.0 CO + 0.48 MO2	J(macr)	IUPAC cross section
MOBA + HO	→	MOBAOO	3.0×10^{-12}	Paulot et al. (2009a)
MOBA + O3	→	0.555 MGLY + 0.89 HO + 0.89 CO + 0.445 HO2 + 0.076 H2O2 + 0.555 GLY + 0.231 KETP + 0.214 ACO3 + 0.214 CO2	2.0×10^{-17}	Paulot et al. (2009a), MCM
MOBAOO + NO	→	ALD + CO2 + HO2 + NO2	8.0×10^{-12}	Paulot et al. (2009a)
MOBAOO + HO2	→	OP2	2.06×10^{-13} ×exp(1300.0/T)	MCM
MOBAOO + MO2	→	0.7 CO2 + 0.7 ALD + 1.4 HO2 + HCHO + 0.3 ROH	3.55×10^{-12}	Madronich and Calvert (1990) RO_2 products and rate assuming 3^o beta hydroxy
MOBAOO + ACO3	→	ALD + 2.0 CO2 + HO2 + MO2	4.23×10^{-12} ×exp(500.0/T)	Tyndall et al. (2001)
MOBAOO + NO3	→	NO2 + HO2 + ALD + CO2	2.3×10^{-12}	Jenkin et al. (1997) RO_2+NO_3 products with MCM rate
HAC + hv	→	ACO3 + HCHO + HO2	J(ch3coch3)	MCM products assume same cross-section as acetone
HAC + HO	→	MGLY + HO2	1.6×10^{-12}×exp(305.0/T)	MCM products, IUPAC rate
GLYC + hv	→	2.0 HO2 + HCHO + CO	J(glyc)	MCM cross section[#]
GLYC + HO	→	0.2 GLY + 0.2 HO2 + 0.8 RCO3	1.0×10^{-11}	MCM

Table D5 (continued) Reactions of isoprene and related species added to RACM2.

Reactants		Products	Rate	Notes
GLYC + NO3	→	RCO3 + HNO3	$1.4\times10^{-12}\times\exp(-1860.0/T)$	MCM
DHMOB + hv	→	HO2 + CO + KETP	J(ald)	Assume aldehyde
DHMOB + HO	→	1.5 CO + 0.5 HO2 + 0.5 HAC + 0.5 ALD	1.0×10^{-11}	Paulot et al. (2009a)
PYAC + HO	→	ACO3 + CO2	8.0×10^{-13}	MCM
PYAC + hv	→	ACO3 + CO2 + HO2	j(Pj_ch3cocho)	Fast-JX 6.5 cross section[#]
MACR + hv		0.5 MACP + 0.175 ACO3 + 0.5 HCHO + 0.325 MO2 + 0.825 CO + HO2	J(macr)	IUPAC cross section
MACR + HO		0.53 MACP + 0.47 MACRO2	$8.0\times10^{-12}\times\exp(380.0/T)$	Paulot et al. (2009a) products, IUPAC rate
MACR + O3		0.902 MGLY + 0.242 HCHO + 0.238 HO + 0.652 CO + 0.098 ACO3 + 0.204 ORA1 + 0.14 HO2 + 0.144 H2O2	$1.4\times10^{-15}\times\exp(-2100.0/T)$	MCM
MACR + NO3		MACP + HNO3	3.4×10^{-15}	MCM
MACP + NO		NO2 + CO + CO2 + HCHO + MO2	$7.5\times10^{-12}\times\exp(290.0/T)$	rate MCM AP + NO prdts Paulot ACP
MACP + HO2		0.4 MAHP + 0.2 O3 + 0.2 ORA2 + 0.4 HO + 0.4 CO2 + 0.26 MO2 + 0.4 HCHO + 0.14 ACO3 + 0.26 CO	$5.2\times10^{-13}\times\exp(980.0/T)$	Hasson et al. (2004) products, MCM rate
MACP + MO2		0.9 HO2 + 0.9 CO2 + 0.585 MO2 + 0.585 CO + 0.315 ACO3 + 0.1 ORA2 + 1.9 HCHO	$2.0\times10^{-12}\times\exp(500.0/T)$	Tyndall et al. (2001)
MACP + ACO3		1.65 MO2 + 2.0 CO2 + 0.35 ACO3 + HCHO + 0.65 CO	$2.9\times10^{-12}\times\exp(500.0/T)$	Tyndall et al. (2001) and IUPAC rate
MACP + NO3		NO2 + CO2 + HCHO + 0.65 MO2 + 0.65 CO + 0.35 ACO3	4.0×10^{-12}	MCM
MACP + NO2		MPAN	TROE(9.0×10^{-28} , 8.9, 7.7×10^{-12} , 0.2, T, M)	Sander et al. (2011) rate for PPN
MPAN		MACP + NO2	TROEE(1.11×10^{28} , 14000.0, 9.0×10^{-28} , 8.9 , 7.7×10^{-12} , 0.2, T , M)	Sander et al. (2011) rate for PPN
MAHP + HO		MACP	1.66×10^{-11}	MCM
UALD + NO3		MACP + HNO3	$5.02\times10^{-13}\times\exp(-1076/T)$	MCM
MAHP + hv		ACO3 + HO + CO2	J(ch3o2h)	MCM CH_3OOH cross section[#]
MACRO2		HAC + CO + HO	$2.9\times\exp10^{7}\times\exp(-5297/T)$	Crounse et al. (2012)

Table D5 (continued) Reactions of isoprene and related species added to RACM2.

Reactants	Products	Rate	Notes
MACRO2 + NO	0.85 NO2 + 0.85 HO2 + 0.425 HAC + 0.425 CO + 0.425 HCHO + 0.425 MGLY + 0.15 MACRN	$2.7\times10^{-12}\times\exp(360.0/T)$	Paulot et al. (2009a) products, MCM rate
MACRO2 + HO2	OP2	$1.8\times10^{-13}\times\exp(1300.0/T)$	MCM
MACRO2 + MO2	0.328 HKET + 1.037 HCHO + 1.344 HO2 + 0.599 HAC + 0.599 CO + 0.036 MOH + 0.073 MGLY	2.04×10^{-13}	Madronich and Calvert (1990) RO_2 products and rate*, from initial $2^o/3^o$ split from MCM
MACRO2 + ACO3	0.855 HAC + 0.855 CO + 0.131 MGLY + 0.131 HCHO + 0.014 HKET + 0.014 ORA2 + 0.986 MO2 + 0.986 HO2 + 0.986 CO2	$2.58\times10^{-13}\times\exp(500.0/T)$	MCM peroxy branching ratio, Madronich and Calvert (1990) RO_2 products and rate*
MACRO2 + NO3	0.855 HAC + 0.855 CO + 0.855 HO2 + 0.145 HO2 + 0.145 MGLY + 0.145 HCHO + NO2	2.3×10^{-12}	MCM
MVK + hv	0.6 OLT + 0.6 CO + 0.4 ACO3 + 0.4 MO2	J(mvk)	Fast-JX 6.5 products and cross-section[#]
MVK + O3	0.28 ACO3 + 0.56 CO + 0.075 ORA1 + 0.09 H2O2 + 0.28 HO2 + 0.2 CO2 + 0.1 ACD + 0.545 HCHO + 0.36 HO + 0.545 MGLY + 0.075 PYAC	$8.5\times10^{-16}\times\exp(-1520.0/T)$	MCM products assuming that the Criegee radical reacts only with H_2O, IUPAC rate
MVKP + NO	0.625 GLYC + 0.625 ACO3 + 0.265 MGLY + 0.265 HCHO + 0.265 HO2 + 0.11 MVKN + 0.89 NO2	$2.7\times10^{-12}\times\exp(360.0/T)$	Paulot et al (2009a) products, MCM rate
MVKP + HO2	0.531 VRP + 0.469 GLYC + 0.469 ACO3 + 0.469 HO	$1.82\times10^{-13}\times\exp(1300.0/T)$	MCM rate and $1^o/2^o$ RO^2 branching, Hasson et al. (2004) products
MVKP + MO2	0.25 ROH + 0.9 HCHO + 0.25 HKET + 0.25 MOH + 0.15 MGLY + 0.35 GLYC + 0.35 ACO3 + 0.65 HO2	1.38×10^{-12}	MCM initial branching ratio, Madronich and Calvert (1990) RO_2 products and rate*
MVKP + ACO3	0.1 HKET + 0.1 ORA2 + 0.27 MGLY + 0.27 HO2 + 0.27 HCHO + 0.63 GLYC + 0.63 ACO3 + 0.9 CO2 + 0.9 MO2	$1.7\times10^{-12}\times\exp(500.0/T)$	Tyndall et al. (2001)
MVKP + NO3	NO2 + 0.3 MGLY + 0.3 HO2 + 0.3 HCHO + 0.7 GLYC + 0.7 ACO3	2.3×10^{-12}	MCM
VRP + hv	HO + 0.7 ACO3 + 0.7 GLYC + 0.3 MGLY + 0.3 HCHO + 0.3 HO2	J(ch3o2h)	MCM CH_3OOH cross section, products split by initial MCM branching ratio for MVKP[#]
VRP + HO	0.7 MVKP + 0.3 KET + 0.3 HO	$3.8\times10^{-12}\times\exp(200.0/T)$	CH3OOH + OH rate and radical branching ratio from Sander et al. (2011)

Table D5 (continued) Reactions of isoprene and related species added to RACM2.

Reactants	Products	Rate	Notes
MACRN + hv	NO2 + CO + HAC + HO2	J(ibutald)	MCM iso-butyraldehyde cross-section[#]
MVKN + hv	GLYC + NO2 + ACO3	J(noa)	MCM nitroxy acetone cross section[#]
MACRN + HO	0.08 ORA2 + 0.08 HCHO + 0.15 NO3 + 0.07 ORA1 + 0.07 MGLY + 0.85 HAC + 0.85 NO2 + 0.93 CO2	5.0×10^{-11}	Paulot et al. (2009a)
MVKN + HO	0.65 ORA1 + 0.65 MGLY + 0.35 HCHO + 0.35 PYAC + NO3	5.6×10^{-12}	Paulot et al. (2009a)

*Using updated rates (Atkinson et al., 2004, 2006; Sander et al., 2011), IUPAC rate or cross section (Atkinson et al., 2006), [#] Cross sections are calculated using the Fast-JX cross-section generator (Wild et al., 2000)., MCM - (Jenkin et al., 1997; Saunders et al., 2003), TROE(k_0(300K),n,k_∞(300K),m,T,M): $k_0(T) = k_{0\_}300K \times (300/T)^n \times M$, $k_\infty(T) = k_\infty(300K) \times (300/T)^m$, $k_{ratio} = k_0(T)/k_\infty(T)$, rate $= k_0(T)./(1+k_{ratio}) \times 0.6\text{^}(1/(1+\log10(k_{ratio})^2))$, TROEE(A, B, k_0(300K),n,k_∞(300K),m,T,M): $k_0(T) = k_{0\_}300K \times (300/T)^n \times M$, $k_\infty(T) = k_\infty(300K) \times (300/T)^m$, $k_{ratio} = k_0(T)/k_\infty(T)$, $k = k_{0(}T)/(1+k_{ratio}) \times 0.6\text{^}(1/(1+\log10(k_{ratio})^2))$, rate = $A\times\exp(-BT/) \times k$

Table D5 (continued) Reactions of isoprene and related species added to RACM2.